MATHEMATICAL MODELING OF FLUIDIZED BED COMBUSTORS WITH RADIATION MODEL

A THESIS SUBMITTED TO
THE GRADUATE SCHOOL OF NATURAL AND APPLIED SCIENCES
OF
MIDDLE EAST TECHNICAL UNIVERSITY

BY

D. ECE ALAGÖZ

IN PARTIAL FULFILLMENT OF THE REQUIREMENTS
FOR
THE DEGREE OF MASTER OF SCIENCE
IN
CHEMICAL ENGINEERING

AUGUST 2006

Approval of the Graduate School of Natural and Applied Sciences.

Prof. Dr. Canan Özgen
Director

I certify that this thesis satisfies all the requirements as a thesis for the degree of Master of Science.

Prof. Dr. Nurcan Baç
Head of Department

This is to certify that we have read this thesis and that in our opinion it is fully adequate, in scope and quality, as a thesis and for the degree of Master of Science.

Assist. Prof. Dr. Görkem Kırbaş
Co-Supervisor

Prof. Dr. Nevin Selçuk
Supervisor

Examining Committee Members

Prof. Dr. Nurcan Baç (METU, CHE)

Prof. Dr. Nevin Selçuk (METU, CHE)

Assist. Prof. Dr. Görkem Kırbaş (METU, CHE)

Prof. Dr. Faruk Arınç (METU, ME)

Assist. Prof. Dr. Nimeti Döner (Dumplupınar Unv., ME)

I hereby declare that all information in this document has been obtained and presented in accordance with academic rules and ethical conduct. I also declare that, as required by these rules and conduct, I have fully cited and referenced all material and results that are not original to this work.

Name, Last name : D. Ece ALAGÖZ

Signature :

ABSTRACT

MATHEMATICAL MODELING OF FLUIDIZED BED COMBUSTORS WITH RADIATION MODEL

Alagöz, D. Ece
M.S., Department of Chemical Engineering
Supervisor: Prof. Dr. Nevin Selçuk
Co-Supervisor: Assist. Prof. Dr. Görkem Kırbaş

August 2006, 120 Pages

Simultaneous solution of the conservation equations for energy and chemical species in conjunction with radiative transfer equation was carried out by coupling a previously developed and tested system model of fluidized bed combustion (FBC) to an existing radiation model.

The predictive accuracy of the coupled code was assessed by applying it to 0.3 MW_t METU Atmospheric Bubbling Fluidized Bed Combustor (ABFBC) Test Rig burning lignite in its own ash and comparing its predictions with the measured temperatures and concentrations of gaseous species along the combustor and radiative heat fluxes incident on the refractory-lined freeboard walls on two combustion tests, with and

without recycle. The predictions of the coupled code were found to be in good agreement with the measurements.

For the investigation of the significance of coupling of the radiation model to the system model, temperature predictions of the coupled code were compared with those obtained by the original system model. It was found that the effect of incorporating a radiation model into the system model on the predictions was not significant because the high temperatures of refractory-lined freeboard walls and high surface to volume ratio of the test rig under consideration cause the incident radiative heat fluxes to be dominated by walls rather than the particle laden gas emissions. However, in industrial boilers, freeboard is surrounded by water-cooled membrane walls and boilers have much lower surface to volume ratio. In order to examine the effects of both on radiation in industrial boilers, an investigation was carried out on 16 MW_t Stationary Fluidized Bed Boiler (SFBB) by applying radiation model, in isolation from the system model, to the freeboard of the boiler. It was found that in the boiler, incident radiative heat fluxes were dominated by particle laden gas emissions.

In brief, the coupled code proposed in this study proves to be a useful tool in qualitatively and quantitatively simulating the processes taking place in an atmospheric fluidized bed boilers.

Keywords: Fluidized bed combustion; System model; Radiation model; Radiative heat transfer in freeboard; MOL solution of DOM.

ÖZ

AKIŞKAN YATAKLI YAKICILARIN RADYASYON MODELİ İLE MATEMATİKSEL MODELLENMESİ

Alagöz, D. Ece
Yüksek Lisans, Kimya Mühendisliği Bölümü
Tez Yöneticisi: Prof. Dr. Nevin Selçuk
Yardımcı Tez Yöneticisi: Yrd. Dç. Dr. Görkem Kırbaş

Ağustos 2006, 120 Sayfa

Enerji ve madde korunumu denklemlerinin ışınım ısı transfer denklemi ile eş zamanlı çözümü, daha önceden geliştirilmiş ve test edilmiş akışkan yataklı bir yakıcı modeli ile varolan bir radyasyon modelinin birleştirilmesiyle sağlanmıştır.

Birleşik kod, kendi külü içinde linyit yakan ODTÜ 0.3 MW Atmosferic Kabarcıklı Akışkan Yataklı Yakıcı (AKAYY) Test Ünitesinin davranışının belirlenmesine uygulanmış ve öngörülerinin doğruluğu aynı test ünitesi üzerinden alınan geri döngülü ve geri döngüsüz ölçümlerle yapılan karşılaştırma ile değerlendirilmiştir. Karşılaştırma sonucu, yakıcı boyunca, sıcaklık, gaz derişimleri ve serbest bölge duvarlarına düşen ışınım ısı akıları öngörülerinin deneysel verilerle uyum içerisinde olduğu görülmüştür.

Radyasyon modeli ile sistem modelinin birleştirilmesinin önemini incelemek için birleşik kodun sıcaklık öngörüleri orjinal sistem modelin sıcaklık öngörüleri ile karşılaştırılmıştır. Test ünitesinin serbest bölge duvar sıcaklıklarının ve yüzey/hacim oranının yüksek olması, ışınım ısı akılarının tanecik saçınımlarından ziyade, serbest bölge duvar yayınımları tarafından kontrol edilmesine neden olduğu için, radyasyon modeli ile sistem modelinin birleştirilmesinin öngörülere etkisinin önemli ölçüde olmadığı görülmüştür. Fakat, endüstriyel kazanlarda, serbest bölge soğutma sulu membran duvarlar ile çevrili olup kazanlar daha düşük yüzey/hacim oranına sahiptir. Bu iki faktörün endüstriyel kazanlarda ışınım ısı transferine etkisini incelemek için radyasyon modeli sistem modelden ayrı bir şekilde 16 MW Kabarcıklı Akışkan Yataklı Kazana (KAYK) uygulanmış ve serbest bölge duvarlarına düşen ışınım ısı akılarının tanecik saçınımları tarafından kontrol edildiği görülmüştür.

Özetle, geliştirilen birleşik kodun akışkan yataklı kazanlarda gerçekleşen olayların nicel ve nitel temsilinde yararlı olduğu görülmüştür.

Anahtar kelimeler: Akışkan yataklı yakıcı; Sistem modeli; Radyasyon modeli; Serbest böldede ışınım ısı transferi; Çizgiler yöntemi

To

my dearest family

and

Müjdat Çelikkan

ACKNOWLEDGEMENTS

I would like to express my deepest gratitude to my supervisor, Prof. Dr. Nevin Selçuk for her guidance and encouragement throughout this study.

I would like to show my appreciation to my co-supervisor, Assist. Prof. Dr. Görkem Kırbaş for insightful conversations and helpful comments on the text.

I would like to thank Dr. Bengt-Åke Andersson whose thesis was a constant guide for the case study in the freeboard of the fluidized bed boiler.

I really would like to thank Mr. Emin Peynirci and Mr. Tamer Bozacı from the Investment and Projects Department of AKSA, for their tolerance and patience during this study.

Many thanks go to Zuhal Göğebakan, Yusuf Göğebakan and especially to Ertan Karaismail for their advice and guidance throughout my thesis study.

I also thank to the members of AFBC research team for their friendship and support during my study; Mehmet Kürkçü, Mehmet Onur Afacan, Mehmet Ekrem Moralı, Fatma Nihan Çayan, Işıl Ayrancı and Ahmet Bilge Uygur.

Furthermore, I would like to thank all my friends for their encouragement and motivation during this study.

Finally, my special thanks go to my family and Müjdat Çelikkan for their great support, encouragement and unshakable faith in me when it was most required.

TABLE OF CONTENTS

LIST OF TABLES

LIST OF FIGURES

LIST OF SYMBOLS

a	Decay constant, cm^{-1}
A	Cross-sectional area, cm^2
A_{mc}	Mass specific cross section, $m^2 kg^{-1}$
Ar	Archimedes number, -
B	Particle load, $kg\ m^{-3}$
c_p	Specific heat capacity, $cal\ g^{-1}\ K^{-1}$
C	Concentration, $mol\ cm^{-3}$
C_d	Drag coefficient, -
d	Diameter, cm
D	Diffusivity of oxygen in nitrogen, $cm^2\ s^{-1}$
E	Activation energy, $cal\ mol^{-1}$
$E(r)$	Elutriation rate constant, s^{-1}
f	Friction factor, -
$f(E)$	Activation energy distribution function for devolatilization, $mol\ cal^{-1}$
F	Char flow rate, $g\ s^{-1}$
F_c	Carryover flow rate, $kg\ h^{-1}$
$f_N(D_p)$	Number distribution of particles, -
F_z	Upward flow rate of entrained particles at any height z in freeboard, $g\ s^{-1}$
g	Gravitational acceleration, $cm\ s^{-2}$
h	Individual heat transfer coefficient, $cal\ cm^{-2}\ s^{-1}\ K^{-1}$
H	Height, m or cm
ΔH^0	Heat of reaction at standard state, $cal\ mol^{-1}$
k	Overall sulfation rate constant, cm/s; thermal conductivity, $cal\ cm^{-1}\ s^{-1}\ K^{-1}$

$k(E)$	First-order reaction rate constant for devolatilization, s^{-1}
k_C	Reaction rate constant for char combustion, $cm\ s^{-1}$
k_{CO}	Reaction rate constant for CO oxidation, $(cm^3\ mol^{-1})^{0.8}\ s^{-1}$
k_f	Film mass transfer coefficient, $cm\ s^{-1}$
k_s	First order surface reaction rate constant for char combustion, $cm\ s^{-1}$
k_t	Time constant, $m^{-1}\ s^{-1}$
K_{be}	Interphase mass transfer coefficient, s^{-1}
$K^*_{i\infty}$	Dispersed non-cluster flux of entrained particles in size i, $g\ cm^{-2}\ s^{-1}$
K^*_{ih}	Cluster flux of entrained particles in size i, $g\ cm^{-2}\ s^{-1}$
K^*_i	Total flux of entrained particles in size i, $g\ cm^{-2}\ s^{-1}$
I	Radiative intensity, $W\ m^{-2}\ sr$
L	Length, m or cm
L_m	Mean beam length, m
m	Mass flow rate, $g\ s^{-1}$; discrete direction,-
M	Molecular or atomic weight, $g\ mol^{-1}$; hold-up in the bed, g; total number of ordinates, -
M_t	Total weight of particles, kg
n	Index of the dimension; molar flow rate, $mol\ s^{-1}$; unit normal vector, -
$\boldsymbol{n}$	Unit normal vector, -
n_C	Carbon consumption rate, $mol\ cm^{-3}\ s^{-1}$
N	Order of approximation, -
$P(D_p)$	Differential weight distribution, -
$P(r)$	Size distribution function, cm^{-1}
Pr	Prandtl number, -
$P_z(r)$	Size distribution of entrained particles at any height z in freeboard, cm^{-1}
$\boldsymbol{q}$	Heat flux vector, $W\ m^{-2}$
Q	Volumetric flow rate, $cm^3\ s^{-1}$; energy generation/loss rate, $cal\ s^{-1}$
Q_a , Q_s	Absorbtion and scattering efficiencies, -
$\boldsymbol{r}$	Position vector, m

r	Position vector, *m*; spatial independent variable, *cm*;
r_C	Carbon consumption rate on the surface of char particle, $mol\ cm^{-2}\ s^{-1}$
r_{CO}	Rate of CO combustion, $mol\ cm^{-3}\ s^{-1}$
r_{SO_2}	Rate of sulfation reaction, $mol\ s^{-1}$
R	Energy generation/loss rate in freeboard, $cal\ cm^{-3}\ s^{-1}$
$\Re$	Species generation/depletion rate, $mol\ cm^{-3}\ s^{-1}$
$\Re(r)$	Shrinkage rate of char particles, $cm\ s^{-1}$
Re_p	Particle Reynolds number, -
s	Geometric path length, *m*
S	External sorbent surface area, cm^2
t	Time, *s*; pseudo-time variable, *s*
T	Temperature, *K*
TF	Final time of integration, *s*
TP	Print interval, *s*
u_o	Superficial velocity in the bed, $cm\ s^{-1}$
u_b	Superficial bubble phase velocity, $cm\ s^{-1}$
u_e	Superficial velocity in emulsion phase, $cm\ s^{-1}$
u_{mf}	Superficial minimum fluidization velocity, $cm\ s^{-1}$
u_t	Terminal velocity of the particles, $cm\ s^{-1}$
u_{tf}	Superficial throughflow velocity in bubbles, $m\ s^{-1}$
U	Overall heat transfer coefficient, $cal\ cm^{-2}\ s^{-1}\ K^{-1}$
U_f	Unit filter function
v	Volatiles released, *%*
v_∞	Ultimate yield of volatiles released, *%*
V	Volume, cm^3
$V_p\ (D_p)$	Volume of particle of diameter, D_p, m^3
w_m	Quadrature weight of ordinate, *m*
W	Width of the enclosure, *m*
x	Mass fraction, -; spatial independent variable, *cm*; size parameter -
x_{vl}	Fraction of volatiles released in the bed

y	Mole fraction
z	Spatial independent variable, *cm*

Greek Letters

α	Thermal diffusivity, $cm^2\ s^{-1}$
β	Extinction coefficient
δ	Bubble phase volume fraction
ε	Voidage; emissivity; convergence criterion
ε_f	Voidage at fluidization conditions
ε_{mf}	Voidage at minimum fluidization conditions
ε_s	Solids volume fraction
η	Contact efficiency; direction cosine
θ	Polar angle, *rad*
Θ	Scattering angle, ^{o} or *rad*
κ	Absorption coefficient
λ^0	Latent heat of vaporization at standard state, $cal\ g^{-1}$
μ	Direction cosine, viscosity, $g\ cm^{-1}\ s^{-1}$
ξ	Direction cosine
ρ	Density, $g\ cm^{-3}$
σ	Standard deviation of activation energy distribution, $J\ mol^{-1}$; stephan-boltzmann constant, $cal\ cm^{-2}\ s^{-1}\ K^{-4}$; fractional sorbent surface area
σ_s	Scattering coefficient
τ	Optical thickness, Residence time, s^{-1}
ϕ	Azimuthal angle, *rad*; sphericity
Φ	Scattering phase function, sr^{-1}
ω	Single scattering albedo
Ω	Direction of radiation intensity

$d\Omega$	Solid angle, *sr*
Ω_m	Ordinate direction

Subscripts

32	Surface/volume mean
a	Air; ash; attrition
av	Size averaged property
avg	Average
b	Bubble; blackbody
bd	Bed drain
bed	Bed
bw	Bed wall
c	Combustion
C	Carbon
co	Carryover
cw	Cooling water
d	Char
e	Emulsion
elut	Elutriation
f	Freeboard; fine; feed coal
fc	Fixed carbon
fw	Freeboard wall
g	Gas
H	Hydrogen
i	Inert; inner
inc	Incident
j	Species index
lst	Limestone
m	Outgoing ordinate direction

m'	Incoming ordinate direction
max	Maximum
maxe	Maximum elutriated
min	Minimum
o	Feed; outer; at the bed surface; initial
p	Particle
r	Radiation; reference
recy	Recycle
rxn	Reaction
S	Sulfur
s	Surface; solid
T	Tube
vm	Volatile matter
w	Wall; water
'	Incoming

Abbreviations

ABFBC	Atmospheric Bubbling Fluidized Bed Combustor
ABFBB	Atmospheric Bubbling Fluidized Bed Boiler
AFBC	Atmospheric Fluidized Bed Combustor
DOM	Discrete ordinate Method
FBC	Fluidized Bed Combustion
MOL	Method of Lines
OHTC	Overall Heat Transfer Coefficient
RTE	Radiative Transfer Equation
SFBB	Stationary Fluidized Bed Boiler

CHAPTER 1

INTRODUCTION

Applications of fluidized bed combustion technology developed for burning coal with high efficiency and within acceptable levels of gaseous pollutant emissions have been steadily increasing in both capacity and number over the past decade. However, mathematical models are required for, (i) confirmation of design parameters of new units in order to alleviate long delays during start-up and initial operation of these units, (ii) investigation of the effect of any change in operation conditions or fuel composition on the performance of the existing units. In order to satisfy these requirements, extensive research on mathematical modeling of fluidized bed combustion systems has been carried out in the last three decades. These studies have mainly focused on heat transfer in the bed section since this region is the dominant source where heat of combustion is liberated. However, it was found that the contribution of freeboard region to total heat transfer in fluidized bed combustors (FBCs) was of comparable magnitude compared to that of the bed region and the major effect on freeboard heat transfer was from radiation of gases and particles [1-3]. Moreover, the efficiency of fluidized bed combustor depends upon the heat recovered in the freeboard region where the dominant mode of heat transfer is radiation.

In literature, radiation in the freeboard of FBCs was taken into consideration by two different approaches: (i) incorporating particle to gas heat exchange through Stefan-Boltzmann law in freeboard energy balance of the system model, (ii) using a radiation

model in isolation from system model for calculation of radiative heat exchange once temperature and concentration profiles are available from either measurements or the system model. Using Stefan-Boltzmann law is a very poor approach to model the radiative heat transfer in absorbing, emitting and scattering freeboard medium. On the other hand, utilizing a radiation model in isolation from a system model requires significant amount of input data obtained from experiments or predictions of a system model. Although experimental investigations, providing useful information regarding the thermal radiation in the freeboard of fluidized bed combustors, are the most reliable way, they are most of the time limited due to their costly setup and relative inconvenience to parametric study. Therefore, accurate treatment of radiative heat transfer can be achieved by the coupled solution of conservation equations for energy and chemical species together with the Radiative Transfer Equation (RTE). There is no study available to date that follows this approach.

Therefore, the principal objective of the present study has been the incorporation of a radiation model of the freeboard region previously developed and tested in isolation from the system model [4] into formerly developed comprehensive system model, originally proposed by Selçuk and Sivrioğlu [5] and later improved, extended and validated against experimental data by Selçuk and her colleagues [6, 7]. To achieve this goal, the main tasks undertaken were as follows:

- incorporation of the radiation model of the freeboard region into a system model of fluidized bed combustion,
- validation of the coupled model by comparing its predictions with experimental data,
- investigation of significance of coupling of the radiation model to the system model,
- determination of performance of the radiation model in an industrial boiler.

CHAPTER 2

LITERATURE SURVEY

2.1. System Models on Fluidized Bed Combustors

In the last three decades, extensive research on mathematical modeling of atmospheric bubbling fluidized bed combustors (ABFBC) has been carried out. Table 2.1 is arranged to give an insight into these models. Table 2.2 describes the nomenclature of Table 2.1.

The system models are compared on the basis of sub-models utilized for bed hydrodynamics, combustion, coal develotilization, SO_2 capture, NO_x formation and reduction, freeboard and radiative heat transfer in freeboard. Models are also compared with respect to the presence of validation against measurements.

Table 2.1: Summary of models on fluidized bed coal combustors.

Author(s)	Year	A	B	C	D	E	F	G	H	I	J	K
Becker et al. [8]	1975	2c	1	2	1,2,4,5	1,2b	1	3	3	3	2	No
Gordon and Amundson [9]	1976	2a	3	2	1,4	6	1,2	3	3	3	2	Yes
Chen and Saxena [10]	1977	3	1	1	1,4,5	6	1	2	3	3	2	Yes
Horio and Wen [11]	1978	2c	2	1	1,4,5	6	3	3	3	3	2	Yes
Sarofim and Beer [12]	1978	2a	3	2	1,2,4,5	4	1	3	1	1	2	Yes
Saxena et al. [13]	1978	3	1	1	1,4,5	6	1	3	3	3	2	No
Gordon et al. [14]	1978	2a	3	2	1,4	6	2	3	3	3	2	No
Beer et al. [15]	1978	2a	3	2	1,2,4	1,4	3	3	3	3	2	Yes
Fan et al. [16]	1979	2a	3	3	1,4	6	1	3	3	3	2	No
Rajan and Wen [17]	1980	2c	2	1	1,2,3,4,5	3	3	1	2	2	2	Yes
Congalidis and Georgakis [18]	1981	2c	3	2	1,2,3,4,5	1	2	3	3	3	2	No
Chakraborty and Howard [19]	1981	1	1	1	1,4	6	2,3	3	3	3	2	Yes
Park et al. [20]	1981	1	1	1	1,2,4,5	2a	3	3	3	1	2	No
Bukur and Amundson [21]	1982	2a	3	2	1,4	6	1	3	3	3	2	Yes
Chang et al. [22]	1982	2a	3	2	1,4	6	1	3	3	3	2	No

Table 2.1: Summary of models on fluidized bed coal combustors (continued).

Author(s)	Year	A	B	C	D	E	F	G	H	I	J	K
Chen and Wen [23]	1982	-	-	-	1,2,4,5	3	3	1	2	2	1	Yes
Overturf and Reklaitis [24]	1983	2c	3	2	1,2,4,5	1	3	3	3	1	2	Yes
Walsh et al. [25]	1984	-	-	-	1,3,4,5	6	2,3	3	3	1	2	Yes
Preto [26]	1986	2c	1	1	1,2,3,4,5	1,3	3	2	2	2	2	Yes
Dixit et al. [27]	1986	-	-	-	1,4,5	6	-	3	3	1	1	Yes
Lemcoff [28]	1988	2a	1	2	1,4	6	3	3	3	2	2	Yes
Brem [29]	1988	2c	1	1	1,2,3,4,5	1,3	3	1	1	2	2	Yes
Ho et al. [30]	1989	2a	3	2	1,4,5	6	1	3	3	3	2	No
de Souza-Santos [31]	1989	2a	1	2	1,2,4,5	1	3	2	2	1	1	Yes
Trevino et al. [32]	1990	2a	3	2	1,4	6	1	3	3	3	2	No
Adanez et al. [33]	1991	2a	1	2	1,2,4,5	1,2	3	3	3	1	2	Yes
Lin et al. [34]	1993	1	2	1	1,2,4	1	1	1	1	3	2	Yes
Goel et al. [35]	1995	2a	1	2	1,2,4	2b	3	3	1	1	2	Yes
Sriramulu et al. [36]	1996	3	1	1	1,4	6	3	3	3	3	2	Yes
Reddy and Sinha [37]	1997	3	1	1	1,4	6	3	3	3	3	2	Yes

Table 2.1: Summary of models on fluidized bed coal combustors (continued).

Author(s)	Year	A	B	C	D	E	F	G	H	I	J	K
Huilin et al. [38]	1999	3	1	1	1,4	6	3	2	3	3	2	No
Kulesekaran et al. [39]	1999	3	1	1	1,4	6	3	3	3	1	2	Yes
Ilic et al. [40]	1999	3	1	1	1,4	6	3	3	3	3	2	Yes
Mançuhan [41]	1999	2c	2	1	1,2,4,5	2	1	3	3	2	2	Yes
Değirmenci [42]	2000	2b	3	2	1,2,3,4,5	1,4,5	4	3	3	1	1	Yes
Chen et al. [43]	2001	3	1	1	1,2,4	2b	3	3	1	1	2	Yes
Altındağ [44]	2004	2b	3	2	1,2,3,4,5	1,4,5	4	1	3	1	1	Yes
Afacan [45]	2005	2b	3	2	1,2,3,4,5	1,4,5	4	1	1	1	1	Yes

Table 2.2: Nomenclature for Table 2.1.

A. Fluidized Bed Model

1. One phase model; slow bubble regime; no distinction between the bubble and emulsion phases.
2. Two phase model; bubble phase and emulsion phase;
    a. bubble with cloud; bubble size dependent on bed height; gas exchange between bubble and emulsion phases axially distributed,
    b. bubble without cloud; average bubble size; average gas exchange coefficient,
    c. compartments in series model; 2 phases in each compartment.
3. Three phase model; bubble, cloud-wake and emulsion phase; bubble size dependent on bed height; gas exchange between phases based on average bubble volume.

B. Gas Flow Pattern in the Bed

1. Plug flow in all phases.
2. Mixed flow in all phases.
3. Plug flow in bubble phase; well mixed in emulsion phase.

C. Mixing of Solids in the Bed

1. Well mixed.
2. Well mixed in the emulsion phase.
3. Finite dispersion of solids.

D. Stages of Combustion

1. Heating and drying.
2. Devolatilization and volatiles combustion.
3. Attrition.
4. Char combustion.
5. Elutriation.

Table 2.2: Nomenclature for Table 2.1 (continued).

E. Devolatilization Pattern of Feed Coal

1. Uniform in the dense bed.
2. Instantaneous release
    a. at the feed point,
    b. at the bottom of the bed (grid section).
3. Volatiles release rate related to solids mixing rate.
4. Devolatilization kinetics.
5. Particle-movement model.
6. Not considered.

F. Kinetics of Coal Combustion

1. Diffusionally controlled.
2. Rate of CO oxidation is comparable to that of other chemical reactions.
3. Both kinetically and diffusionally controlled but oxidation of CO to CO_2 in bubble phase is assumed to be very fast.
4. Both kinetically and diffusionally controlled but oxidation of CO to CO_2 in bubble and emulsion phases is kinetically controlled.

G. SO_2 capture

1. Desulphurization model.
2. Semi-empirical sulfur dioxide capture kinetic equation.
3. Not considered.

H. NO_x formation and reduction

1. NO_x formation and reduction model.
2. Semi-empirical NO_x formation and reduction kinetic equations.
3. Not considered.

Table 2.2: Nomenclature for Table 2.1 (continued).

I. Freeboard Model

1. Plug flow gas phase with solids dispersed in it.
2. Mixed flow gas phase with solids dispersed in it.
3. Not considered.

J. Radiative Heat Transfer in Freeboard

1. Particle to gas heat exchange through Stefan-Boltzmann law.
2. Not considered.

K. Validation

Model validated against experimental measurements: Yes/No.

As can be seen from Table 2.1, bed hydrodynamics is based on one, two or three phase theory. Chakraborty and Howard [19], Park et al. [20] and Lin et al. [34] simply defined the bed region by one phase model, where no distinction between gas and solid phases is made. On the other hand, in most of the system models, bubbling bed hydrodynamics was described by two phase theory in which bed is assumed to consist of two phases; bubble and emulsion phase. Bubble phase is solids-free gas phase in plug flow and emulsion phase is well-mixed solid laden gas mixture. Modifications were made to several two phase fluidized bed models to represent the gas and solid motion [8, 9, 11, 12, 14-18, 21, 22, 24, 26, 28-33, 35, 41, 42, 44, 45]. Modeling of hydrodynamics was further improved by utilizing three phase theory. In this theory, in addition to bubble and emulsion phases, cloud-wake phase at minimum fluidization condition, where gas in the cloud region is well mixed with respect to gas in the wake region and solid particles are well mixed with respect to solids in emulsion phase, exists [10, 13, 36-40, 43]. Due to its complex description of bed hydrodynamics, application of the three phase model has been limited.

In most of the previous studies, only heating and drying and coal combustion were taken into account as the stages of combustion [9, 14, 16, 19, 21, 22, 28, 32, 36-40]. In order to obtain more realistic predictions, researchers also included devolatilization and volatiles combustion, attrition and elutriation into their system models [17, 18, 26, 29, 42, 44, 45].

The comprehensive models treated devolatilization pattern of coal by five different approaches: uniform, instantaneous, proportional release, devolatilization kinetics and particle movement model. Uniform and instantaneous volatiles release are the most common assumptions during devolatilization [8, 18, 20, 24, 31, 33-35, 41, 43]. In the models of Rajan and Wen [17], Chen and Wen [23], Preto [26] and Brem [29] devolatilization time was evaluated with respect to mixing rate of solid particles. Sarofim and Beer [12] and Beer et al. [15] took into consideration volatiles release pattern by devolatilization kinetics. Finally, in the system models of Selçuk and her colleagues [42, 44, 45], particle movement model combined with devolatilization kinetics.

In early studies, it was assumed that the external gas diffusion is the only rate controlling step and no homogenous reaction of CO oxidation takes place in the bed [8, 10, 12, 13, 16, 21, 22, 30, 32, 34, 41]. Saxena et al.[13], Lemcoff [28] and Lin et al. [34] included also ash diffusion resistance. Gordon and Amundson [9], Gordon et al. [14], Congalidis and Georgakis [18], Chakraborty and Howard [19] and Walsh et al. [25] indicated that CO oxidation was comparable to that of other chemical reactions. In several studies, coal combustion was taken to be both kinetically and diffusionally controlled but oxidation of CO to CO_2 in bubble phase was assumed to be very fast [11, 15, 17, 19, 20, 23-26, 28, 29, 31, 33, 35-40, 43]. Recently, Selçuk and her coworkers [42, 44, 45] improved this approach by introducing kinetically controlled oxidation of CO to CO_2 in both bubble and emulsion phases.

In the last two decades, the requirement to control sulfur dioxide (SO_2) and nitrogen oxides (NO_x) emissions when burning fossil fuels have led researchers to pay attention to the processes of SO_2 capture and NO_x reduction. SO_2 is released from combustion of char and volatiles and captured by sorbent particles such as limestone or dolomite. Due to relatively low combustion temperatures of fluidized beds (~ 1123 K), the major source of nitrogen is originated from coal. Coal decomposes into first char nitrogen and volatile nitrogen and then undergoes NO_x formation and reduction reactions. Since these processes are very complex, only Brem [29], Lin [34] and Afacan [45] included both sulfur retention and NO_x formation and reduction via comprehensive sub-models.

The dilute zone above the fluidized bed combustor is defined as freeboard region. The solids thrown up into the freeboard contain the whole spectrum of particle sizes present in the bed. Among these particles, small ones pass through the freeboard region whereas large ones turn back to bed region. Thus, the solid hold-up in the freeboard changes with height. Particle hold-up in this region not only affects NO_x reduction, SO_2 capture and CO emission but also contributes to physical phenomena such as heat transfer. Despite the importance of these physical and chemical phenomena, few researchers included a freeboard model in their system models [12, 17, 20, 23-29, 31, 33, 35, 39, 41-45].

Heat transfer is one of the important components of the system model. Among other modes of heat transfer, radiative heat transfer in coal firing systems becomes significant due to the presence of particle laden combustion gases at high operating temperatures. Most of the studies have mainly focused on heat transfer in the bed section. However, it was found that the contribution of freeboard region to total heat transfer in fluidized bed combustors was of comparable magnitude compared to that of the bed region and the major effect on freeboard heat transfer was from radiation of gases and particles [1-3]. Therefore, in modeling such systems, contribution of radiation to total heat transfer in freeboard section cannot be ignored. To date, radiative heat transfer in system models [23, 27, 31, 42, 44, 45] has been taken into account only

by a simple treatment which is the incorporation of particle to gas heat exchange through Stefan-Boltzmann law into the energy conservation equations.

In summary, among the aforementioned system models, the most comprehensive model was developed by Selçuk and her co-workers [42, 44, 45]. The model is based on modified two phase bed model and plug flow gas phase freeboard model and it accounts for volatiles release and combustion, char particles combustion and size distribution, attrition, elutriation, sulfur retention, nitrogen dioxides formation and reduction, heat transfer, and thermal radiation in bed and freeboard region by using Stefan-Boltzmann law in energy conservation equation. The predictive performance of this model was tested by comparing the model predictions with measurements obtained from the combustion tests carried out by burning indigenous lignites in METU 0.3 MW_t Atmospheric Bubbling Fluidized Bed Combustor (ABFBC). The predictive ability, flexibility in the incorporation of various sub-models and the computational efficiency of this code makes it a promising tool for the evaluation of performance of industrial fluidized bed boilers. This model can further be improved by incorporation of a radiation model into the existing model and solving conservation equations for mass, momentum, energy, species and radiant energy simultaneously in the freeboard region of combustor. All the radiation models published in the literature were developed in isolation from the system model. A review of these radiation models is given in the following section.

2.2. Modeling of Radiation in Freeboard of Fluidized Bed Combustors

The lean phase of a fluidized bed combustor above the bed region is defined as freeboard region. The solid particles in varying sizes are transported from bed surface to freeboard of combustor by means of fluidizing gas. Among the entrained particles, fines are carried out of bed while coarse particles fall back to the bed. As coal particles burn away, they decrease in size until they are small enough to be carried out of the

combustor. These unburnt particles significantly affect the combustion efficiency. This efficiency can be improved by recycling the elutriated particles back to the combustor. However, once they return to the bed, small particles percolate through the larger bed material simply to be elutriated again to the freeboard. For this reason, it is essential to extract as much heat as possible from the off-gases and their associated fine materials [46]. Therefore, the efficiency of fluidized bed combustion depends upon the amount of heat recovered in the freeboard region where the predominant mode of heat transfer is radiation.

Modeling of radiative heat transfer in the freeboard of fluidized bed combustors requires the accurate knowledge of radiative properties of solid laden combustion gases because major contribution to thermal radiation is from emittance of participating combustion gases and fly ash particles. For this reason, it is necessary to obtain data on freeboard temperature and gas composition in addition to concentration, composition and size distribution of solid particles collected at the freeboard outlet. Once the required information is collected, gas to wall and wall to wall radiative heat exchanges can be readily calculated.

In literature, radiation models for the freeboard of FBCs were treated in isolation from the system model for calculation of radiative heat exchange once temperature and concentration profiles are available from either measurements or a system model. Only few studies exist on the investigation of thermal radiation in the freeboard section and they are summarized in Table 2.3.

Table 2.3: Freeboard radiation models treated in isolation from system models.

Author (Year)	System	Medium*	Method	Work carried out	Validation
Andersson [47] (1988)	Freeboard of a 16 MW_t ABFBB	G,A,E	Single zone method	Prediction of heat fluxes on water-cooled freeboard walls	Against measurements
Filla et al. [3, 48] (1996)	Freeboard of a 1 MW_t ABFBC	G,A,E,S	Discrete ordinate flux method	Prediction of radiative properties of particle cloud in the freeboard	No validation
Kozan and Selçuk [49] (2000)	Freeboard of a 0.3 MW_t ABFBC	G,A,E,S	Well-stirred enclosure model with RIM	Prediction of radiative heat fluxes on refractory-lined freeboard walls	Against measurements
Batu and Selçuk [50] (2001)	Freeboard of a 0.3 MW_t ABFBC	G,A,E,S	Zone method	Prediction of radiative heat fluxes on refractory-lined freeboard walls	Against measurements
Selçuk et al. [4, 51] (2005)	Freeboard of a 0.3 MW_t ABFBC	G,A,E,S	MOL solution of DOM	Prediction of radiative heat fluxes on refractory-lined freeboard walls	Against predictions of zone method and measurements

* G: Gray, A: Absorbing, E: Emitting, S: Scattering

The first model on radiative heat transfer in the freeboard of fluidized bed was developed by Andersson [47]. The physical system under consideration was the freeboard of 16 MW_t atmospheric stationary fluidized bed boiler (SFBB) located at Chalmers University of Technology, Sweden. This boiler was used to burn coal in the bed of silica sand. In the model, the freeboard was assumed to be well-stirred enclosure containing gray, absorbing and emitting medium with constant temperature and concentration obtained from measurements. The enclosure was bounded by water-cooled gray and diffuse walls. Calculated total heat flux to the side walls was a result of the convective and radiative heat exchange between the particle laden gas, the splashing bed surface and the water-cooled freeboard walls. In the model, gas convection was evaluated according to conventional relationships. For radiative heat exchange, single zone method was applied in the freeboard of the boiler. However, the contribution of scattering and particle convection to total heat flux was neglected. The predictions of total heat flux to the side walls of freeboard were compared with the measurements. Due to the single zone treatment of freeboard and no consideration of particles in participating medium, only reasonably good agreement was achieved.

In the model of Filla et al. [3, 48], the virtues of particle scattering on radiation in freeboard of the 1 MW_t FBC, burning coal in a bed of sand particles with and without limestone addition, were investigated. The effect of scattering on total heat transfer to the walls of freeboard was studied by physical and chemical characterization of solid particles collected at the freeboard exit. Particle cloud was assumed to consist of char and fly ash together with sand particles formed due to comminution of the inert bed material. Freeboard medium was assumed to be gray, absorbing, emitting and scattering. Mie theory was applied to calculate the absorption and scattering coefficients of solid particles. The emissivity of particle cloud was determined as a function of absorption thickness and effective albedo by using discrete ordinate flux method. Significant effect of scattering on the transmissivity of particle cloud in the freeboard was observed. The shortcoming of this study is that it only provides a parametric study on the effect of radiative properties of the particles on the emissivity

of the particle laden flue gases. It does involve neither measurements nor predictions of radiative heat flux on the walls and also does not include the effect of flue gases on medium radiative properties.

Radiative heat exchange in the freeboard of METU 0.3 MW_t ABFBC Test Rig burning lignite in its own ash was modeled by Kozan and Selçuk [49], Batu and Selçuk [50] and Selçuk et al. [4, 51]. In all three studies, freeboard region was considered as a 3-D rectangular enclosure containing gray, absorbing, emitting and scattering medium. The radiative properties of the medium were based on experimental measurements of freeboard temperature and gas composition in addition to concentration, composition and size distribution of solid particles collected at the freeboard outlet. For property estimation, gas mixture was assumed to consist of only carbon dioxide and water vapor while particle cloud was treated as pure ash according to the chemical analysis of the fly ash particles. Leckner's correlations [52] were used to determine gas absorption coefficient and Mie theory [53] was employed to evaluate absorption and scattering coefficients of solid particles. Utilizing three different radiation models, the authors predicted radiative heat exchange in the freeboard of fluidized bed combustor and validated their results against incident radiative heat fluxes measured by a radiometer probe on the refractory-lined freeboard walls.

In the model of Kozan and Selçuk [49], radiative heat flux incident on the refractory-lined freeboard walls were calculated by using a well-stirred freeboard model in conjunction with radiosity irradiation model (RIM). Freeboard was considered to have three surfaces which are top, bottom and side surfaces. Radiosity equation was written for each surface and simultaneously solved for radiative heat fluxes leaving the surfaces. The incident radiative heat fluxes were then obtained by using the calculated radiosities at each surface. Significant discrepancies between the predicted and measured incident radiative heat fluxes were observed. This was considered to be due to the single zone treatment of freeboard, where a constant and uniform incident

radiative heat flux is used to represent the relatively steep variation of measured profile along the freeboard walls.

Batu and Selçuk [50] utilized the zone method proposed by Hottel and Cohen [54] to analyze the radiative heat exchange in the freeboard of fluidized bed combustor. In this model, freeboard was subdivided into isothermal 10 volume and 12 surface zones and each zone was assumed to be well mixed with uniform properties. For the zones, incident radiative heat flux equations were solved simultaneously by using Gauss-Jordan elimination method. Between any pair of zones, direct numerical integration technique was applied to multiple integrals which define the direct exchange areas between any pair of zones [55]. The predictions of incident radiative heat fluxes reproduced measurements reasonably well. It was found that the presence of particles in the participating medium does not affect the magnitude of the predicted incident fluxes significantly due firstly to low particle load in the freeboards of bubbling fluidized bed combustors and secondly to the compensation of higher extinction by higher emissivity caused by the particles.

Recently, Selçuk et al. [4, 51] used Method of Lines solution of Discrete Ordinate Method (MOL solution of DOM), which has been shown to be an accurate method upon its assessment on idealized test problems with participating media [56-58], to predict radiative fluxes in the freeboard of the fluidized bed combustor. DOM is applied to radiative transfer equation for angular domain discretization resulting in system of partial differential equations (PDEs). Further application of false transients method makes this system suitable for MOL solution by incorporating initial value variable. After spatial discretization by Taylor series expansion, the result is an initial value problem governed by ordinary differential equations (ODEs). Once the radiation intensity distribution in the enclosure is evaluated by using the RTE together with its boundary conditions, incident radiative heat flux on side walls are readily calculated. Predictive accuracy of the model was assessed by comparing its predictions with those of the zone method [4] and measurements [4, 51]. MOL solution of DOM was found to

be as accurate as zone method and much faster for lightly scattering media. Parametric studies were carried out to analyze the sensitivity of predicted heat flux profiles to the presence of particles, particle load and anisotropic scattering. Conclusions drawn from the parametric studies were: (i) presence of particles in the participating medium did not affect the magnitude of predicted incident fluxes significantly due to low particle load in the freeboards of bubbling fluidized bed combustors, (ii) increasing the particle load to the order of magnitude typically encountered in circulating FBCs led to significant rise in incident radiative heat fluxes at the wall, (iii) effect of anisotropy on incident radiative heat fluxes on the side walls was negligible even in the presence of high particle loads. The effect of recycle on radiative heat transfer in the freeboard of fluidized bed combustor was also studied [51]. Comparisons between radiative heat fluxes with and without recycle revealed that recycle significantly enhances radiative fluxes due to higher freeboard temperatures caused by recycling particles. It was concluded that MOL solution of DOM provides both accurate and computationally efficient solutions for prediction of radiative heat fluxes and can be used with confidence in conjunction with FBC system models.

CHAPTER 3

ABFBC SYSTEM MODEL

3.1. General

A system model on fluidized bed combustion, originally proposed by Selçuk and Sivrioğlu [5] and later extended and validated against experimental data by Selçuk and her colleagues [6, 7], was chosen as a basis for incorporation of a radiation model, based on method of lines solution of discrete ordinate method (MOL solution of DOM), for the freeboard region which was developed and tested in isolation from the system model previously [4]. The system model was developed on the basis of first principles and used to correlate data from METU 0.3 MW_t ABFBC Test Rig. The model in its present form accounts for bed and freeboard hydrodynamics, volatiles release and combustion, char particles combustion and size distribution, attrition, elutriation, sulfur retention and heat transfer. In this study, radiative transfer equation is solved simultaneously with the conservation equations for mass, momentum, energy and species compared to original system model where radiation was taken into account by incorporation of particle to gas heat exchange through Stefan-Boltzmann law.

The behavior of the fluidized bed combustor under consideration is described by a model based on conservation equations for energy and chemical species in conservative form for both bed and freeboard sections. The assumptions involved are illustrated in Figure 3.1 and Figure 3.2 for the bed and freeboard sections, respectively. The

correlations used in estimating important parameters in the model are listed in Table 3.1. Five chemical species, O_2, CO, CO_2, H_2O, and SO_2 are considered in the model.

Chemical reactions included in the model together with their rate expressions are given in Table 3.2. Details of the system model before incorporation of radiation model in the freeboard region can be found elsewhere [44]. However, for the sake of integrity, a brief summary of the system model will be provided in the following sections. Modifications required for the consideration of radiative heat exchange in the freeboard region will be explained in detail in the next chapter.

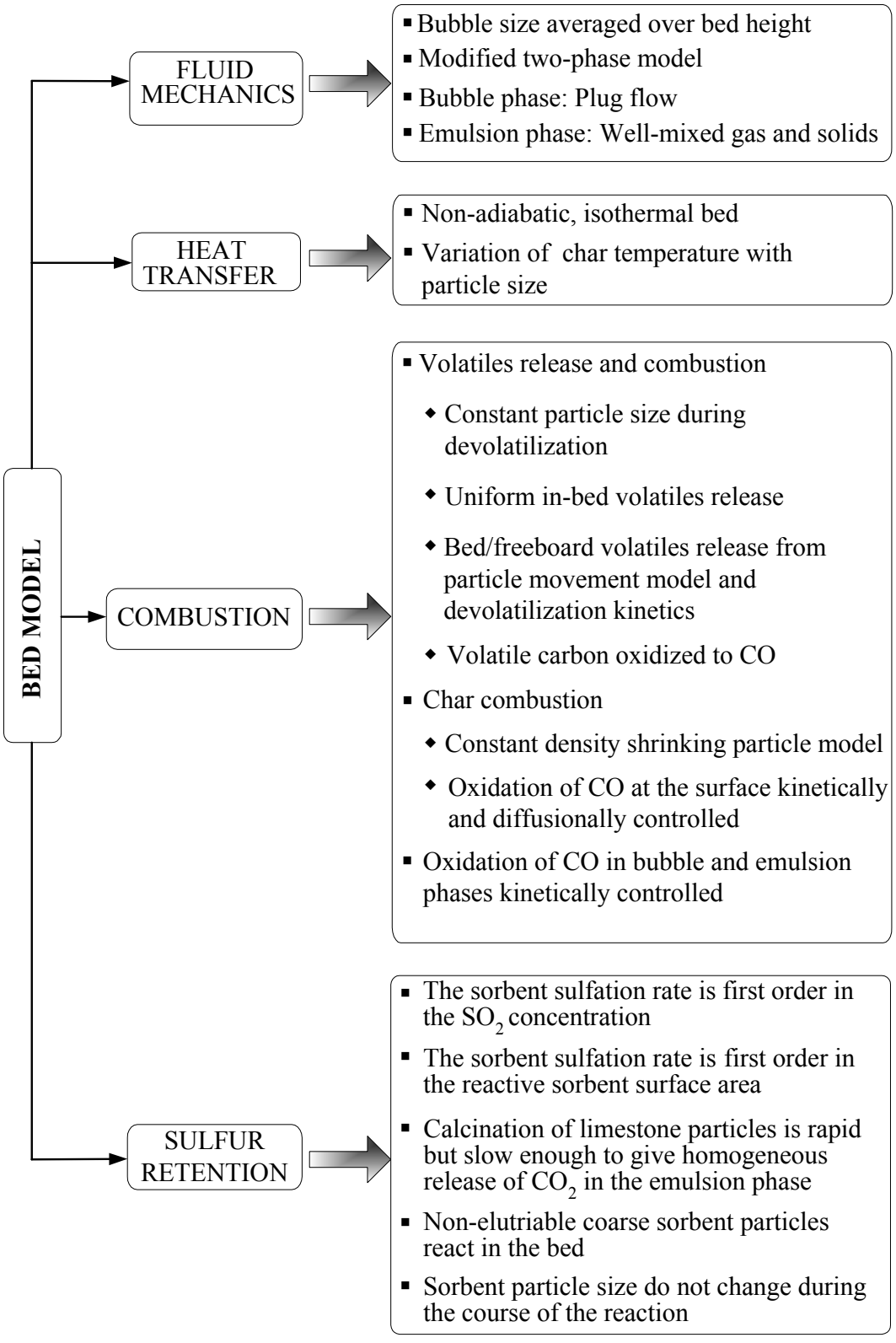

Figure 3.1: An overview of the steady state bed model assumptions.

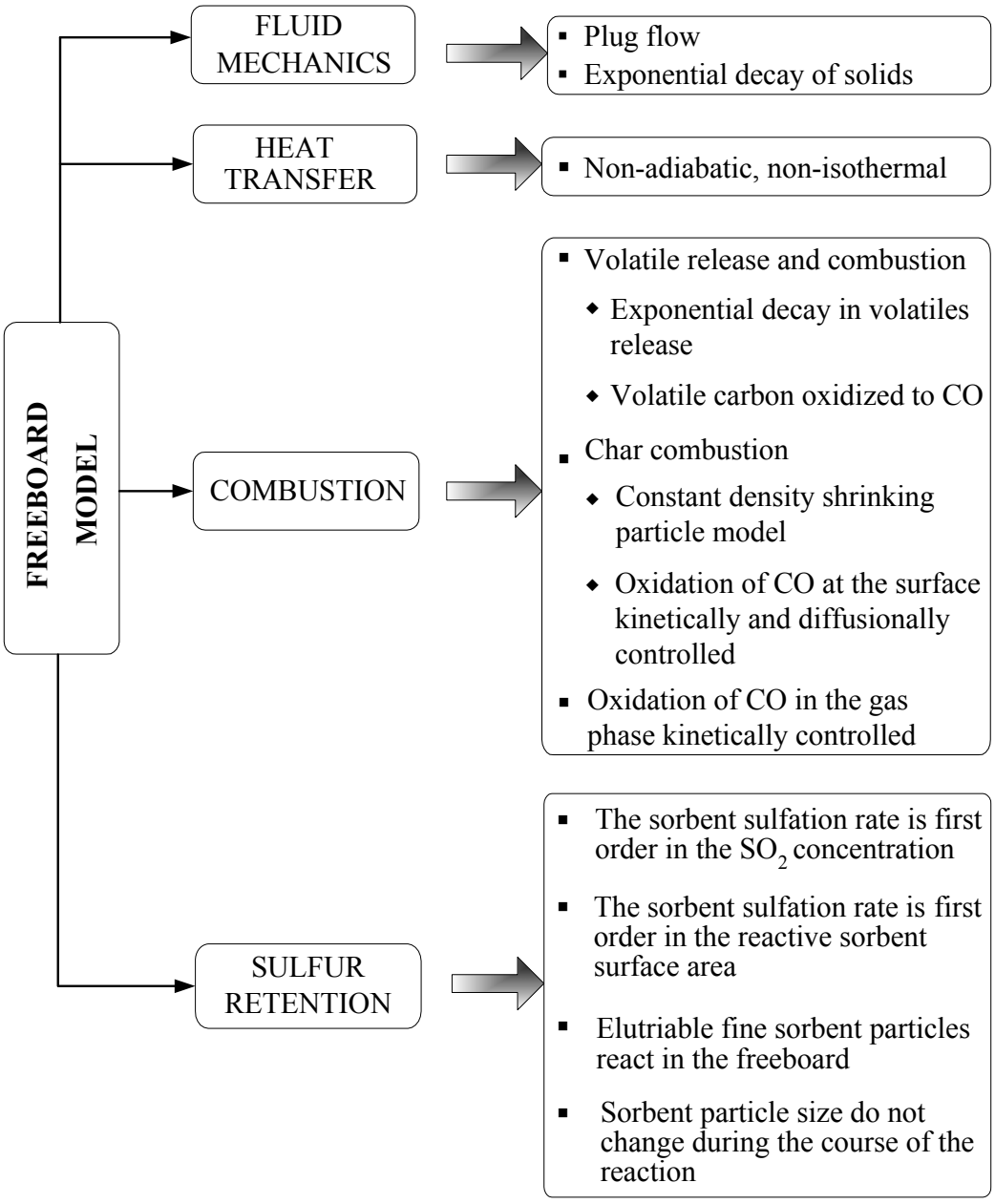

Figure 3.2: An overview of the steady state freeboard model assumptions.

Table 3.1: Correlations used in the model.

	Reference
Mass transfer to particles in the emulsion phase, k_f	[19]
Heat transfer to particles in the emulsion phase, h_p	[59]
Specific elutriation rate constant, $E(r)$	[60]
Terminal velocity of the particles, u_t	[61]
Bubble to emulsion mass transfer, K_{be}	[62]
Minimum fluidization velocity, u_{mf}	[63]
Bubble size, d_b	[64]
Emulsion phase velocity, u_e	[65]
Bubble phase volume fraction, δ	[65]
Convective heat transfer coefficient of bed wall, h_{bw}	[61]
Convective heat transfer coefficient of cooling tubes, h_{cw}	[66]
Convective heat transfer coefficient of cooling water, h_i	[67]
Exponential decay constant, a	[60]
Gas side heat transfer coefficient in freeboard, h_g	[59]

Table 3.2: Reactions and rate expressions.

#	Reaction	Place	Rate Expression	Unit	Ref.
R1	$C_s + 1/2O_2 \rightarrow CO$	char surface	$5.95\times10^{4} T_p \exp(-17967/T_p) C_{O_{2,s}}$	$mol\ cm^{-2}\ s^{-1}$	[68]
R2	$C + 1/2O_2 \rightarrow CO$	gas phase	Instantaneous		-
R3	$CO + 1/2O_2 \rightarrow CO_2$	gas phase	$3.0\times10^{10} T \exp(-8052/T_g) C_{0_2}^{0.3} C_{CO} C_{H_2O}^{0.5}$	$mol\ cm^{-3}\ s^{-1}$	[69]
R4	$H_2 + 1/2O_2 \rightarrow H_2O$	gas phase	Instantaneous		-
R5	$S + O_2 \rightarrow SO_2$	gas phase	Instantaneous		-
R6	$CaCO_3 \rightarrow CaO + CO_2$	sorbent surface	Instantaneous		-
R7	$CaO + SO_2 + 1/2O_2 \rightarrow CaSO_4$	sorbent surface	$14.9 C_{SO_2} S_o \sigma_{avg}$	$mol\ s^{-1}$	[7]

3.2. Bed Model

Bed model can be described in terms of bed hydrodynamics, volatiles release and combustion, char combustion, particle size distribution of bed char and bed char hold-up desulfurization and species and energy conservation equations.

3.2.1. Bed Hydrodynamics

Bed hydrodynamics is based on modified two-phase theory suggested by Grace and Clift [70],

$$u_o = \frac{Q_b}{A_{bed}} + u_{tf} + u_e(1-\delta) \tag{3.1}$$

where throughflow velocity, u_{tf}, can be expressed in terms of emulsion phase velocity, u_e, using modified n-type two-phase theory of Grace and Harrison [71],

$$u_{tf} = (n+1)u_e\delta \tag{3.2}$$

where $n = 2$ for three dimensional beds. Gas/solids in the emulsion phase and gas in the bubble phase are assumed to be well-stirred and in plug flow, respectively.

An improved expression for the emulsion phase velocity was suggested by Gogolek and Becker [65] for a bed of coarse particles,

$$u_e = \frac{u_{mf}}{1-1.5\delta^{2/3}} \tag{3.3}$$

where δ is found by the solution of following nonlinear equation,

$$\frac{u_o}{u_{mf}} - \frac{u_b}{u_{mf}}\delta - \frac{1+2\delta}{1-1.5\delta^{2/3}} = 0 \tag{3.4}$$

In Equation (3.4), the rise velocity of bubbles in the bubbling bed is obtained from Davidson and Harrison [72],

$$u_b = 0.711(gd_b)^{1/2} + u_o - u_{mf} \tag{3.5}$$

and minimum fluidization velocity can be obtained from Ergun equation [63],

$$\frac{1.75}{\varepsilon_{mf}^3 \phi_s}\left(\frac{d_p u_{mf} \rho_g}{\mu}\right)^2 + \frac{150(1-\varepsilon_{mf})}{\varepsilon_{mf}^3 \phi_s^2}\left(\frac{d_p u_{mf} \rho_g}{\mu}\right) = \frac{d_p^3 \rho_g (\rho_i - \rho_g) g}{\mu^2} \tag{3.6}$$

An integrated average mean bubble size found from bubble size expression proposed by Mori and Wen [64] is utilized in the sections unoccupied by the tube bank. In the portion of the bed occupied by the horizontal tube bank, bubble diameter was assumed to be equal to the horizontal clearance between the tubes.

Bubbles are assumed to be free of solids. The gas interchange coefficient between bubble and emulsion phases is defined as,

$$K_{be} = \frac{\begin{pmatrix} \textit{volume of gas going from bubbles} \\ \textit{to emulsion or from emulsion to bubbles} \end{pmatrix}}{(\textit{volume of bubbles in the bed})(\textit{time})} \tag{3.7}$$

In this thesis study, the following relationship was used for K_{be} [62],

$$K_{be} = 7.14\frac{u_e}{d_b} + 5.46\frac{D^{1/2}}{g^{1/4} d_b^{5/4}}\frac{\varepsilon_{mf}}{1+\varepsilon_{mf}} \tag{3.8}$$

This is a modified Davidson-Harrison [72] equation put forward to allow for the observation that bubbles in a real fluid move faster than was assumed in the original theory. In utilizing Equation (3.8) the second term is neglected since it is approximately two orders of magnitude smaller than the first term.

3.2.2. Volatiles Release and Combustion

Volatiles are assumed to be released uniformly in the emulsion phase. The amount released in bed is determined by using the volatiles release model of Stubington et al. [73], and to describe the devolatilization kinetics, the parallel independent reaction model of Anthony and Howard [74] is used. In the presence of radial temperature profile and with the assumption of evenly distributed volatile matter in the particle, total amount of volatile matter released with respect to time is given by,

$$\frac{v_{avg}}{v_{\infty}} = \frac{3}{R^3}\int_0^R \left[1 - \int_0^{\infty} exp\left(-\int_0^t k(E)dt \right) f(E)\,dE \right] r^2 dr \tag{3.9}$$

Devolatilization history of the particle yields the fraction of volatiles released in bed. The remaining volatiles release is assumed to decrease exponentially as a function of distance from the surface of bed. With regard to combustion of volatiles released, volatile carbon and hydrogen are assumed to burn instantaneously to carbon monoxide *(CO)* and water vapor *(H_2O)*, respectively. The oxidation of *CO* takes place in both bubble and emulsion phases according to the rate expression of Hottel et al. [69]. Further details of the volatiles release model can be found in [42].

3.2.3. Char Combustion

Char particles are assumed to burn only to *CO*, as it is the major product of char combustion for typical FBC temperatures. Using the shrinking particle model and taking film mass transfer and the kinetics resistance into consideration, the rate of carbon oxidation at the particle surface can be obtained as,

$$r_{C,e} = \frac{2}{1/k_f + 2/k_s}\bar{C}_{O_2,e} \tag{3.10}$$

Film mass transfer coefficient, k_f, is obtained from the equation suggested by Chakraborty and Howard [19]. Kinetics of combustion of char particles is assumed to be represented by equation of Field et al. [68]. Average emulsion phase oxygen (O_2) concentration is used to calculate combustion rate.

3.2.4. Char Particles Size Distribution

Since carbon consumption rate depends on the surface area provided by burning char particles, calculation of particle size distribution and hold-up of char particles is of fundamental importance in the prediction of behavior of ABFBCs.

In order to derive a population balance based on the mass fractions for shrinking char particles, the following assumptions are made:

1. Char particles enter the bed at a rate of F_o with size distribution of $P_o(r)$ which is expressed by Rosin-Rammler size distribution function.
2. As char particles are well-mixed, bed drain char size distribution represents the bed char size distribution,

$$P_{bd}(r) = P_{bed}(r) \tag{3.11}$$

3. The rate of elutriation of char particles of size r is directly proportional to their concentration in the bed, *i.e.*,

$$F_{co}P_{co}(r)dr = M_d P_{bed}(r)E(r)dr \tag{3.12}$$

   where $E(r)$ is the elutriation rate constant [60], M_d is the total mass of char in the bed and $P_b(r)$ is the size distribution of char particles in the bed.
4. Carryover char size distribution represents the recycle char size distribution, since both streams are elutriated from the bed,

$$P_{co}(r) = P_{recy} \tag{3.13}$$

5. Densities of char particles do not change during the burn-out.
6. Fragmentation of char particles is negligible since there is no noticeable fragmentation for particles having diameters less than 3 mm [75].
7. Char particles can be attrited until reaching the upper size limit of the fines, r_f, and then becomes a fine particle itself. Fines have a size distribution of $P_f(r)$. Fines generated by attrition are not attritable themselves.
8. Char particles are considered to shrink by combustion and attrition according to shrinking particle model at a rate of

$$\left(-\frac{dr}{dt}\right)=\left(-\frac{dr}{dt}\right)_c + U_f\left(r_{max}, r_f\right)\left(-\frac{dr}{dt}\right)_a \tag{3.14}$$

where U_f is unit filter function defined to differentiate particle size ranges attained due to both combustion and attrition and due to combustion only. A detailed discussion on definition of unit filter function can be found elsewhere [75].

The working form of the population balance is given in Equation (3.15). A detailed derivation of the following equation can be found elsewhere [44, 75].

$$\frac{dW(r)}{dr} = W(r)\left[\frac{F_{bd}}{M_d \Re(r)} + \left(1-\frac{F_{recy}}{F_{co}}\right)\frac{E(r)}{\Re(r)} + \frac{3}{r}\right] - F_o P_o(r) - U_f\left(r_f, 0\right) F_a P_f(r) \tag{3.15}$$

$W(r)$ is the dummy variable in which M_d, $P_{bed}(r)$ and shrinkage rate of char particles, $\Re(r)$, are combined,

$$W(r) = M_d P_{bed}(r)\Re(r) \tag{3.16}$$

where char particle shrinkage rate, $\Re(r)$, is expressed as,

$$\Re(r) = -\frac{dr}{dt} \tag{3.17}$$

Equation (3.15) is subjected to the following boundary condition,

$$\text{at } r = r_{max} \qquad W(r) = 0 \tag{3.18}$$

as the probability of having solid particles of size r_{max} in the bed, *i.e.,* P_{bed}, is practically zero, due to the shrinkage of maximum particle size in the bed. Once the solution for $W(r)$ becomes available, the bed char hold-up, M_d, bed char size distribution, $P_{bed}(r)$, carryover rate, F_{co}, and carryover char size distribution, $P_{co}(r)$, can be obtained by using Equations (3.12) and (3.16).

3.2.5. Desulfurization Model

It is assumed that desulfurization involves two consecutive steps, instantaneous calcination of limestone followed by sulfation reaction. The rate expression for the reaction between SO_2 and lime, reaction R7 in Table 3.2, was assumed to be first order in SO_2 concentration and proportional to the reactive external surface area of the particles [7].

The sorbent fed has a wide particle size distribution and it is assumed that particle size of sorbent does not change during reaction. Attrition of limestone particles is not considered. Therefore, for any particle with size r, the rate equation takes the following form,

$$r_{SO_2} = k C_{SO_2} S(t) \tag{3.19}$$

Overall sulfation rate constant, k, is a combination of film mass transfer limitations and sulfation kinetics. It was determined from fluidized bed combustion experiments in this study.

As sulfation continues, sulfation reaction rate decreases due to pore blocking of the $CaSO_4$ product. Therefore, the reactive external surface area, $S(t)$, is expressed in terms of fractional external surface area, $\sigma(t)$, and described by an exponential decay with time.

$$\frac{S(t)}{S_o} = \sigma(t) = exp\left[-\frac{6M_{CaCO_3}kC_{SO_2}}{x_{CaCO_3}\rho_{lst}d_p}t\right] \tag{3.20}$$

where total initial external surface area for spherical limestone particles, S_o, is expressed as,

$$S_o = \frac{6M_{lst}}{\rho_{lst}d_p} \tag{3.21}$$

In order to model sulfation reaction at steady state, it is necessary to assess an average fractional external surface area, σ_{avg}, which is calculated from the solids residence time distribution function, and the fractional external surface area as a function of time $\sigma(t)$,

$$\sigma_{avg} = \frac{1}{\left[1+\frac{6M_{CaCO_3}kC_{SO_2}}{x_{CaCO_3}\rho_{lst}d_p}\tau\right]}\left[1-exp\left(-\left\{\frac{1}{\tau}+\frac{6M_{CaCO_3}kC_{SO_2}}{x_{CaCO_3}\rho_{lst}d_p}\right\}\tau_{max}\right)\right] \tag{3.22}$$

Calculation of average fractional external surface area, σ_{avg}, and determination of residence time of sorbent particles, τ, are given in detail elsewhere [44].

Finally, rate of sulfation reaction becomes,

$$r_{SO_2} = k\,C_{SO_2}S_o\,\sigma_{avg} \tag{3.23}$$

and the total reaction rate can be calculated from the summation of the rates obtained at different sizes,

$$r_{SO_2} = \sum_{i=1}^{n} r_{SO_2,i} \tag{3.24}$$

3.2.6. Species Conservation Equations

Spatial variations of species concentrations are described by the conservation equations for chemical species in bubble and emulsion phases,

$$\frac{dn_{j,b}}{dz} = A_{bed}\delta\left[\Re_{j,b} + K_{be}(C_{j,e} - C_{j,b})\right] \tag{3.25}$$

$$n_{j,e}\,|_{z=0} - n_{j,e} + V_{bed}\delta\left[\frac{1-\delta}{\delta}\varepsilon_{mf}\,\Re_{j,e} - K_{be}(C_{j,e} - \bar{C}_{j,b})\right] = 0 \tag{3.26}$$

These equations are subject to the following boundary conditions,

$$\text{at } z = 0 \qquad n_{j,b} = y_{j,b}\frac{n_a}{1 + \dfrac{u_e}{u_b}\dfrac{1-\delta}{\delta}\varepsilon_{mf}} \tag{3.27}$$

$$\text{at } z = 0 \qquad n_{j,e} = y_{j,e}\frac{n_a}{1 + \dfrac{u_b}{u_e}\dfrac{\delta}{(1-\delta)\varepsilon_{mf}}} \tag{3.28}$$

The expressions for the species generation or depletion terms appearing in Equations (3.25) and (3.26), $\Re_{j,b}$ and $\Re_{j,e}$, take the following forms for each species considered,

j=1 (O_2)

$$\Re_{1,b} = -0.5r_{CO,b} \tag{3.29}$$

$$\begin{aligned}\Re_{1,e} = &-\frac{m_{vm}x_{vl}}{V_{bed}(1-\delta)\varepsilon_{mf}}\left\{0.5\frac{x_{C,vm}}{M_C} + 0.5\frac{x_{H,vm}}{M_{H_2}} + \frac{x_{S,vm}}{M_S} - \frac{x_{O,vm}}{M_{O_2}}\right\} \\ &- 0.5n_{C,e} - 0.5r_{CO,e} - \frac{0.5r_{SO_2,e}}{V_{bed}(1-\delta)\varepsilon_{mf}}\end{aligned} \tag{3.30}$$

j=2 (CO)

$$\Re_{2,b} = -r_{CO,b} \tag{3.31}$$

$$\Re_{2,e} = \frac{m_{vm} x_{vl}}{V_{bed}(1-\delta)\varepsilon_{mf}} \left\{ 0.5 \frac{x_{C,vm}}{M_C} \right\} + n_{C,e} - r_{CO,e} \tag{3.32}$$

j=3 (CO_2)

$$\Re_{3,b} = r_{CO,b} \tag{3.33}$$

$$\Re_{3,e} = r_{CO,e} + \frac{F_{lst} x_{CaCO_3}}{M_{CaCO_3} V_{bed}(1-\delta)\varepsilon_{mf}} \tag{3.34}$$

j=4 (H_2O)

$$\Re_{4,b} = 0 \tag{3.35}$$

$$\Re_{4,e} = \frac{1}{V_{bed}(1-\delta)\varepsilon_{mf}} \left\{ m_{vm} x_{vl} \frac{x_{H,vm}}{M_{H_2}} + m_f \frac{x_{H_2O}}{M_{H_2O}} \right\} \tag{3.36}$$

j=5 (SO_2)

$$\Re_{5,b} = 0 \tag{3.37}$$

$$\Re_{5,e} = \frac{1}{V_{bed}(1-\delta)\varepsilon_{mf}} \left\{ \frac{m_{vm} x_{vl} x_{S,vm}}{M_S} - r_{SO_2,e} \right\} \tag{3.38}$$

where,

$$n_{C,e} = \frac{3W_d}{V_{bed}(1-\delta)\varepsilon_{mf} M_C} \frac{x_{fc}}{x_{fc} + x_a} \int_{r_{\min}}^{r_{\max}} \frac{P_{bed}(r)}{r} \Re(r) dr \tag{3.39}$$

3.2.7. Energy Conservation Equations

Since the contribution of radiative heat transfer to total heat transfer in bed region is not significant compared to freeboard region, the radiative heat transfer in this section can be treated as a simple engineering approach, which is utilized in the original system model [44] by using Stefan-Boltzmann law in the following energy conservation equation.

On the assumption that the gas and the inert particles are at the same temperature and that the mass of combustion gases and char particles are negligible compared to the mass of inerts, a combined gas/solid phase energy balance can be written as,

$$\begin{aligned} & n_A \int_{T_r}^{T_A} c_{pA} dT - \alpha \frac{A_T}{L_T} \int_0^{L_T} U_{cw}(T_{bed} - T_{cw}) dx - A_{bw} h_{bw} (T_{bed} - T_{bw,s}) \\ & - m_{recy} c_{pi} \left(T_{bed} - T_{recy} \right) - m_{co} c_{pi} (T_{bed} - T_r) - m_{bd} c_{pi} (T_{bed} - T_r) \\ & - n_g \sum_{j=1}^{8} y_j \int_{T_r}^{T_{bed}} c_{pg,j} dT - m_f x_w \lambda^0 + Q_{rxn} + Q_p = 0 \end{aligned} \tag{3.40}$$

where enthalpy generated by chemical reactions, Q_{rxn}, and energy transferred from burning char particles, Q_p, are obtained from following equations,

$$\begin{aligned} Q_{rxn} = {} & m_f x_{vm} x_{vl} \left[\frac{x_{C,vm}}{M_C} \Delta H_{R2}^0 + \frac{x_{H,vm}}{M_{H_2}} \Delta H_{R4}^0 + \frac{x_{S,vm}}{M_S} \Delta H_{R5}^0 \right] - \frac{F_{lst} x_{CaCO_3}}{M_{CaCO_3}} \Delta H_{R6}^0 \\ & + A_{bed} \left\{ \Delta H_{R3}^0 \left[\varepsilon_{mf} (1-\delta) \int_0^{H_{bed}} r_{CO,e} dz + \delta \int_0^{H_{bed}} r_{CO,b} dz \right] + \frac{\Delta H_{R7}^0}{V_{bed} \varepsilon_{mf} (1-\delta)} \int_0^{H_{bed}} r_{SO_2,e} dz \right\} \end{aligned} \tag{3.41}$$

$$Q_p = \frac{3 M_d}{\rho_d} \int_{r_{min}}^{r_{max}} \left[h_p (T_d - T_{bed}) + \sigma \varepsilon (T_d^4 - T_{bed}^4) \right] \frac{dr}{r} \tag{3.42}$$

and particle temperature is calculated by solving an energy balance around the particle, which is assumed to have uniform temperature,

$$\frac{\rho_d}{M_C}\frac{x_{fc}}{x_{fc}+x_a}\Delta H^o_{R1}\Re(r)-\left[h_p\left(T_d-T_{bed}\right)+\sigma\varepsilon\left(T_d^4-T_{bed}^4\right)\right]=0 \tag{3.43}$$

Energy loss through the bed walls is taken into account by making a one-dimensional heat transfer analysis. For a combustor with square cross-section and wall thickness of L_{bw}, the temperature profile inside the wall of variable cross section is given by the following equation,

$$\frac{d^2T_{bw}}{dx^2}\left(x+A_{bed}^{0.5}/2\right)+\frac{dT_{bw}}{dx}=0 \tag{3.44}$$

Equation (3.44) is subject to the following boundary conditions,

$$at\ x=0 \qquad h_{bw}\left(T_{bed}-T_{bw}\right)=-k_{bw}\frac{dT_{bw}}{dx} \tag{3.45}$$

$$at\ x=L_{bw} \quad T_{bw}=T_{bw,o} \tag{3.46}$$

where the heat transfer coefficient, h_{bw}, is calculated by using semi-empirical correlation developed by Kuni and Levenspiel [61].

In order to account for the energy absorbed by the in-bed heat exchanger, a separate energy balance is performed on the cooling water. Neglecting the heat transfer resistance of the tubes, the spatial variation of the temperature of the cooling water is given by the following equation,

$$\frac{4m_{cw}}{\pi}\frac{dT_{cw}}{dx}-\frac{4d_{T,o}}{c_{pcw}}h_{cw}\left(T_{bed}-T_w\right)=0 \tag{3.47}$$

The overall bed to tube surface heat transfer coefficient, h_{cw}, consists of three modes; gas convective, particle convective and radiative heat transfer,

$$h_{cw}=h_g+h_p+h_r \tag{3.48}$$

In the model, gas convective, h_g, particle convective, h_p, heat transfer coefficients are calculated by adopting the correlations proposed by Denloyee and Botterill [66],

$$h_g = \frac{k_g}{d_p^{0.5}} 0.86 Ar^{0.39} \tag{3.49}$$

$$h_p = \frac{k_g}{d_p} 0.843 Ar^{0.15} \tag{3.50}$$

and radiative heat transfer coefficient by the following equation,

$$h_r = \varepsilon_{cw} \sigma \left(T_{bed} + T_w \right) \left(T_{bed}^{\ 2} + T_w^{\ 2} \right) \tag{3.51}$$

The inlet temperature of the cooling water is set as boundary condition to Equation (3.47). Surface temperature of tube wall, T_w, is calculated by solving a surface energy balance,

$$h_{cw} d_{T,o} \left(T_{bed} - T_w \right) - h_i d_{T,i} \left(T_w - T_{cw} \right) = 0 \tag{3.52}$$

where is the water side heat transfer coefficient, h_i, calculated by using the correlation of Sleicher and Rouse [67],

$$h_i = \frac{k_{cw}}{d_{T,i}} \left[5 + 0.015 \,\mathrm{Re}^m \,\mathrm{Pr}^{\mathrm{n}} \right] \tag{3.53}$$

$$m = 0.88 - \frac{0.24}{4 + \mathrm{Pr}} \,; \qquad n = 0.333 + 0.5 \exp\left(-0.6 \,\mathrm{Pr} \right) \tag{3.54}$$

3.3. Freeboard Model

3.3.1. Solids distribution

The hold-up of particles in the freeboard is expressed with an exponential decay function Choi et al. [60],

$$\frac{\varepsilon_s}{\varepsilon_{s,0}} = \exp\left(-az_f\right) \tag{3.55}$$

where a is the decay constant calculated using the empirical correlation provided by Choi et al. [60],

$$\begin{aligned} a = \frac{1}{d_p}\exp\left(-11.2 + 210\frac{d_p}{d_{bed}-d_p}\right)\left(\frac{d_p\rho_g\left(u_o-u_{mf}\right)}{\mu}\right)^{-0.492} \\ \times\left(\frac{d_p g\rho_g}{\rho_g\left(u_o-u_{mf}\right)^2}\right)^{0.725}\left(\frac{\rho_p-\rho_g}{\rho_g}\right)^{0.731} C_d^{\,-1.47} \end{aligned} \tag{3.56}$$

where

$$C_d = \begin{cases} 24/\mathrm{Re}_p & for\ \mathrm{Re}_p \le 5.8 \\ 10/\mathrm{Re}_p^{\,0.5} & for\ 5.8 < \mathrm{Re}_p \le 540 \\ 0.43 & for\ 540 < \mathrm{Re}_p \end{cases} \tag{3.57}$$

This empirical equation covers column diameters from 0.05 to 0.4 *m*, bed particle diameters from 46 to 720 μm, particle densities from 930 to 3050 kg/m^3, gas velocities from 0.3 to 6.2 *m/s* and temperatures from 24 to 600 ^oC.

The total volume fraction of solids just above the surface of dense bubbling bed, $\varepsilon_{s,o}$ is and is obtained from,

$$\varepsilon_{s,o} = 1 - \varepsilon_f \tag{3.58}$$

The volume fractions of char and inert particles of size r at bed surface are obtained from the following equations respectively,

$$\varepsilon_{d,o} = \varepsilon_{s,o} \frac{M_d P_{bed}(r)\Delta r / \rho_d}{M_d / \rho_d + M_i / \rho_i} \tag{3.59}$$

$$\varepsilon_{i,o} = \varepsilon_{s,o} \frac{M_i P_{bed}(r)\Delta r / \rho_i}{M_d / \rho_d + M_i / \rho_i} \tag{3.60}$$

The entrainment flux of particles, K_i^*, is calculated by assuming that it consists of a cluster flux, K_{ih}^*, and a dispersed noncluster flux, $K_{i\infty}^*$ as suggested by Hazlett and Bergougnou [76],

$$K_i^* = K_{ih}^* + K_{i\infty}^* \tag{3.61}$$

and are obtained from empirical correlations proposed by Choi et al. [60]. The elutriation rate constant, *E(r)*, used in Equation (3.12) is then calculated from,

$$E(r) = \frac{A_{bed}}{M_d} K_{i\infty}^* \tag{3.62}$$

The elutriated particles are assumed to rise at the superficial gas velocity in the freeboard. Size distribution of entrained solid particles at any height in the freeboard is calculated by assuming that probability of finding particles of size r at any height is proportional to their presence in bed with proportionality constant being K_{ih}^*,

$$F_z P_z(r) = K_{ih}^* A_{bed} P_{bed}(r) \tag{3.63}$$

Multiplying both sides of Equation (3.63) by *dr* and integrating yields the flow rate of entrained particles and their size distribution as follows,

$$F_z = A_{bed} \int_{r_{\min}}^{r_{\max}} K_{ih}^{*} P_{bed}(r) dr \tag{3.64}$$

$$P_z(r) = A_{bed} K_{ih}^{*} P_{bed}(r) / F_z \tag{3.65}$$

3.3.2. Species Conservation Equations

The gases in the bubble and emulsion phases are assumed to mix instantaneously at the top of the bed and then enter freeboard. The gas flow in freeboard is assumed to be in plug flow. A mass balance for j^{th} gas component in the freeboard results in the following equation,

$$\frac{dn_{j,f}}{dz} = A_f (1-\varepsilon_s) \Re_{j,f} \tag{3.66}$$

Boundary condition for Equation (3.66) is expressed as,

$$\text{at } z_f = 0 \qquad n_{j,f} = n_{j,e} + n_{j,b} \tag{3.67}$$

The expression for species generation/depletion term, $\Re_{j,f}$, appearing in Equation (3.66) takes the following forms for the species considered,

j=1 (O_2)

$$\Re_{1,f} = -\frac{m_{vm}(1-x_{vl})}{V_f(1-\varepsilon_s)} \left\{ 0.5\frac{x_{C,vm}}{M_C} + 0.5\frac{x_{H,vm}}{M_{H_2}} + \frac{x_{S,vm}}{M_S} - \frac{x_{O,vm}}{M_{O_2}} \right\} - \frac{0.5 r_{SO_2,f}}{V_f(1-\varepsilon_s)} - 0.5 n_{C,f} - 0.5 r_{CO,f} \tag{3.68}$$

j=2 (CO)

$$\Re_{2,f} = \frac{m_{vm}(1-x_{vl})}{V_f(1-\varepsilon_s)}\left\{0.5\frac{x_{C,vm}}{M_C}\right\} + n_{C,f} - r_{CO,f} \tag{3.69}$$

j=3 (CO_2)

$$\Re_{3,f} = r_{CO,f} \tag{3.70}$$

j=4 (H_2O)

$$\Re_{4,f} = \frac{m_{vm}(1-x_{vl})}{V_f(1-\varepsilon_s)}\left\{\frac{x_{H,vm}}{M_{H_2}}\right\} \tag{3.71}$$

j=5 (SO_2)

$$\Re_{5,f} = \frac{1}{V_f(1-\varepsilon_s)}\left\{m_{vm}(1-x_{vl})\frac{x_{S,vm}}{M_S} - r_{SO_2,f}\right\} \tag{3.72}$$

where $n_{C,f}$, the solid carbon consumption rate at any height in freeboard is the sum of carbon consumption rates for coarse and fine particles, as shown below,

$$n_{C,f} = -\frac{3\eta}{M_C}\frac{x_{fc}}{x_{fc}+x_a}\left[\rho_d \int_{r_{\max e}}^{r_{\max}} \frac{\varepsilon_{s,d}P_z(r)}{r}\Re_f(r)dr + \frac{F_{co}}{A_f}\int_{r_{\min}}^{r_{\max}} \frac{P_{co}(r)}{r\ u_p(r)}\Re_f(r)dr\right] \tag{3.73}$$

η in Equation (3.73) represents the contact efficiency between gas and solids in freeboard and it is calculated from the following equation proposed by Kunii and Levenspiel [77],

$$\eta = 1-(1-\eta_0)\exp(-6.62\,z_f) \tag{3.74}$$

where,

$$\eta_0 = \frac{u_e}{u_0}(1-\delta) \tag{3.75}$$

3.3.3. Energy Conservation Equation

The incorporation of the radiation model into the system model necessitates modification in the freeboard energy conservation equation utilized in previous studies [6, 7]. The system model is coupled with radiation model through the radiative source term, $\nabla \cdot \boldsymbol{q}_R$. The energy conservation equation takes the following form after the addition of the radiative source term.

The gas temperature profile in freeboard is obtained by solving an energy balance which considers convective transport, and generation and loss of energy. On a differential volume element of thickness Δz in freeboard, the energy balance can be written as,

$$\begin{aligned} 0 = {} & M_g\, n_f\, c_{p,g} \left(T_f - T_r\right)\Big|_z - M_g\, n_f\, c_{p,g} \left(T_f - T_r\right)\Big|_{z+\Delta z} \\ & + A_f\, \Delta z \left(1-\varepsilon_s\right) R - A_f\, \Delta z\, \nabla \cdot \boldsymbol{q_R} \end{aligned} \tag{3.76}$$

Dividing both sides of Equation (3.76) by $A_f \Delta z$ and taking $lim_{\Delta z \to 0}$ results in,

$$\frac{dT_f}{dz} = \frac{A_f}{M_g\, n_f\, c_{p,g}} \left[R\left(1-\varepsilon_s\right) - \nabla \cdot \boldsymbol{q}_R \right] \tag{3.77}$$

Equation (3.77) has the following boundary condition,

$$\text{at } z = 0 \qquad T_f = T_{bed} \tag{3.78}$$

In Equations (3.76) and (3.77) R is the combined energy generation and loss rate per unit volume of freeboard. It is the sum of energy generated by chemical reactions, R_{rxn}, energy loss from freeboard walls, R_{fw} and energy transferred from/to char and ash particles present in the freeboard, R_p. These terms can be expressed as follows,

$$R_{rxn} = \frac{m_{vm}\left(1-x_{vl}\right)}{V_f\left(1-\varepsilon_s\right)}\left[\frac{x_{C,vm}}{M_C}\Delta H^0_{R2} + \frac{x_{H,vm}}{M_{H_2}}\Delta H^0_{R4} + \frac{x_{S,vm}}{M_S}\Delta H^0_{R5}\right] + \Delta H^0_{R3} r_{CO,f} + \frac{1}{V_f\left(1-\varepsilon_s\right)}\left[\Delta H^0_{R7} r_{SO_2,f}\right] \tag{3.79}$$

$$R_{fw} = -\frac{4 d_{bed}}{A_{bed}\left(1-\varepsilon_s\right)} h_{fw}\left(T_f - T_{fw}\right) \tag{3.80}$$

$$R_p = \frac{3F_{co}}{A_{bed}\rho_d}\int_{r_{\min}}^{r_{\max e}} \frac{P_{z,d}(r)}{r\,u_p(r)}\left[h_p\left(T_d - T_f\right)\right]dr + 3\varepsilon_d \int_{r_{\max e}}^{r_{\max}} \frac{P_{z,d}(r)}{r}\left[h_p\left(T_d - T_f\right)\right]dr + 3\varepsilon_i \int_{r_{\max e}}^{r_{\max}} \frac{P_{z,i}(r)}{r}\left[h_p\left(T_i - T_f\right)\right]dr \tag{3.81}$$

where particle convective heat transfer coefficient, h_p, is calculated by adopting the correlation proposed by Davidson and Harisson [62] and Botterill [78],

$$h_p = \frac{k_g}{d_p}\left[0.03\,\mathrm{Re}_p^{\,1.3}\right] \tag{3.82}$$

The gas side heat transfer coefficient, h_{fw}, is calculated by using the correlation of Kunii and Levenspiel [61],

$$\frac{h_{fw} - h_g}{h_{zf=0} - h_g} = \exp\left(-a\,z_f / 2\right) \tag{3.83}$$

In utilizing Equation (3.83), the radiative heat transfer coefficient, h_r, is neglected since the radiative heat exchange between particle surface to wall surface is taken into account in the radiation model.

The gas convective heat transfer coefficient, h_g is obtained by employing the correlation proposed by Gnielinski [59],

$$h_g = \frac{k_g}{d_{bed}}\left[\frac{(f/8)(\mathrm{Re}-1000)\mathrm{Pr}}{1+12.7(f/8)^{0.5}\left(\mathrm{Pr}^{2/3}-1\right)}\right] \tag{3.84}$$

In solving energy conservation equation (Equation (3.77)) together with its boundary condition (Equation (3.78)), it is assumed that in freeboard, temperatures of char particles are equal to their temperatures in bed as calculated by Equation (3.43) and temperatures of inert particles remain at T_{bed}.

CHAPTER 4

RADIATION MODEL FOR THE FREEBOARD OF FLUIDIZED BED COMBUSTOR

4.1. General

Modeling of fluidized bed combustors necessitates the accurate treatment of radiative heat transfer. In an attempt to achieve this objective in this thesis study, a radiation model, which was developed and tested in isolation from the system model for calculation of radiative heat exchange [4], was incorporated into the system model described in Chapter 3. The radiation model is based on method of lines solution of discrete ordinates method ((MOL solution of DOM) for 3-D rectangular enclosure containing gray, absorbing, emitting and isotropically scattering medium surrounded by gray and diffuse walls. For the sake of integrity, equations representing MOL solution of DOM derived starting from the radiative transfer equation for three-dimensional rectangular coordinate system and the numerical solution procedure utilized for the MOL solution of DOM are described in this chapter.

4.2. Radiative Transfer Equation

The propagation of radiation in a participating medium is governed by the radiative transfer equation which is derived by drawing up a balance on the flux of radiant

energy in specified direction through a small volume element. The details of derivation can be found elsewhere [79, 80]. The RTE for gray, absorbing, emitting and scattering medium can be written in the form,

$$\frac{dI}{ds} = (\boldsymbol{\Omega}.\nabla) I(\boldsymbol{r},\boldsymbol{\Omega}) = -\kappa I(\boldsymbol{r},\boldsymbol{\Omega}) + \kappa I_b(\boldsymbol{r}) - \sigma_s I(\boldsymbol{r},\boldsymbol{\Omega}) + \frac{\sigma_s}{4\pi}\int_{4\pi} \Phi(\boldsymbol{\Omega}',\boldsymbol{\Omega}) I(\boldsymbol{r},\boldsymbol{\Omega}')\, d\boldsymbol{\Omega}' \tag{4.1}$$

where, $I(\boldsymbol{r},\boldsymbol{\Omega})$ is the radiation intensity at position $\boldsymbol{r}$ in the direction $\boldsymbol{\Omega}$ defined as the quantity of radiant energy passing in specified direction $\boldsymbol{\Omega}$ along a path s per unit solid angle $d\boldsymbol{\Omega}'$, per unit area normal to the direction of travel, per unit time. κ and σ_s are the absorption and scattering coefficients of the medium, respectively, $I_b(\boldsymbol{r})\left(\equiv \sigma T^4(\boldsymbol{r})/\pi\right)$ is the black-body radiation intensity and $\Phi(\boldsymbol{\Omega}',\boldsymbol{\Omega})$ is the phase function for scattering which describes the fraction of energy scattered from incoming direction $\boldsymbol{\Omega}'$ to the outgoing direction $\boldsymbol{\Omega}$. The expression on the left-hand side represents the change of the intensity in the specified direction $\boldsymbol{\Omega}$. The terms on the right-hand side stand for absorption, emission, out-scattering and in-scattering, respectively. For the case of isotropic scattering, which means that equal amounts are scattered into all directions, phase function is equal to unity.

For rectangular coordinate system, the gradient of intensity can be expressed in terms of the derivatives with respect to space coordinates x, y, and z and hence RTE in rectangular coordinates can be written as,

$$\frac{dI}{ds} = \mu\frac{\partial I}{\partial x} + \eta\frac{\partial I}{\partial y} + \xi\frac{\partial I}{\partial z} = -\kappa I(\boldsymbol{r},\boldsymbol{\Omega}) + \kappa_b I_b(\boldsymbol{r}) - \sigma_s I(\boldsymbol{r},\boldsymbol{\Omega}) + \frac{\sigma_s}{4\pi}\int_{4\pi} I(\boldsymbol{r},\boldsymbol{\Omega}')\, d\boldsymbol{\Omega}' \tag{4.2}$$

where the direction cosines can be expressed in terms of the polar angle θ and the azimuthal angle ϕ (Figure 4.1) as $\mu = \cos\theta$, $\eta = \sin\theta\cdot\sin\phi$ and $\xi = \sin\theta\cdot\cos\phi$.

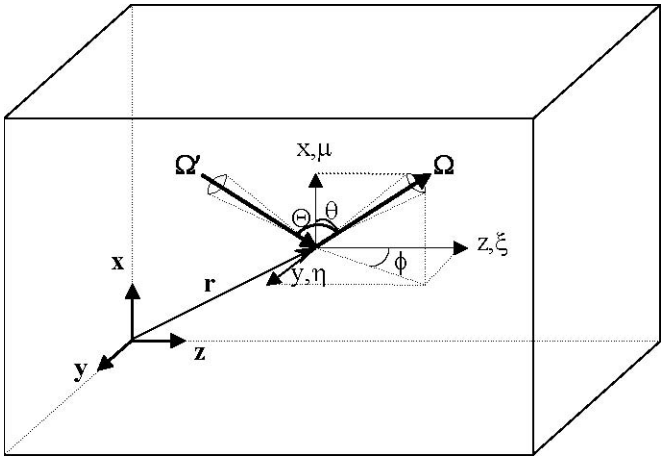

Figure 4.1: Coordinate system [81].

If the surface bounding the medium is a gray and diffuse wall at specified temperature, then Equation (4.2) is subject to the boundary condition,

$$I\left(\boldsymbol{r}_w,\boldsymbol{\Omega}\right)=\varepsilon_w I_{b,w}+\frac{1-\varepsilon_w}{\pi}\int\limits_{\boldsymbol{n}\cdot\boldsymbol{\Omega}'<0}\left|\boldsymbol{n}\cdot\boldsymbol{\Omega}'\right|I\left(\boldsymbol{r}_w,\boldsymbol{\Omega}'\right)d\boldsymbol{\Omega}' \qquad \boldsymbol{n}\cdot\boldsymbol{\Omega}>0 \tag{4.3}$$

where $I\left(\boldsymbol{r}_w,\boldsymbol{\Omega}\right)$ is the radiative intensity leaving the surface at a boundary location, ε_w is the surface emissivity, $I_{b,w}\left(\equiv\sigma T_w^{\,4}(\boldsymbol{r})/\pi\right)$ is the black-body radiation intensity at the surface temperature, $\boldsymbol{n}$ is the local outward surface normal and $\boldsymbol{n}\cdot\boldsymbol{\Omega}'$ is the cosine of the angle between incoming direction $\boldsymbol{\Omega}'$ and the surface normal. The first and second terms on the right-hand side of Equation (4.3) stand for the contributions to the leaving intensity due to emission from the surface and reflection of the incoming radiation, respectively.

Equations (4.2) and (4.3) represent governing equation and its boundary condition for radiative heat transfer, respectively. Once the intensity distribution is determined, quantities of interest such as radiative heat flux and energy source term distributions along the freeboard region can be readily evaluated.

4.3. Discrete Ordinates Method

This method is based on representation of the continuous angular domain by a discrete set of ordinates with appropriate angular weights, spanning the total solid angle of 4π steradians. The RTE is replaced by a discrete set of equations for a finite number of directions and each integral is replaced by a quadrature summed over the ordinate directions [82]. The discrete ordinates representation of RTE for a 3-D rectangular enclosure containing a uniform, gray, absorbing, emitting and isotropically scattering medium takes the following form,

$$\mu_m \frac{\partial I^m}{\partial x} + \eta_m \frac{\partial I^m}{\partial y} + \xi_m \frac{\partial I^m}{\partial z} = -\kappa I^m + \kappa I_b - \sigma_s I^m + \frac{\sigma_s}{4\pi} \sum_{m'=1}^{M} w_{m'} I^{m'} \tag{4.4}$$

where $I^m \left[\equiv I\left(\mathbf{r}; \mu_m, \eta_m, \xi_m\right) \right]$ is the radiation intensity at position $\mathbf{r}\left(x, y, z\right)$ in the discrete ordinate direction $\mathbf{\Omega}_m$, m denotes the discrete ordinate $\left(m = 1, 2, ...M\right)$, M is the total number of ordinates used in the approximation, μ_m, η_m and ξ_m are the direction cosines of $\mathbf{\Omega}_m$ with x, y and z axes, respectively and $w_{m'}$ is the angular quadrature weight associated with the incoming direction $\mathbf{\Omega}_{m'}$.

The boundary conditions at the two opposite, diffuse, gray surfaces with normal vectors parallel to x axis can be written as,

$$at \quad x = 0, \qquad I^m = \varepsilon_w I_{b,w} + \frac{1 - \varepsilon_w}{\pi} \sum_{\mu_{m'} < 0} w_{m'} \left|\mu_{m'}\right| I^{m'} \qquad \mu_m > 0 \tag{4.5}$$

$$at \quad x = L, \qquad I^m = \varepsilon_w I_{b,w} + \frac{1 - \varepsilon_w}{\pi} \sum_{\mu_{m'} > 0} w_{m'} \left|\mu_{m'}\right| I^{m'} \qquad \mu_m < 0 \tag{4.6}$$

where I^m is the intensity of radiation leaving the surface, ε_w is the surface emissivity, $I_{b,w}$ is the total black-body radiation intensity at the temperature of the surface. Similar expressions hold for boundaries in other coordinate directions.

Using the DOM, the RTE is transformed into a set of simultaneous partial differential equations containing only space coordinates as independent variables. The angular derivative term, which makes the solution of DOM complicated, is discretized by introducing the S_N angular quadrature scheme proposed by Carlson and Lathrop [83]. The quadrature ordinates and weights for S_N approximations are listed in Appendix A. The choice of S_4 order of approximation was selected based on an assessment study carried out by Selçuk and Kayakol [84].

4.4. Method of Lines Solution of Discrete Ordinates Method

The solution of discrete ordinates equations with MOL is carried out by adoption of the false-transients approach which involves incorporation of a pseudo-time derivative of intensity into the discrete ordinates equations [56]. Application of the false-transients approach to Equation (4.4) yields,

$$k_t \frac{\partial I^m}{\partial t} = -\mu^m \frac{\partial I^m}{\partial x} - \eta_m \frac{\partial I^m}{\partial y} - \xi_m \frac{\partial I^m}{\partial z} - \kappa I^m + \kappa I_b - \sigma_s I^m + \frac{\sigma_s}{4\pi} \sum_{m'=1}^{M} w_{m'} I^{m'} \qquad (4.7)$$

where t is the pseudo-time variable and k_t is a time constant with dimension $[(m/s)^{-1}]$ which is introduced to maintain dimensional consistence in the equation and it is taken as unity.

The system of PDEs with initial and boundary-value independent variables is then transformed into an ODE initial-value problem by using the method of lines approach [85]. The transformation is carried out by representation of the spatial derivatives with algebraic finite-difference approximations. For the difference relations of spatial derivatives, three-point upwind differencing scheme, DSS014, assessed previously for accuracy [56-58] is employed. Starting from an initial condition for radiation intensities in all discrete directions, the resulting ODE system is integrated until steady state by using a powerful ODE solver. The utilized ODE solver is the RKF45 (Runge–Kutta–

Fehlberg integration) subroutine previously found to be as accurate but less CPU intensive than Livermore solver for ordinary differential equations (LSODE) [58]. Any initial condition can be chosen to start the integration, as its effect on the steady state solution decays to insignificance. As a result, evolution of radiative intensity with time at each node and ordinate is obtained. The steady-state intensity values give the solution to Equation (4.4) because the artificial time derivative vanishes at steady-state.

Once the intensity distribution is determined by solving Equation (4.7) together with its boundary conditions, radiative energy source term used in the freeboard energy conservation equation of FBC system model and the incident radiative heat fluxes on freeboard side walls which is the quantity of interest for comparison with measurements can be readily calculated by using the following equations,

$$\nabla \cdot \boldsymbol{q}_R = \kappa \left(4\pi I_b - \sum_{m'=1}^{M} w_{m'} I^{m'} \right) \tag{4.8}$$

$$q''_{w,inc} = \sum_{\boldsymbol{n}\cdot\boldsymbol{\Omega}_{m'}<0} w_{m'} \left| \boldsymbol{n} \cdot \boldsymbol{\Omega}_{m'} \right| I^{m'} \tag{4.9}$$

4.5. Treatment of Freeboard for Radiation

The physical situation under consideration is the freeboard section of METU 0.3 MW_t Atmospheric Bubbling Fluidized Bed Combustor. The details of the ABFBC are given in Chapter 6. The freeboard section of the combustor is treated as a 3-D rectangular enclosure containing gray, absorbing, emitting and isotropically scattering medium bounded by refractory-lined gray and diffuse walls. The cooler boundary at the top, which consists of gas lanes and cooler tubes, is represented by an equivalent gray surface of effective emissivity and temperature related to area weighted average emissivity and emissive power of the components, respectively. Details of the treatment of tube-row/gas-lane combination can be found elsewhere [49, 86]. The

boundary with the bed section at the bottom is represented as a black surface due to Hohlraum effect [86]. The physical system and the treatment of the freeboard is illustrated in Figure 4.2.

4.5.1. Radiative Properties of Combustion Gases

The radiative properties of the participating combustion gases, composed of CO_2 and H_2O, are estimated by using Leckner's correlations [52], which require the partial pressures of carbon dioxide and water vapor, the gas temperature and mean beam length, L_m. Calculation of the gas emissivity ε_g through Leckner's correlations leads to gas absorption coefficient expressed by,

$$\kappa_g = -\frac{1}{L_m} ln\left(1-\varepsilon_g\right) \tag{4.10}$$

For the estimation of uniform absorption coefficient, average gas composition and temperature and mean beam length based on the entire freeboard region are required. For the estimation of non-uniform absorption coefficient, on the other hand, the point values of gas and temperature and mean beam length based on each control volume are utilized.

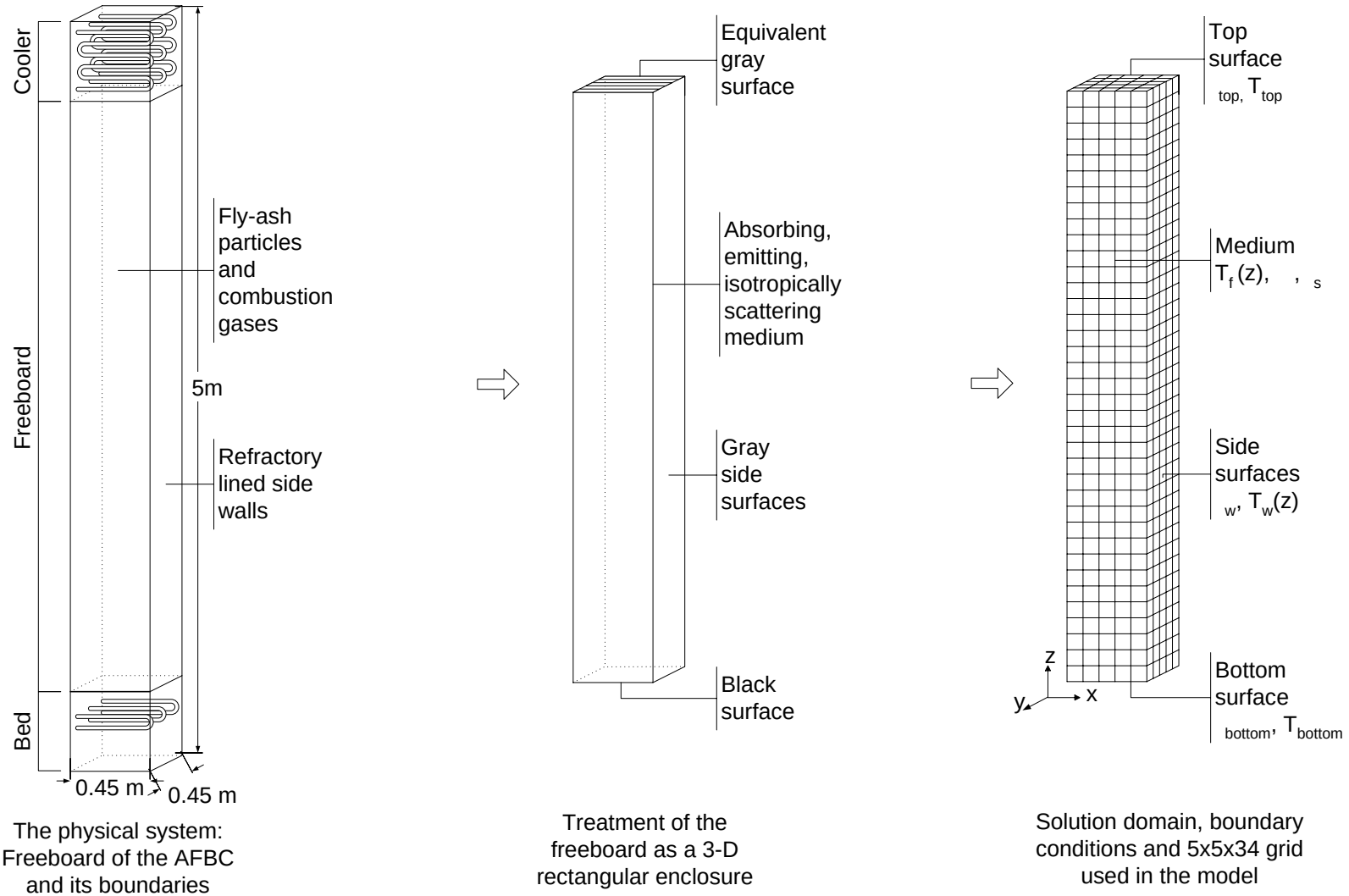

The physical system: Freeboard of the AFBC and its boundaries

Treatment of the freeboard as a 3-D rectangular enclosure

Solution domain, boundary conditions and 5x5x34 grid used in the model

Figure 4.2: Treatment of freeboard as a 3-D rectangular enclosure and solution domain for MOL solution of DOM [81].

4.5.2. Radiative Properties of Particles

Radiative properties of the cloud of fly ash particles depend on the composition, size distribution and particle loading. In this study, particle concentration and size distribution were assumed to be uniform and constant throughout the freeboard and represented by the material sampled from the cyclone and baghouse filter. The ash content of the fly ash particles determined by chemical analysis was 98% indicating that the fly ash can be treated as pure ash in the radiative property estimation. The spectral dependence of complex index of refraction is neglected and a representative value of $m = 1.5 - 0.02i$ is used as given in [87]. Independent scattering is assumed to take place in the freeboard of the test rig as the particle volume fraction is in the order of 10^{-5}. This assumption is confirmed by the scattering regime map of Tien and Drolen [88]. Assuming also that the particles are spherical, efficiency factors of a single particle can be obtained from Mie theory [53] for a given particle size parameter $x = \pi D_p / \lambda$ and complex index of refraction. The size parameter is determined by using a representative wavelength $(3\mu m)$ suggested for combustion systems in [80]. Utilizing the assumption of independent scattering, efficiency factors for the particle cloud can be determined by taking average over the efficiencies of the single particles. In the case of homogeneous polydispersion and single wavelength, size averaged efficiency factors characterize the radiative properties of the particle cloud.

In order to find the size averaged efficiency factors, the cumulative weight distribution of the particles is expressed as a Rosin-Rammler distribution function,

$$W(D_p) = e^{\left(-bD_p{}^n\right)} \tag{4.11}$$

where b and n are constants and $W(D_p)$ is the cumulative weight distribution function. Once the constants b and n are determined, the cumulative weight distribution is related to differential weight distribution $p(D_p)$ and number distribution $f_N(D_p)$ with the following relations.

$$p(D_p) = -\frac{d}{dD_p} W(D_p) \tag{4.12}$$

$$f_N(D_p) = \frac{p(D_p)}{\rho_p V_p(D_p)/M_t} \tag{4.13}$$

where M_t is the total weight of the particles, ρ_p is the density of the particles and $V_p(D_p)$ is the volume of a spherical particle of diameter D_p. The size averaged absorption efficiency of the particle cloud $Q_{a,av}$ is given by [89],

$$Q_{a,av} = \frac{\int_0^\infty Q_a(D_p)\left(\pi {D_p}^2/4\right) f_N(D_p) dD_p}{\int_0^\infty \left(\pi {D_p}^2/4\right) f_N(D_p) dD_p} \tag{4.14}$$

where $Q_a(D_p)$ is the absorption efficiency factor obtained from Mie theory. Similar relation holds for the size averaged scattering efficiency factor $Q_{s,av}$. In this thesis study, size averaged absorption and scattering efficiency factors are calculated by using the Mie code developed by Değirmenci [90]. The absorption and scattering coefficients of a cloud of fly ash particles are then calculated from [89],

$$\kappa_p = Q_{a,av} B A_{mc} \tag{4.15}$$

$$\sigma_s = Q_{s,av} B A_{mc} \tag{4.16}$$

where

$$B = \frac{F_c}{u_o A_c} \tag{4.17}$$

$$A_{mc} = \frac{3/2}{\rho_p D_{32}} \tag{4.18}$$

A_{mc} is the mass specific cross-section, B is the particle load, u_o is the superficial gas velocity, F_c is the carryover flow rate of particles collected from the cyclone with density ρ_p, D_{32} is the Sauter mean diameter of the size distribution of particles and A_c is the cross-section of the combustor.

CHAPTER 5

SOLUTION PROCEDURE

5.1. Coupling between System Model and Radiation Model

In this study, previously developed and validated, (i) FBC system model accounting for bed and freeboard hydrodynamics, volatiles release and combustion, char particles combustion and size distribution, attrition, sulfur retention and heat transfer [5-7], (ii) radiation model based on MOL solution of DOM for a 3-D rectangular enclosure containing gray, absorbing, emitting and scattering medium bounded by gray and diffuse walls [4], are coupled for the solution of conservation equations of mass, momentum, energy and species in conjunction with radiative transfer equation.

Coupling strategy between the FBC and radiation codes is mainly based on periodic transfer of temperature and concentration distributions calculated by the FBC code to the radiation code which in turn provides the source term field to be inserted in the energy conservation equation of the freeboard region of the system model. The schematic representation of the coupling procedure is illustrated in Figure 5.1.

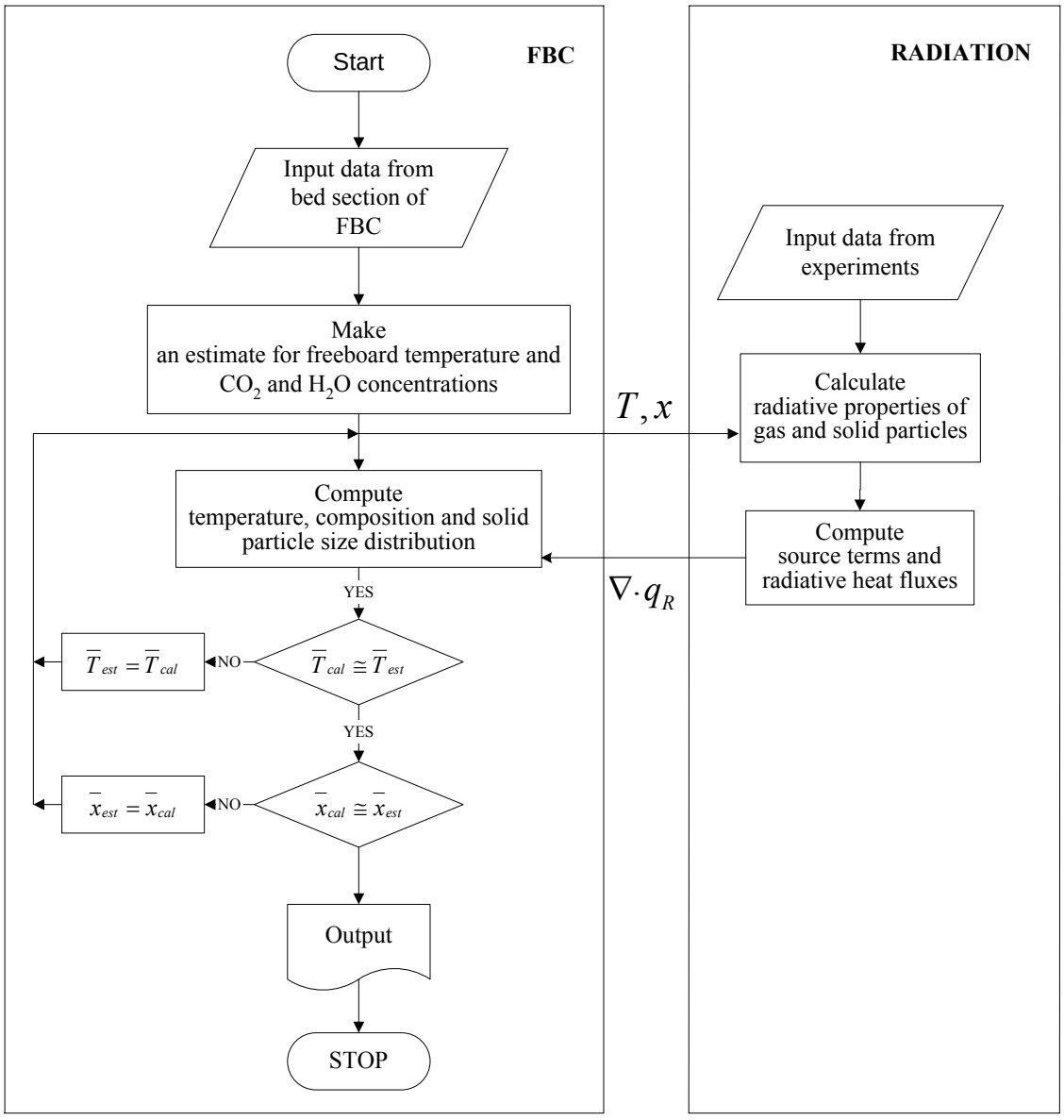

Figure 5.1: Coupling procedure.

5.2. Algorithm of Coupled Code

The algorithms of the coupled code in compact form for the bed and freeboard sections are illustrated in Figure 5.2 and Figure 5.3, respectively. The whole procedure of the coupled code can be summarized as follows.

The input data required by the coupled code are the configuration and dimensions of the rig and its internals; radiative properties of bounding surfaces; air and coal flow rates; coal analysis; all solid and gas properties; inlet temperatures of air, cooling water and feed solids; freeboard wall temperature profile; and size distribution function of feed solids and fly ash particles deduced from sieve analysis.

Apart from these input data, application of the model necessitates empirical and semi-empirical correlations from the literature for heat and mass transfer, combustion kinetics, elutriation and entrainment rates etc., listed in Tables 3.1 and 3.2. These expressions contain empirical or semi-empirical constants which may not always comply with the experimental conditions of the system to be modeled. Therefore, it is the usual practice to adjust some of these constants until a compromise is found to reproduce the measured data as accurately as possible [91]. In this study, minimum number of fitting parameters was utilized. These were pre-exponential factor for carbon monoxide oxidation, exponential decay constant for entrained particles and elutriation rate constant previously deployed in the system model.

CO concentrations predicted by using the rate expression of Hottel et al. [69] was found an order of magnitude lower than the measurements. To match the measured CO concentration at the exit of the combustor, the rate constant from Hottel et al. was multiplied by 0.3 and this value was used for model validation.

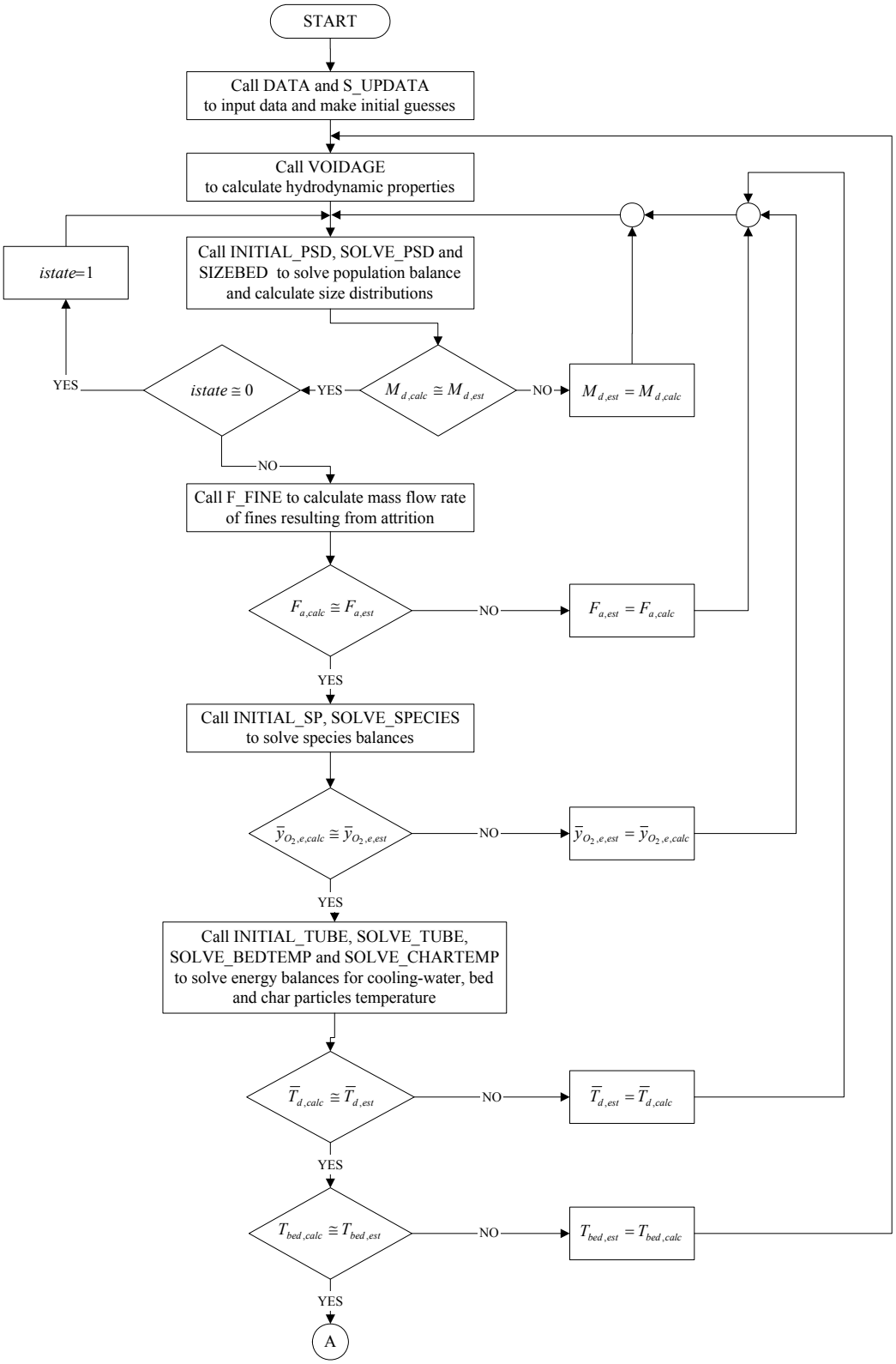

Figure 5.2: Algorithm of the coupled code for the bed section.

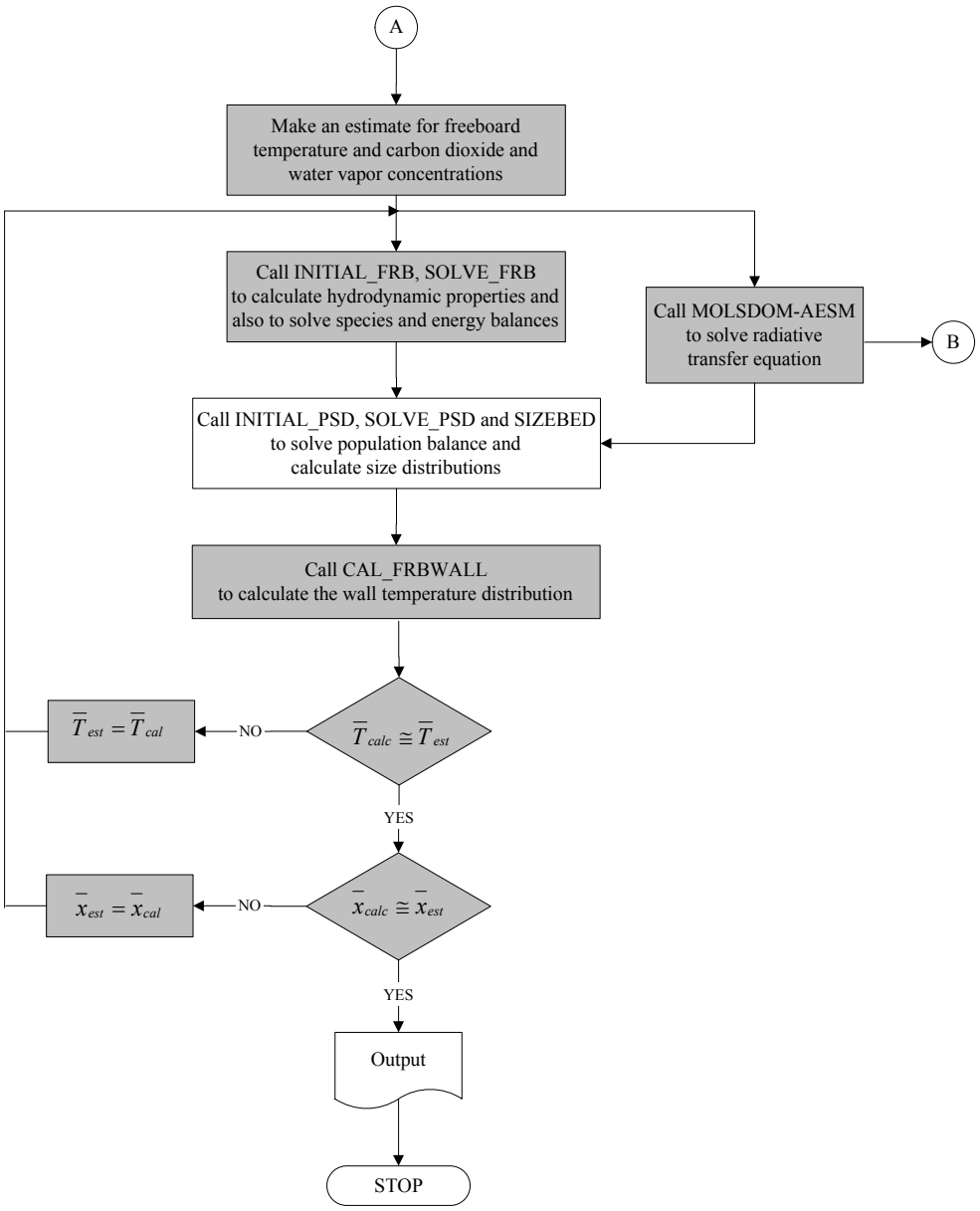

Figure 5.3: Algorithm of the coupled code for the freeboard section showing the modified sections in this study in shade.

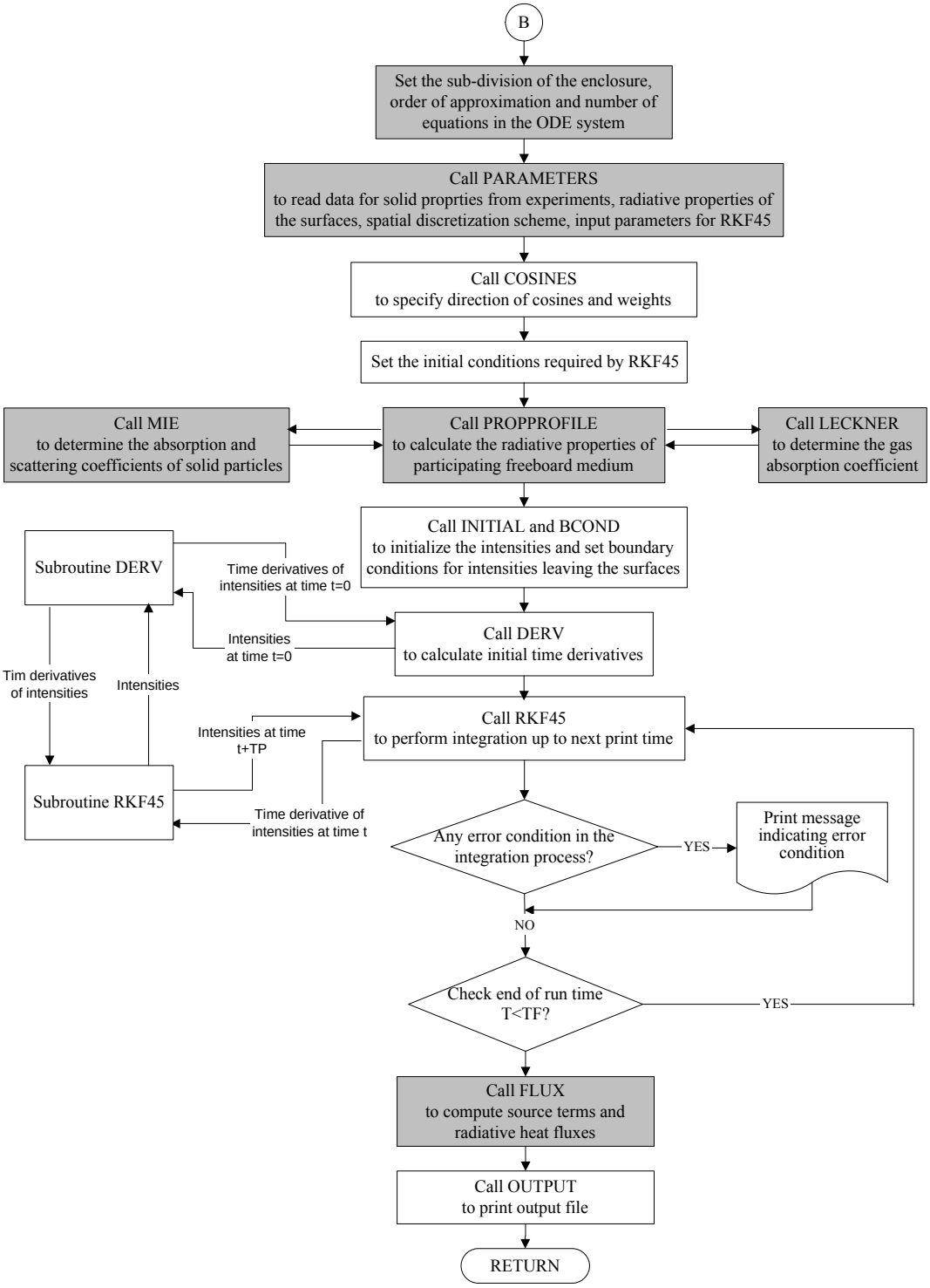

Figure 5.3: Algorithm of the coupled code for the freeboard section showing the modified sections in this study in shade (continued).

With regard to entrainment, direct use of the entrainment rate expression of Choi et al.[60], in the model resulted in higher char hold-up and hence lower O_2 concentrations in the freeboard compared to measurements. To match the measured O2 concentration at the exit of the freeboard, the decay constant of the entrainment rate expression of given in Equation (3.56) was multiplied by 5 and used in the simulations for model validation.

Direct use of elutriation rate expression of Choi et al. [60] in the model yielded higher carryover flow rate at the cyclone exit. To match the measured carryover flow rates, elutriation rate constant of Choi et al. was multiplied by 0.02 for Run 1 and 0.01 for Run 2. Fine-tuning for the carryover flow rates at the cyclone exit was the simplest approach as the carryover flow rate was only a function of elutriation.

The solution starts with making initial guesses for T_{bed}, $\bar{y}_{O_2,e}$, M_d, F_a, and $T_{bw,o}$ in the bed section. This is followed by computation of $\overline{T}_d$ and by using estimated parameters. There are five loops of iterations to be converged for M_d, F_a, $\bar{y}_{O_2,e}$, $\overline{T}_d$ and T_{bed}. In the freeboard section, three loops of iterations for $\overline{T}_f$, $\bar{y}_{CO_2,f}$ and $\bar{y}_{H_2O,f}$, which are estimated to initialize the freeboard, are converged. For each loop, a convergence criterion, ε, is set as the absolute difference between calculated and estimated values of the parameters. In this study, the set values of ε are 5×10^{-1}, 5×10^{-3}, 5×10^{-5}, 1, 1, 1, 5×10^{-5} and 5×10^{-5} for iterations on M_d, F_a, $\bar{y}_{O_2,e}$, $\overline{T}_d$, T_{bed}, $\overline{T}_f$, $\bar{y}_{CO_2,f}$ and $\bar{y}_{H_2O,f}$, respectively.

The integration of ODEs of system model is carried out by Backward-Differentiation Formula (BDF) method embedded in the ODE solver LSODES [92] whereas RKF45 [85] is applied to ODEs of radiation model. Solution of the non-linear algebraic equations is performed by using the subroutine ZERO. Details of the solution procedure of steady state code can be found in [42].

CHAPTER 6

EXPERIMENTAL

6.1. General

Measurements used for benchmarking predictions of the coupled code have previously been carried out on the 0.3 MW_t ABFBC Test Rig of Chemical Engineering Department of Middle East Technical University (METU) within the scope of a research project MİSAG-159, financed by The Scientific and Technical Research Council of Turkey (TÜBİTAK).

It was also intended to validate the predictions of the coupled code against experimental data available on an industrial scale boiler in order to evaluate the effects of presence of water walls and surface to volume ratio on the predictions. However, due to the absence of detailed information on experimental data, it was only possible to benchmark the validation of radiation model in isolation from the system model. For this purpose, data available on 16 MW_t Stationary Fluidized Bed Boiler of Chalmers University of Technology were utilized.

6.2. 0.3 MW_t ABFBC Test Rig

0.3 MW_t ABFBC Test Rig in its present form is shown schematically in Figure 6.1. As can be seen from the figure, the test rig basically consists of a forced draft (FD) fan, a windbox with an ash removal system, a modular combustor, a cyclone with a recycle leg, a baghouse filter, an induced draft (ID) fan and a coal and limestone feeding systems.

6.2.1. The Combustor

The main body of the test rig is the modular combustor formed by five modules of equal dimensions. Modular structure of the combustor is intended to provide flexibility in burning various fuels by addition or removal of heating surfaces. Each module has an internal cross-section of 0.45 × 0.45 m^2 and 1 *m* height. Inner walls of each module are refractory-lined with firebricks with a thickness of 6 *cm*. Outer walls of the refractory bricks are insulated with insulation bricks with thickness of 20 *cm*. Further insulation is provided by leaving an air gap of 6 *mm* between the outer wall of the insulation brick and the inner wall of the steel construction of each module.

The first and fifth modules from the bottom are referred as bed and cooler, respectively, and the ones in between are referred as freeboard modules. The bed module provides an expanded bed height of 1 *m*. It contains 6 water-cooled U-tubes (25 *mm* OD, stainless steel) for cooling purposes, 5 ports for thermocouples, 4 ports for gas sampling probes, one port for LPG distributor, one port for the ignitor and two ports for feeding coal/limestone mixture. One of the feeding ports is 22 *cm* and the other is 85 *cm* above the distributor plate. There are 6 ports for gas sampling probes and 9 ports for thermocouples in freeboard and cooler modules. There exists a water-cooled tube bundle consisting of 11 tubes (26.7 *mm* OD, carbon steel) with 14 passes installed across the cross-section of the cooler module for cooling the stack gases before leaving the combustor.

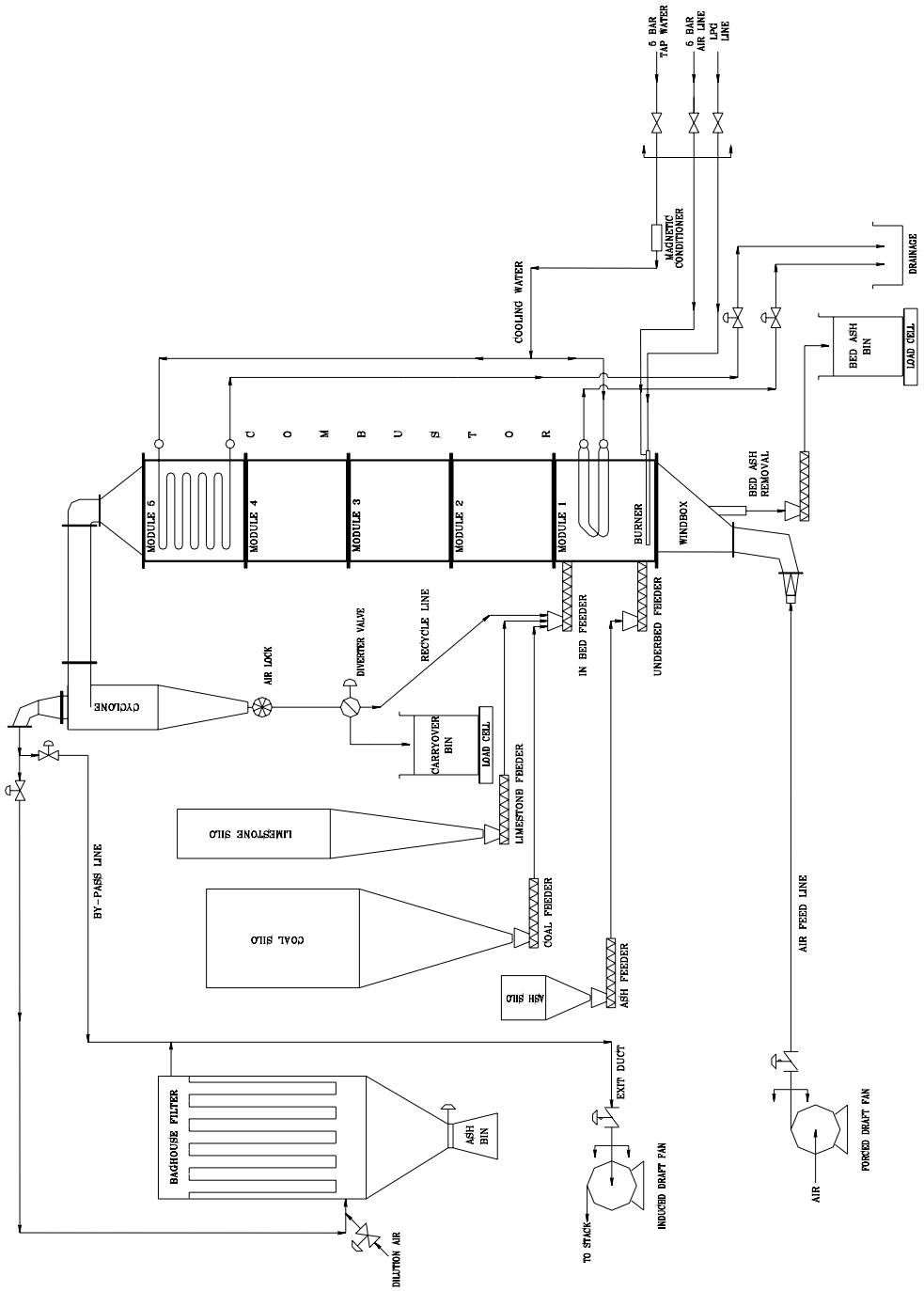

Figure 6.1: Flow sheet of 0.3 MW_t ABFBC Test Rig. [42].

6.2.2. Air and Gas System

The fluidizing air fed by the FD fan enters the bottom of the windbox through a pipe of 6.5 *m* long and 7.8 *cm* ID on which a manual gate valve, an automatic butterfly valve and a vortex flow meter are installed. The design of the windbox allows the installation of bed ash removal system as shown in Figure 6.1. It is a mobile windbox supported by four wheels and a distributor plate is placed on the top. Air supplied to the windbox by means of the pipe of 7.8 *cm* ID diverges to the full cross-section of the combustor at the distributor plate located 1.4 *m* above the entrance port. Sieve type distributor plate contains 412 holes, each 4.5 *mm* in diameter, arranged in a triangular pattern. Within the bed module air mixes with lignite and limestone to affect combustion and sulfur capture.

Flue gases and elutriated fines leaving the bed surface enter the freeboard. Sufficient freeboard height is provided to permit burnout of elutriated lignite fines and combustible gases.

After leaving the freeboard, flue gases pass through the cooler module to cool the hot combustion gases. Flue gases leaving the modular combustor enter the cyclone and then the baghouse filter to leave the elutriated particles before passing through ID fan to exit from the stack.

6.2.3. Solids Handling System

Crushed and sieved lignite and limestone are stored in two separate silos and conveyed into the hoppers of feeders at controlled flow rates via precalibrated volumetric feeders placed under their respective silos. The lignite/limestone mixture is continuously fed to the bed through water-cooled screw feeders. Both screw feeders are operated at

controlled speed in such a way as to maintain certain amount of accumulated material in the hopper in order to prevent backflow of combustion gases from the combustor.

Bed ash is withdrawn from the bed through 5 *cm* diameter, 1.1 *m* long water-cooled ash removal pipe. Some of the bed ash is disposed and the rest is stored to provide bed inventory when required. Bed ash drain rate is adjusted from the computer to obtain the desired bed pressure drop and hence the expanded bed height. Bed ash particles are collected in a continuously weighted ash storage bin.

The majority of the elutriable fines produced from solid in the bed and those fed within the solid streams are captured by the cyclone, having dimensions of 45 *cm* OD and 2.12 *m* height. Cyclone catch particles pass through an air lock (i.e. a rotary valve) and fall onto a diverter. Depending on the position of the diverter, particles are either discharged from the system to a continuously weighted ash storage bin for experiments without recycle or flow back to the combustor for refiring. The fraction of a short time interval over which the position of the diverter remains on the recycle mode determines the recycle ratio. Continuity of flow is provided by repeating this time interval periodically. In order to provide a wider range of recycle ratio and yet not to disturb the steady state conditions within the combustor, a periodic time interval of 10 *s* was selected.

In order to catch fine particles of fly ash ($d_p \leq 40\ \mu m$) leaving the cyclone, a *pulse-jet* type baghouse filter with a 100 % collection efficiency for particles greater than 1 μm was utilized. As mentioned in the previous section, the bag material used is P84-Polyimide and it can resist temperatures up to 260 °*C*. Hence, if the inlet temperature of the flue gases exceeds 220 °*C*, dilution or bypass of flue gases is employed.

6.2.4. Cooling Water System

Cooling water required for the test rig is passed through a magnetic conditioner and is then divided into two streams, one for the in-bed tube bundles, and the other for the tube bundle in the cooler module. Heat transfer areas provided by the bed and cooler modules are 0.30 m^2 and 4.3 m^2, respectively. The cooling water in bed enters lower header and leaves the bed through the upper header. The cooling water for the cooler module enters the upper header and flows downward to provide counter-current flow to the up flowing flue gases. Water flow rates are adjusted by means of either a manual or a pneumatic control valve located at the drain of each stream to maintain maximum exit temperature of about 60 $°C$.

6.2.5. Gas Sampling System

Sample gas extracted from the combustor through the sampling probe is passed through a solenoid valve and sent to the gas conditioning and analysis system of the test rig by means of sample line. The sample line itself is maintained at 150 $°C$ by means of a variable DC power supply so that no water, sulfuric acid or hydrocarbons would condense along the sampling interface. In addition, all lines and fittings in contact with the gas sample are made of teflon or stainless steel to prevent interferences due to gas adsorption or heterogeneous reactions. The existing analytical system of the test rig consists of a bank of analyzers for O_2, CO, CO_2, SO_2 and NO/NO_x. The positions of the gas sampling probes and the details of gas conditioning and analysis system are given in Table 6.1 and Figure 6.2, respectively. Gas is sampled at a rate of 13 cm^3/s at STP which is small enough to cause minimal interference to the combustion system. After passing through the probe, sample gas is transported through the heated stainless steel line to a hygroscopic, ion exchange membrane type gas drier. Once through the drier, the gas is cooled, filtered and pumped to the analyzers via a teflon-coated diaphragm-type sample pump. Then, sample gas is divided into two parallel lines; one passing

through O_2, CO/CO_2 and SO_2 analyzers in series, the other through NO/NO_x analyzer. After the measurement of species concentrations, sample gas is vented to the atmosphere. On-line wet analyses of O_2 and CO are also carried out at the exit of the combustor.

Table 6.1: Relative positions of gas sampling probes.

Thermocouple No	Distance above the distributor plate, *cm*
P10	25
P9	56
P8	69
P7	85
P6	123
P5	183
P4	291
P3	344
P2	419
P1	500

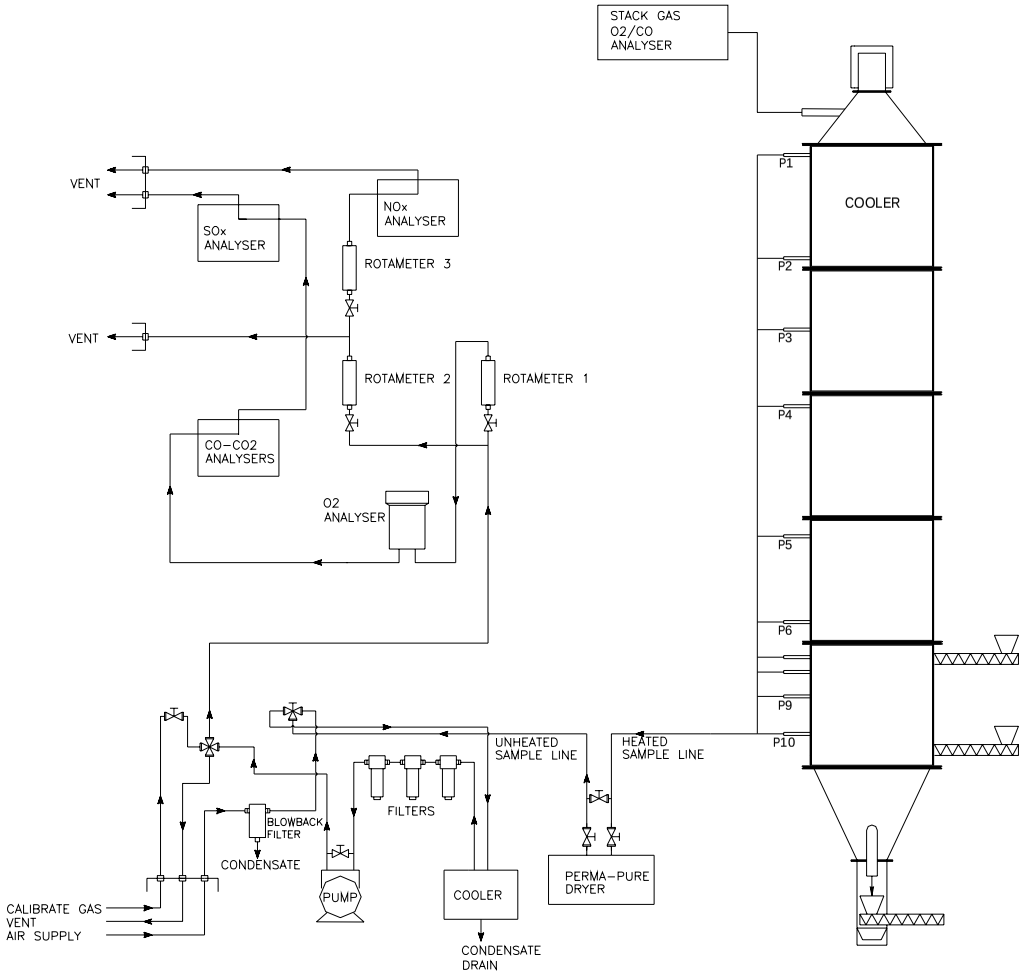

Figure 6.2: Gas conditioning and analysis system. [42].

6.2.6. Instrumentation and Analytical Systems

Instrumentation and analytical systems can be divided into following categories:

i. Data acquisition and control system
ii. Solid flow control and monitoring
iii. Air and gas flow control and monitoring
iv. Cooling water flow control and monitoring
v. On-line continuous gas analyzers
vi. Pressure sensors
vii. Temperature sensors
viii. Solids analyses

The test rig is equipped with a data acquisition and control system namely Bailey INFI 90. Real time process data is monitored, manipulated, collected and analyzed with the aid of a control software called Bailey LAN-90 Process Control View installed on an IBM compatible PC 486 computer running under QNX operating system. The control system scans the signals coming from all of the instruments attached to it in a fraction of a second and reports and logs their averages discretely for 30 seconds of intervals. An uninterruptible power supply is connected to Bailey INFI 90 and PC in order to enable proper shut-down in case of a electricity cut-off by preventing corruption of data logged.

Fuel and sorbent feed rates are controlled manually by adjusting the fuel feeder or sorbent feeder control dial from the computer. The flow rates of fuel and sorbent are normally set to such values that provide desired excess air and *Ca/S* molar ratio, respectively. Bed ash drain rate can also be adjusted from the computer to obtain the desired bed pressure drop and hence the expanded bed height. The interface between the controller and driving motors of fuel and sorbent feeders and bed ash drain are provided with three speed transmitters. Cyclone ash and bed ash are collected in

respective bins and their flow rates are followed by load cells placed under respective bins.

The volumetric flow rate of air is measured by a vortex flow meter and adjusted with an automatic butterfly valve driven by a computer controlled pneumatic actuator. In order to achieve conversion from volumetric to molar flow, a static pressure tap and a temperature sensor is placed downstream of the vortex flow meter. The flow rate of air is normally set to a value to achieve the desired superficial velocity in the combustor. In order to achieve almost neutral pressure on the bed surface, the flow rate of exhaust gases is adjusted with an automatic butterfly valve driven by a computer controlled pneumatic actuator.

In order to measure flow rates of cooling water flowing through bed and cooler bundles, two orifices are located up streams of their lower and upper headers, respectively. The pressure drops across the orifice meters are measured by means of pressure transmitters. The signals from the transmitters are interpreted in the control system to yield mass flow rate of the cooling water flowing through in-bed and cooler bundles. There exist two pneumatic control valves installed on the downstream of upper and lower headers of bed and cooler bundles, respectively, to adjust the cooling water flow in each bundle. The flow rates of cooling water in bed and cooler bundles are normally set to a value which provides exit water temperature in the range 40-60°*C*.

The on-line continuous gas analyzers with which the test rig is equipped are listed in Table 6.2. Analyzers except Bailey SMA 90 are used for measuring spatial variation of species O_2, CO, CO_2, NO/NO_x and SO_2 along the combustor at the positions given in Table 6.1 on dry basis. Bailey SMA 90 uses close-coupled sampling system which does not remove water vapor from the sample. The analyzer reports *CO* equivalent indicating mostly *CO*, but also responds to other combustibles present in the flue gas. It is used for measuring temporal variation of O_2 and *CO* at the combustor exit.

Table 6.2: On-line gas analyzers.

Instrument	Gas species	Sensor type	Range
Leeds & Northrup	O_2	Paramagnetic	0-15 %
Anarad AR 600	CO	IR	0-5 %
	CO_2	IR	0-20 %
Siemens Ultramat 6	SO_2	NDIR	0-1 %
Servomex 1491	NO/NOx	Chemiluminescence	0-0.2 %
Bailey SMA 90	O_2	Zirconium oxide	0-25 %
	CO	Catalytic RTD	0-2 %

Pressure sensors are used for measuring differential and gauge pressures at various positions on the test rig. Measured differential pressures are the pressure drops over orifice meters, bed and distributor plate pressure drop, and gauge pressures are the pressure at the bed surface and pressure of air feed at the downstream of the vortex flow meter.

Spatial and temporal variations of gas temperatures along the height of the combustor are measured by means of thermocouples of K type (Chromel-Alumel) with grounded junction to minimize their response time. The tips of the thermocouples are on the symmetry axis of the combustor. The axial positions of thermocouples are given in Table 6.3. The temperature of air feed at the downstream of vortex flow meter and temperatures of cooling water at the exits of bed and cooler bundles are measured by resistance thermocouples of type Pt-100. Further details of the test rig and operating procedures such as procedures before cold start-up, during runs, after shut down can be found elsewhere [93].

Table 6.3: Relative positions of thermocouples.

Thermocouple No	Distance above the distributor plate, *cm*
TC1	25
TC2	44
TC3	73
TC4	73
TC5	97
TC6	133
TC7	154
TC8	226
TC9	257
TC10	285
TC11	330
TC12	361
TC13	425
TC14	500

6.2.7 Radiative Heat Flux Measurement

Radiative heat flux incident on the refractory-lined side walls of the freeboard is measured by a Medtherm 48P-20-22K heat flux transducer during the steady state operation of the test rig.

The transducer is a Gardon gage with a diameter of 19 mm. Gardon gages absorb heat in a thin metallic circular foil and transfer the heat radially to the heat sink attached at the periphery of the foil, and the difference in temperature between the center and edge of the foil is related to the heat flux being absorbed [94, 95]. Design heat flux range of the transducer is 0-227 kW/m^2. The response is linear up to 150 % of this range. The certified calibration of the transducer is accurate to ± 3 % for most ranges. A sapphire

window attachment is installed to the transducer to eliminate convective mode of heat transfer, thus making the basic transducer a radiative heat flux transducer, or a radiometer. The sensor absorptance is 92 % in the spectral range of 0.6-15 μm, but spectrum transmitted by the sapphire window is 85 % in the spectral range of 0.15-5.0 μm. The view angle of the transducer is 150° with the window. With this sapphire window attachment, the sensitivity of the basic transducer is reduced to 79 % of the original. Air purging is provided around the periphery of the sapphire window to keep it clean. Water-cooled body of the transducer is provided with an integral K type thermocouple for body temperature measurement. Figure 6.3 shows a schematic view of the Medtherm heat flux transducer with water-cooling and gas purging provisions. Details of the transducer are available elsewhere [49, 86, 94].

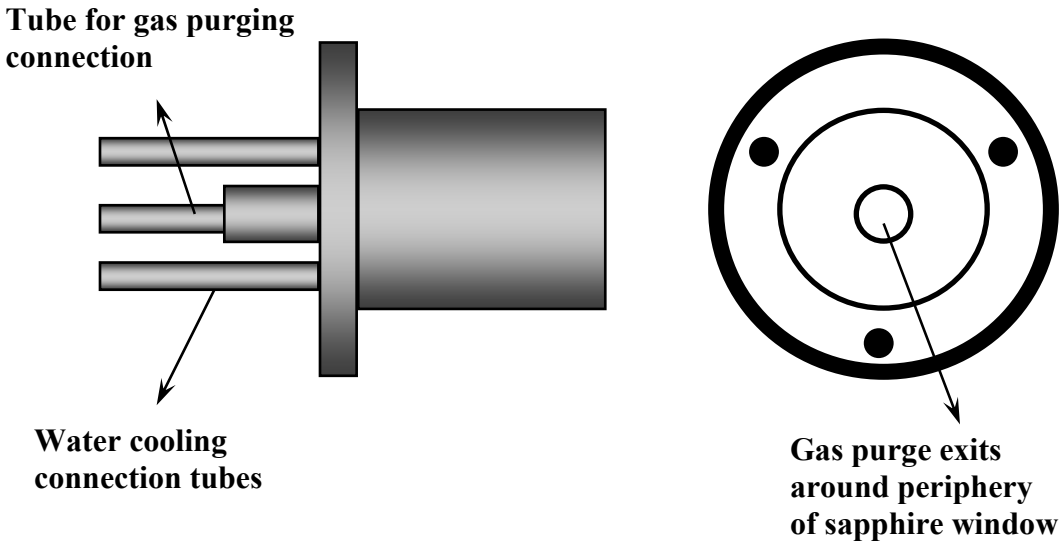

Figure 6.3: Radiative heat flux transducer [86].

Measurements were carried out by means of a probe formed by placing the heat flux transducer in a 25 mm outer diameter stainless steel tube with a provision of air cooling to prevent excessive heating of connection tubes and cables. A photograph of the radiometer probe is shown in Figure 6.4. The view angle of the transducer becomes 135° when it is placed in the probe and the sensitivity of the basic transducer is reduced to 69 % of the original.

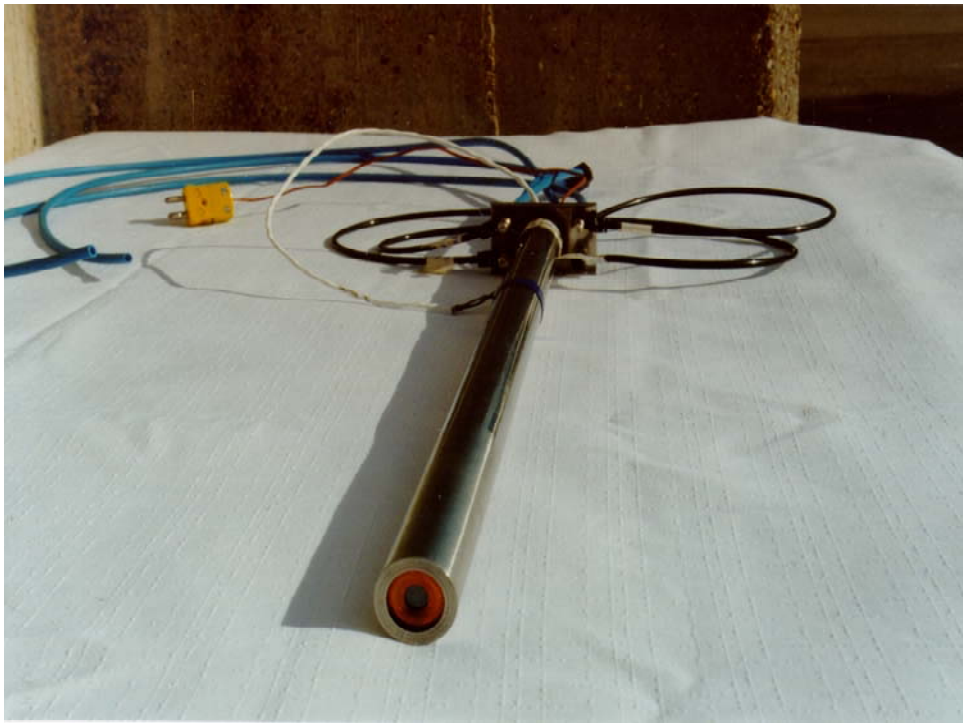

Figure 6.4: Radiometer probe [86].

In order to measure the radiative heat flux incident on refractory-lined side walls of the freeboard, the radiometer probe is inserted into the gas sampling ports flush with the inner surface of the refractory-lined side wall at five different heights along freeboard. The radiometer output for incident radiative heat flux is read from a voltmeter and transducer body temperature is read from a temperature transmitter. The voltmeter readings are then converted to heat fluxes using the certified calibration of the transducer also considering the reduced view angle.

6.2.8. Experimental Data from 0.3 MW_t ABFBC Test Rig

Experiments were carried out with Beypazarı lignite. Beypazarı lignite supplied by Turkish Coal Enterprises (TKİ) was delivered from Çayırhan lignite mine to Çayırhan Power Station of Turkish Electricity Generation and Transmission Co. (TEAŞ) where the coal to be burned in the test rig was prepared by crushing and sieving it through –4/+1.5 mm screens twice. Crushed and sieved lignite was then transported to the laboratory in closed barrels. Representative samples from coals were then subjected to sieve analyses and proximate and ultimate analyses. The results of these analyses together with the calorific value and particle density determined by mercury porosimetry are summarized in Table 6.4. As can be seen from the table, Beypazari lignite is a fuel with high VM/FC ratio (~2), high ash content (~42 %) and high total sulfur content (~4.5 %). Ash constituents of lignites are shown in Table 6.5. Very low calcium content of Beypazarı lignite ash is uncommon to the same lignite investigated previously [96].

The experiments consist of two combustion tests, without (Run 1) and with recycle (Run 2) of fine particles. In all the runs, the lignite was burned in its own ash due to its high ash content and without air staging. Experiments were carried out at recycle ratios of 0.0 and 2.37 without limestone addition for Run1 and Run 2, respectively. Feed point location was 0.85 *m* above the distributor plate for both experiments. Table 6.6 lists the operating conditions of the two experiments at steady-state. The properties of the carryover and baghouse filter streams required for the radiative property estimation is presented in Table 6.7. For radiative property estimation of particle-laden combustion gases, particles collected from both cyclone and baghouse downstream of the freeboard were subjected to particle size distribution analysis by laser light scattering technique. Measured size distributions are expressed by Rosin-Rammler function.

Table 6.4: Characteristics of Beypazarı lignite.

Sieve Analysis		Proximate Analysis (as received)		Ultimate Analysis (dry)	
Size (*mm*)	**Weight (*%*)**	**Component**	**Weight (*%*)**	**Component**	**Weight (*%*)**
4.000-3.350	11.5	Moisture	13.8	C	38.1
3.350-2.360	20.2	Ash	36.4	H	3.1
2.360-2.000	17.7	VM	32.7	O	12.4
2.000-1.700	16.8	FC	17.2	N	1.4
1.700-1.180	15.7	HHV: 3154 *cal/g*		S_{comb}	2.7
1.180-0.710	12.2	d_{32}: 1.26 *mm*		S_{total}	4.5
0.710-0.000	5.9	ρ_p: 1.58 g/cm^3		Ash	42.2

Table 6.5: Ash analyses of the lignite.

Component	Weight (*%*)
SiO_2	45.0
Al_2O_3	15.9
Fe_2O_3	7.7
CaO	1.0
MgO	3.0
SO_3	16.2
Na_2O	8.0
K_2O	1.5
TiO_2	1.8

Table 6.6: Operating conditions of the experiments.

	Run 1	**Run 2**
Coal flow rate, *kg/h*	101	101
Bed drain flow rate, *kg/h*	7	11
Cyclone ash flow rate, *kg/h*	24	27
Baghouse filter ash flow rate, *kg/h*	1.1	3.4
Recycle ratio*	0.0	2.37
Air flow rate, *kmol/h*	22	21
Excess air, *%*	43	36
Superficial velocity, *m/s*	3.0	2.8
Average bed temperature, *°C*	875	846
Average freeboard temperature, *°C*	847	905
Bed height, *m*	0.91	0.91
Feed point location, *m*	0.85	0.85
OHTC in the bed, W/m^2-*°C*	258	230
OHTC in the freeboard, W/m^2-*°C*	41	52
Bed cooling water flow rate, *kg/h*	1867	1839
Freeboard cooling water flow rate, *kg/h*	2214	4298
Mean beam length of freeboard, *m*	0.38	0.38

* Recycle ratio = (Recycle flow rate)/(Coal flow rate)

Table 6.7: Properties of fly ash streams.

	Run 1	**Run 2**
Carryover		
Particle density, kg/m^3	1029	931
Particle size range, μm	$0.5<d_p<710$	$0.5<d_p<850$
Rosin-Rammler coefficient b, -	0.0042	0.0013
Rosin-Rammler coefficient n, -	1.22	1.43
Baghouse filter		
Particle density, kg/m^3	536	633
Particle size range, μm	$0.5<d_p<124$	$0.5<d_p<68$
Rosin-Rammler coefficient b, -	0.078	0.051
Rosin-Rammler coefficient n, -	1.7	1.4

6.3. 16 MW_t Stationary Fluidized Bed Boiler

The effect of radiation in industrial boilers was investigated in the North American bituminous coal fired 16 MW_t SFBB located at Chalmers University of Technology [97]. Figure 6.5 illustrates the flow scheme for the boiler plant.

Due to the absence of detailed information on experimental data, only the radiation model, based on MOL solution of DOM, in isolation from the system model was applied to the freeboard of the boiler.

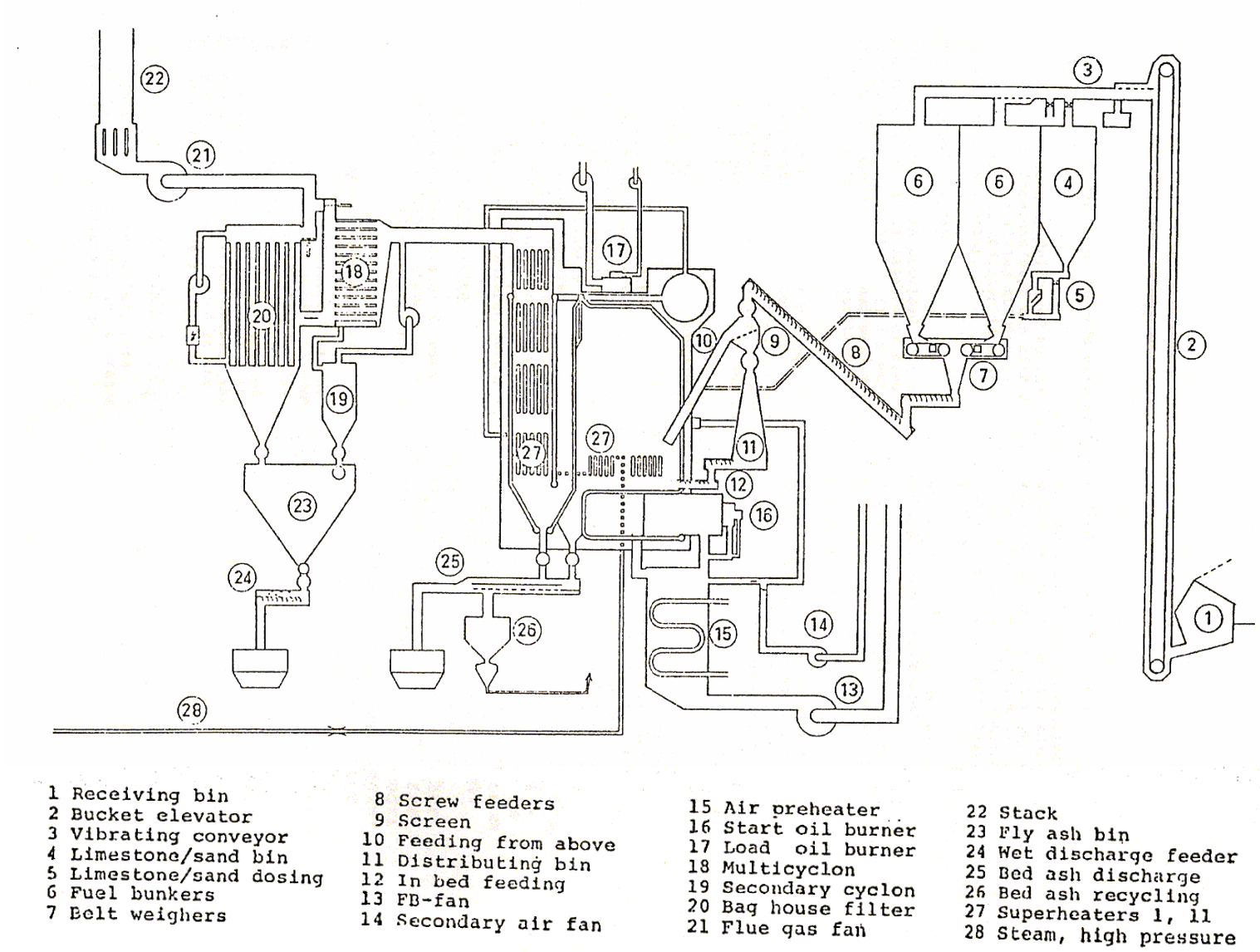

Figure 6.5: Flow sheet of 16 MW_t SFBB [99].

6.3.1. Description of the Boiler

The boiler is used to produce superheated steam (425^{o}C, 3.2 MPa) with a capacity of 16 MW. It is operated in bubbling regime at atmospheric pressure. The boiler has a cross section of 3.4 m × 2.9 m and 5.7 m height. It is bounded by conventional panel tube walls. A superheater tube bundle, which is immersed in the bed region of combustion chamber, consists of 10 double pass tubes with a vertical and horizontal pitch of 0.14 m and 0.15 m, respectively. The tube bundle is located 0.26 – 0.90 m from the rear wall and 0.62 – 1.07 m above the air nozzle openings. At various heights in the freeboard, gas temperature field is measured by a suction pyrometer. The detailed description of the boiler can be found elsewhere [98].

The total heat fluxes to freeboard walls are measured by conductivity type of heat flow meters during the steady-state operation of the boiler. The measured heat flux is the total heat flux including both radiation and particle and gas convection. The further details of the conductivity type of heat flow meter can be found elsewhere [47].

The steady state operating conditions of the experiments with bituminous coal carried out by Andersson et al. [97] are presented in Table 6.8. Temperature measurements were carried out on a discrete grid of points along the freeboard at steady state operation. In order to facilitate the use of these measurements as input data in the calculation of total heat exchange, the experimental data were represented by a high order polynomial given in Figure 6.6.

Table 6.8: Operating conditions for the experiment with bituminous coal [97].

Load, *%*	64
Total excess air ratio based on O_2, -	1.32
Air temperature, *°C*	51
Recycling ratio, *kg/kg fuel*	0.2
Bed height at operation, *m*	0.89
Fluidizing velocity, *m/s*	1.49
Bed temperature, *°C*	895
Flue gas temperature after freeboard exit, *°C*	671
Flue gas temperature at the boiler exit, *°C*	140

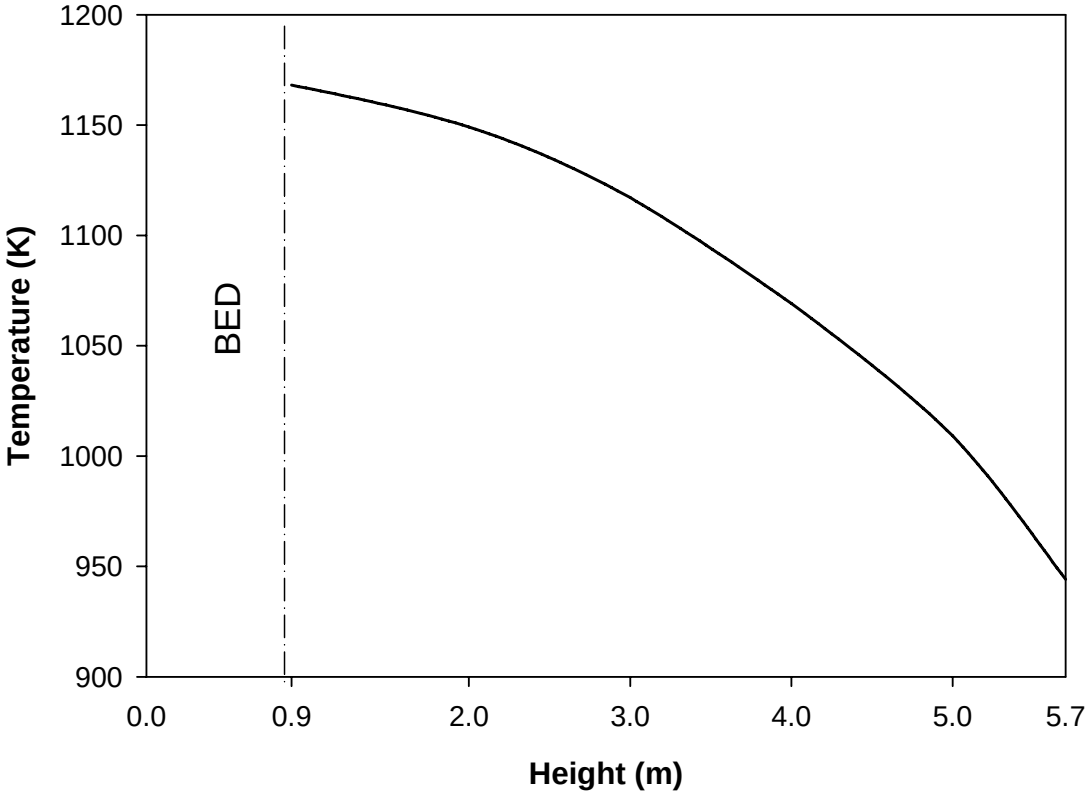

Polynomial for gas temperature profile;

$$T_g(z) = -0.3639\, z^5 + 5.6553\, z^4 - 33.015\, z^3 + 81.818\, z^2 - 104.6\, z + 1216.4$$

Figure 6.6: Temperature profile along the freeboard [97].

6.3.2. Approximation of the Freeboard as a 3-D Radiation Problem

The physical system under consideration is a 3-D rectangular enclosure containing gray, absorbing and emitting medium bounded by gray and diffuse walls (Figure 6.7).

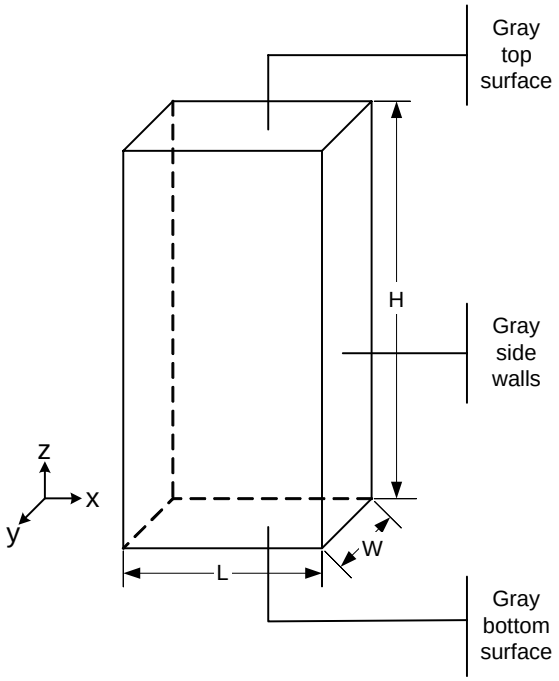

Figure 6.7: The coordinate system for the freeboard section of 16 MW_t SFBB.

In order to apply radiation model to the freeboard region of the boiler, it is required to provide temperatures and radiative properties of the surfaces and the medium in addition to the temperature profile given in Figure 6.6.

The radiative properties of the particle laden gaseous mixture, consisting of combustion gases (CO_2 and H_2O), bed material, ash, soot from combustion of hydrocarbons and ash particles, are assumed to be uniform and constant throughout the freeboard. The effective emissivities of the bounding surfaces, gas mixture and the particle laden gaseous mixture reported by Andersson et al.[97] are tabulated in Table 6.9.

Table 6.9: Effective emissivities of freeboard medium and surfaces.

Bed surface, ε_{bed}	0.8
Water-cooled walls, ε_w	0.8
Gas mixture, ε_g	0.28
Particle laden gaseous mixture, ε_f	0.42

The transmissivity of the gas mixture is calculated by,

$$\tau_g = \left(1 - \varepsilon_g\right) \tag{6.1}$$

The transmissivity of the particle cloud is calculated by using the gas transmissivity, τ_g, and the emissivity of particle laden gaseous mixture, ε_f, from,

$$\tau_p = \frac{\left(1 - \varepsilon_f\right)}{\tau_g} \tag{6.2}$$

The absorption coefficient of gas mixture is calculated by Leckner's correlations,

$$\kappa_g = -\frac{1}{L_m} ln\, \tau_g \tag{6.3}$$

and the particle absorption coefficient is calculated by using Bouguer's law,

$$\kappa_p = -\frac{1}{L_m} ln\, \tau_p \tag{6.4}$$

The dimensions of the enclosure, emissivities and temperatures of the surfaces and properties of the medium presented in Table 6.10 and freeboard temperature profile (Figure 6.6) are the input data for the radiation code.

Table 6.10: Input data for the radiation code.

Dimensions		
Length, L (m)		3.4
Width, W (m)		2.9
Heigth, H (m)		4.81
Mean beam length of freeboard, L_m (m)		2.12
Medium		
Gas absorption coefficient, κ_g (1/m)		0.15
Absorption coefficient of particle cloud, κ_p (1/m)		0.10
Absorption coefficient of the medium, $\kappa = \kappa_p + \kappa_g$ (1/m)		0.25
Boundaries	**Temperature, T (K)**	**Emissivity, ε**
Top surface	537.15	0.8
Side surfaces	537.15	0.8
Bottom surface	1168.15	0.8

The predictive accuracy of the radiation model can be investigated by comparing the predicted and measured incident radiative heat fluxes. However, instead of incident radiative heat fluxes, total heat fluxes were reported by Andersson et al. [97]. Therefore, for comparison, it is required to calculate total heat fluxes which include the convective and radiative heat exchange between the particle laden gas, the splashing bed surface and water-cooled freeboard walls.

In the evaluation of the convective heat transfer contribution, gas convection is calculated by using the gas convective heat transfer coefficient (Equation (3.84)) and particle convection is neglected due to the dilute medium of the freeboard.

In the evaluation of the radiative heat transfer contribution, the effect of scattering on radiation is neglected since scattering is negligible for particles with emissivities less than 0.5 to 0.8 [2].

CHAPTER 7

RESULTS AND DISCUSSION

7.1. General

The assessment of the accuracy of the FBC system model in conjunction with the radiation model was carried out by predicting the behavior of the lignite fired 0.3 MW_t ABFBC test rig for the lignite characteristics and operating conditions shown in Tables 6.4 and 6.6 and comparing the predictions with measurements. Axial temperature profiles, concentration profiles of O_2, CO and CO_2 throughout the combustor and incident radiative heat fluxes on the refractory-lined freeboard side walls were used as measures of performance to test the validity of the coupled code.

The input data required by the model includes the following:

1. Configuration and dimensions of the test rig and its internals
2. Radiative properties of bounding surfaces
3. Air and coal flow rates
4. Coal analysis
5. All solid and gas properties
6. Inlet temperatures of air, cooling water and feed solids
7. Size distribution function of feed solids and fly ash particles deduced from sieve analysis

Apart from these input data, in this study, following the approach of Selçuk et al. [51], a high order polynomial was utilized for the determination of freeboard wall temperature profile for Run 1. The polynomial developed by Selçuk et al. [51] was modified to reproduce the measured radiative heat fluxes incident on freeboard walls as accurately as possible. During Run 2, due to recycling of particles, higher freeboard temperatures and heat transfer between the particle laden flue gas and the walls were observed. Therefore, for Run 2, the wall and gas temperature profiles were assumed to be equal to each other. The freeboard wall temperature profiles used in Run 1 and Run 2 are depicted in Figure 7.1 and 7.2, respectively.

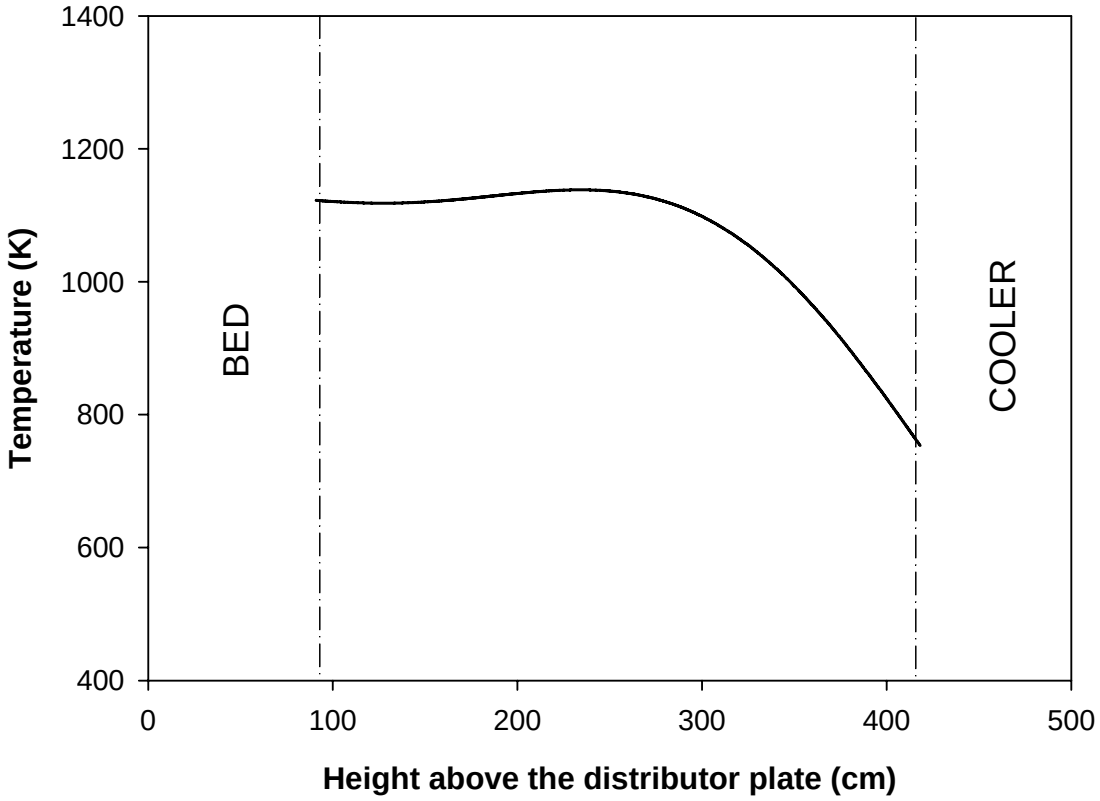

Polynomial for wall temperature profile;

$$T_w(z) = 4.9303\, z^5 - 56.239\, z^4 + 209.66\, z^3 - 318.96\, z^2 + 192.1\, z + 1089.2$$

Figure 7.1: Freeboard wall temperature profile for Run 1.

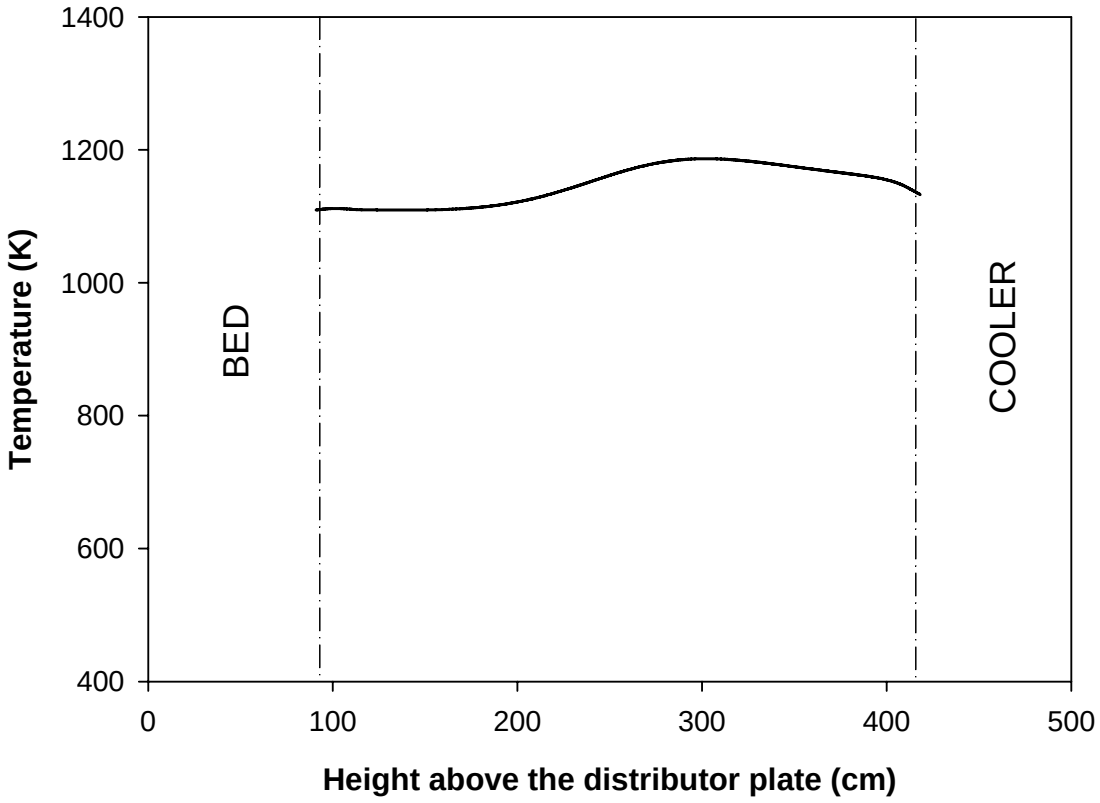

Figure 7.2: Freeboard wall temperature profile for Run 2.

The following sections of this chapter describe the comparison between measured and predicted temperature and concentration profiles and incident radiative heat fluxes on the freeboard walls. In order to investigate the effect of radiation in industrial boilers, the radiation model was applied to North American bituminous coal fired 16 MW_t Stationary Fluidized Bed Boiler at Chalmers University of Technology. In the last section of this chapter, the predictions of the radiation model are compared with the measurements and those of the single zone method.

7.2. 0.3 MW_t Atmospheric Bubbling Fluidized Bed Combustor

7.2.1. Temperature Profiles

Figures 7.3 and 7.4 illustrate the comparison between the predicted and measured medium temperatures along the combustor for Run 1 and Run 2, respectively. Inspection of the temperature profile for Run 1 shows that freeboard temperature decreases toward the cooler. However, the same trend is not observed in the freeboard temperature profile of Run 2. The comparison of the temperature profiles of the runs with and without recycle show that recycling of fly ash results in decrease in bed temperature and increase in freeboard temperature. Predicted and measured values are found to be in good agreement in both runs.

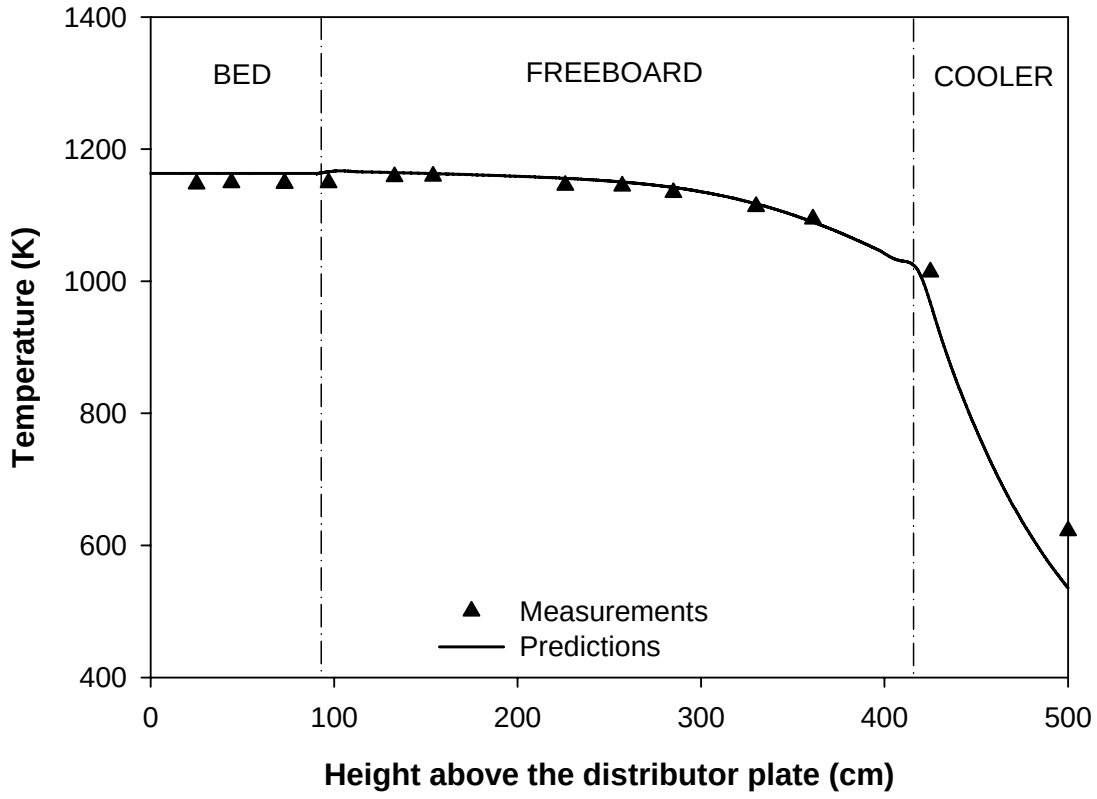

Figure 7.3: Measured and predicted temperature profiles for Run 1.

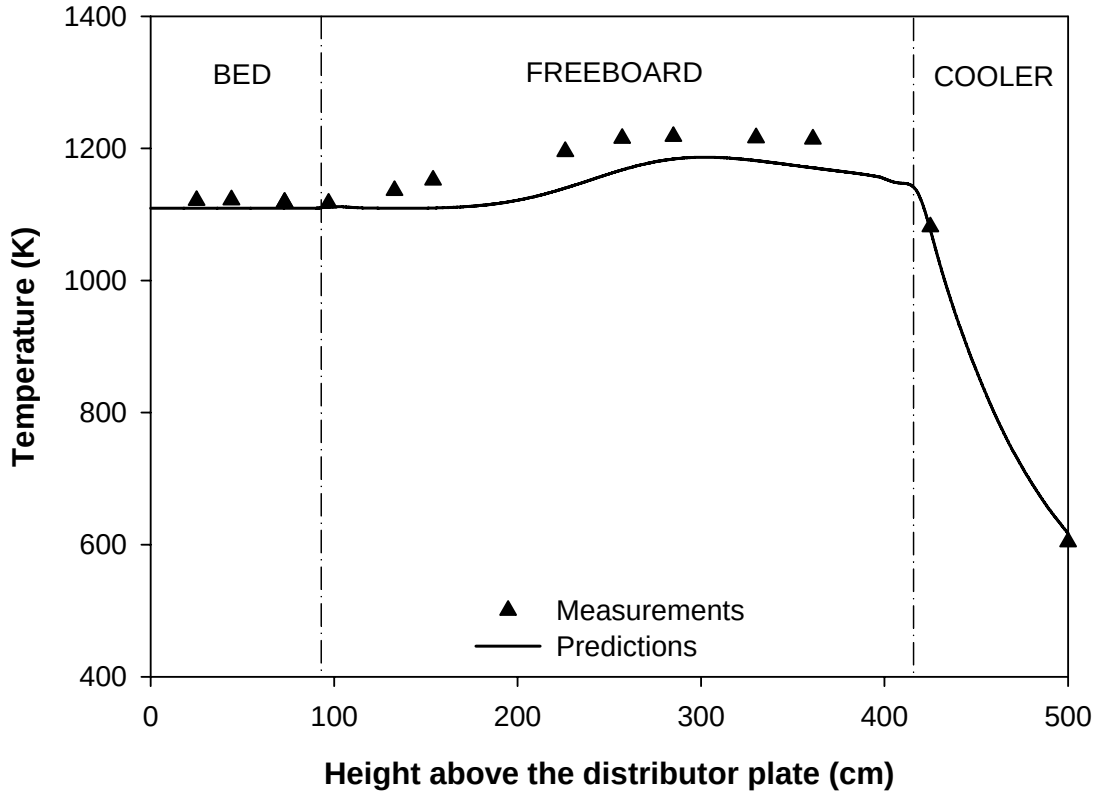

Figure 7.4: Measured and predicted temperature profiles for Run 2.

7.2.2. O_2, CO_2 and CO Concentration Profiles

Figures 7.5 and 7.6 compare the predicted and measured concentrations of O_2, CO_2 and CO on dry basis along the combustor for Run 1 and Run 2, respectively. As can be seen from the figures, measured O_2 concentrations decrease continuously until the bed surface whereas the measured CO_2 concentrations rise steeply along the bed. The same trend exists in the freeboard, however, with smaller gradients. CO measurements, on the other hand, show maxima in the bed and combustion continues in the freeboard rather slowly. As depicted in the figures, favorable comparisons are also obtained between the predicted and measured profiles. Comparison between Figure 7.5 and 7.6 shows that O_2 decreases and CO_2 and CO increase with recycle.

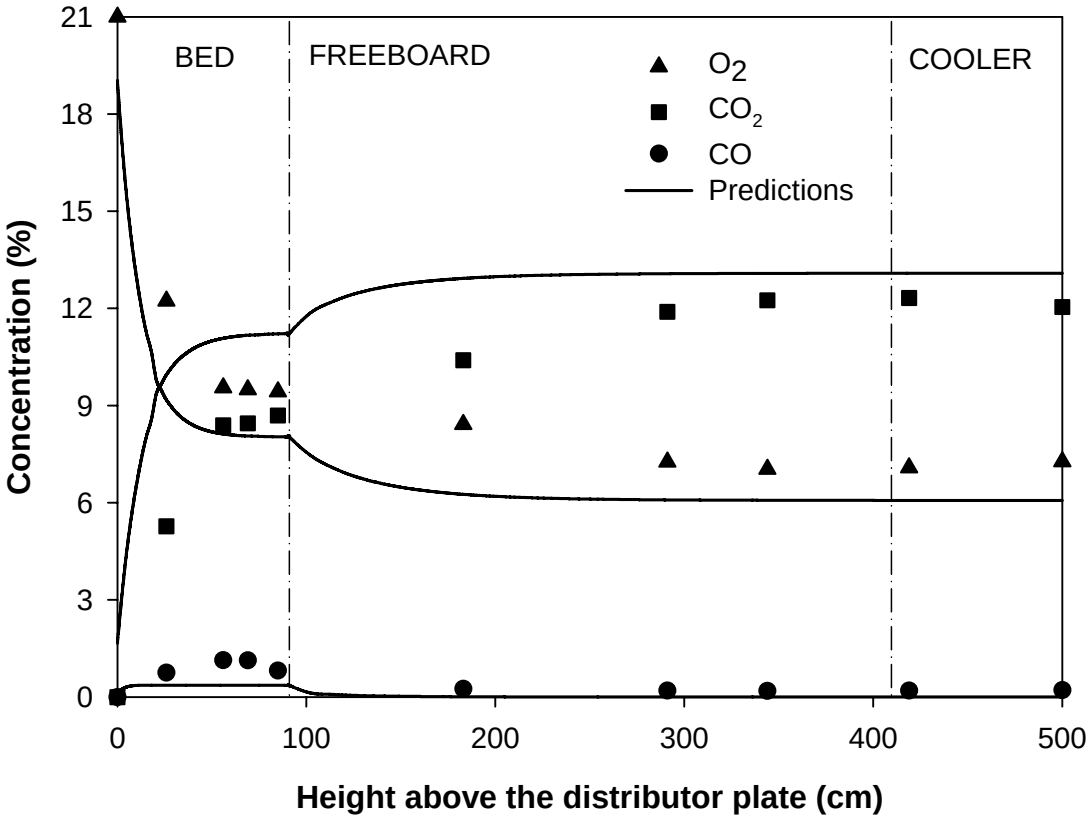

Figure 7.5: Measured and predicted O_2, CO_2, and CO concentrations for Run 1.

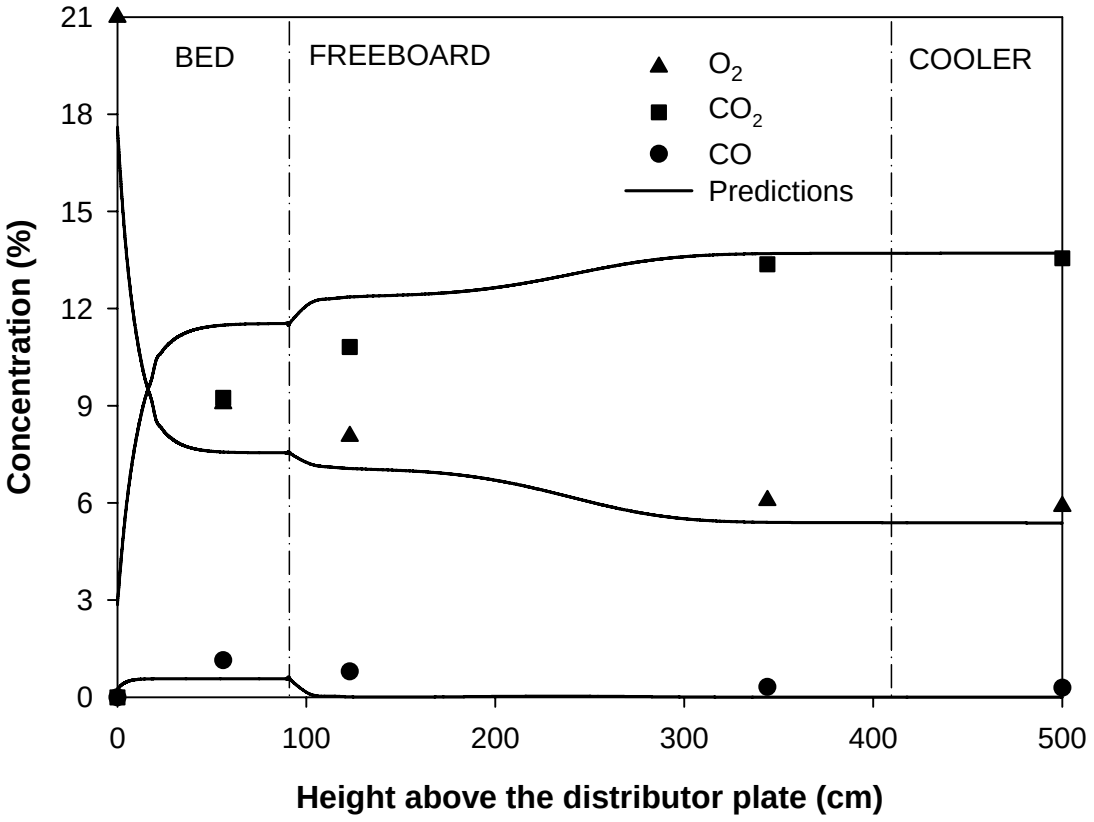

Figure 7.6: Measured and predicted O_2, CO_2, and CO concentrations for Run 2.

7.2.3. Incident Radiative Heat Fluxes on Freeboard Side Walls

For the prediction of source terms and incident radiative heat fluxes on freeboard walls, the radiative properties of the participating medium, consisting of combustion gases and fly ash particles, were assumed to be uniform and constant throughout the freeboard region. This assumption was based on uniform CO_2 and H_2O concentrations measured along the freeboard and the fact that particle concentration and size distribution was represented by the material sampled from the cyclone and baghouse filter [96]. Radiative properties of the medium and surfaces are presented in Table 7.1. As can be seen from the table, absorption and scattering coefficients of particles are

significantly higher in Run 2 compared to Run 1 due to the higher concentration of particles inside the freeboard caused by the recycling fly ash particles.

Table 7.1: Radiative properties of the medium and the surfaces.

	Run 1	**Run 2**
Gas absorption coefficient, κ_g (1/m)	0.44	0.43
Absorption coefficient of particle cloud, κ_p (1/m)	0.48	4.28
Scattering coefficient of particle cloud, σ_s (1/m)	1.80	9.66
Extinction coefficient of the particles, $\beta_p = \kappa_p + \sigma_s$ (1/m)	2.28	13.94
Absorption coefficient of the medium, $\kappa = \kappa_p + \kappa_g$ (1/m)	0.92	4.71
Extinction coefficient of the medium, $\beta = \kappa + \sigma_s$ (1/m)	2.72	14.37
Scattering albedo of the medium, $\omega = \sigma_s / \beta_p$	0.79	0.69
Emissivity of top surface, ε_{top}	0.87	0.87
Emissivity of side surfaces, ε_w	0.33	0.33
Emissivity of bottom surface, ε_{bottom}	1.00	1.00
Temperature of top surface, T_{top} (K)	747	830
Temperature of bottom surface, T_{bottom} (K)	1163	1109

The incident radiative heat flux predictions along the freeboard walls from the first run without recycle and second run with recycle are compared with the measurements in Table 7.2. As can be seen from the table, the predictions are in good agreement with the measurements. For both runs, the incident flux decreases from the bed surface toward the cooler and is minimum at the top due to the effect of cooler tubes. The fluxes near the bed surface are close to each other. As one proceeds higher along the freeboard, radiative heat flux from the case with recycle increases considerably when compared to that of the case without recycle. The recycle causes about 46 % rise of

radiative heat flux at 3.44 m height. This behavior is attributed to the significant freeboard temperature rise in the second run.

Table 7.2: Incident radiative heat fluxes on freeboard side walls.

Height (m)	Measurements (kW/m^2)	Predictions (kW/m^2)	Relative error* (%)
Run 1			
1.23	105.0	97.9	-6.8
1.83	106.3	97.5	-8.2
2.91	100.0	89.4	-10.6
3.44	81.3	71.7	-11.7
4.19	22.5	35.5	57.8
Run 2			
1.23	95.0	86.0	-9.5
3.44	118.8	108.7	-8.5
4.19	62.5	77.6	24.1

* Relative error % = (Prediction - Measurement) / Measurement * 100

Significant discrepancy between the predictions and the measurements at the uppermost port is considered to be due to the fact that the top surface of the enclosure is approximated by an equivalent gray surface consisting of cold tube-row/hot gas-lane combination for modeling purposes whereas the radiometer probe is affected mostly by the cooling tubes as the port for the measurement is located nearly adjacent to a cooler tube.

Effect of using non-uniform gas absorption coefficient instead of a uniform one for the freeboard medium on the accuracy of the predicted temperatures and heat fluxes was also investigated in this thesis study. Non-uniform gas absorption coefficient was calculated by using the point values of gas temperature and composition at each grid point from Leckner's correlation (Equation (4.10)). Figures 7.7 and 7.8 illustrate the

comparison between the gas temperature predictions using uniform and non-uniform absorption coefficients for Run 1 and Run 2, respectively. Comparisons show that use of non-uniform absorption coefficient has no significant effect on the predictions of the medium temperatures.

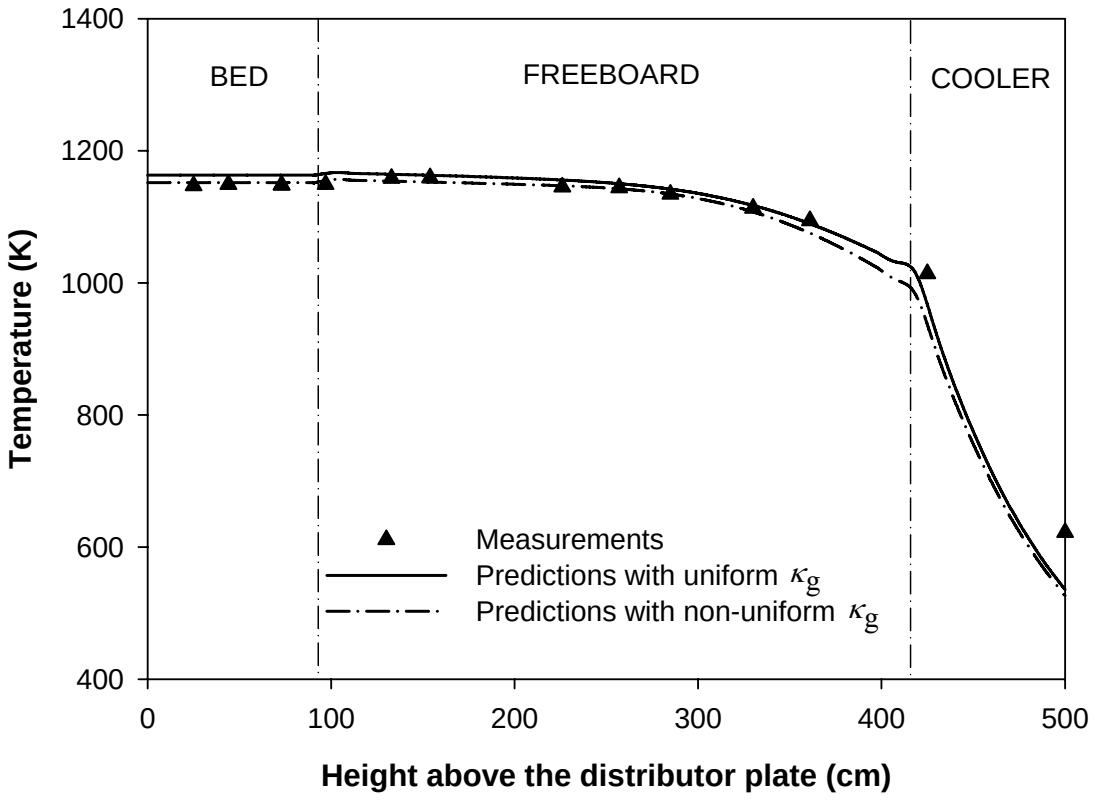

Figure 7.7: Comparison between the measurements and predictions of temperature profiles with uniform and non-uniform gas absorption coefficients for Run 1.

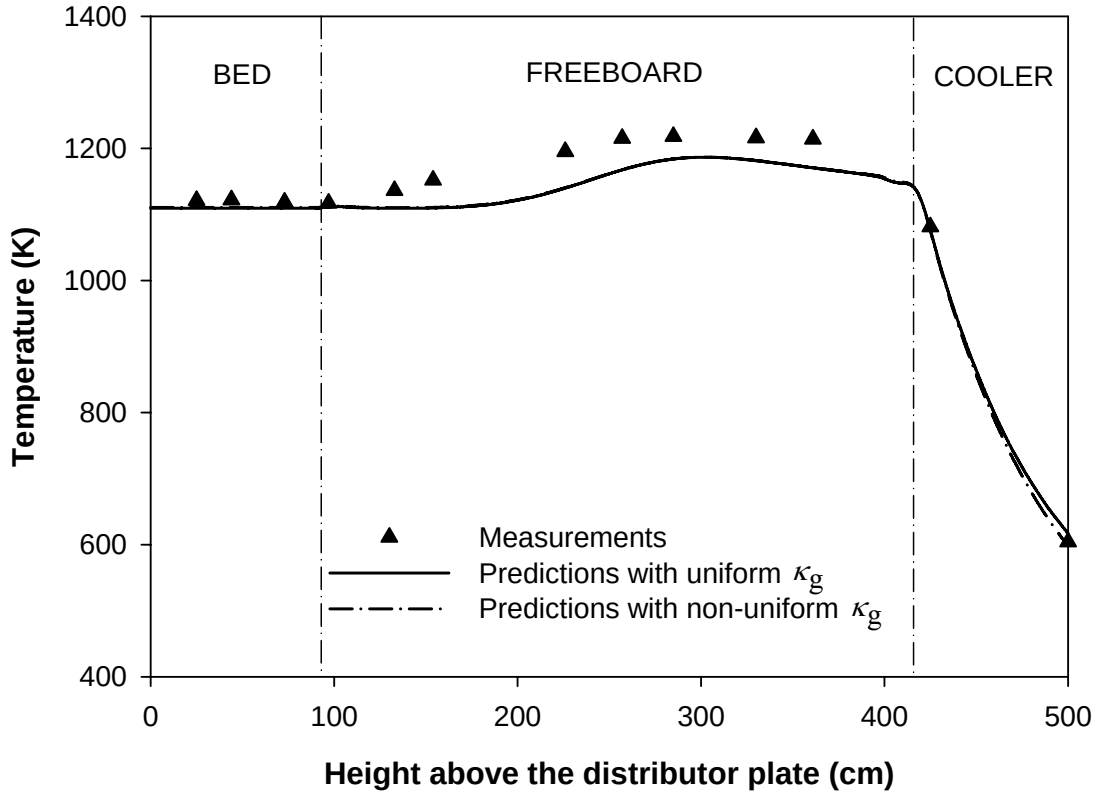

Figure 7.8: Comparison between the measurements and predictions of temperature profiles with uniform and non-uniform gas absorption coefficients for Run 2.

Table 7.3 shows the comparison between the measurements and predictions of incident radiative heat fluxes with uniform and non-uniform absorption coefficients. As can be seen from the table, using non-uniform gas absorption coefficient leads to slight improvement of the accuracy with additional cost in computational time. Therefore, uniform absorption coefficient can be used for the calculation of radiative heat fluxes of 0.3 MW_t ABFBC.

Table 7.3: Comparison between the measurements and predictions of incident radiative heat fluxes with uniform and non-uniform gas absorption coefficients.

Absorption coefficient, κ_g	Height (m)	Measurements (kW/m²)	Predictions (kW/m²)	Relative error* (%)	CPU time** (s)
Run 1					
Uniform	1.23	105.0	97.9	-6.8	294
	1.83	106.3	97.5	-8.2	
	2.91	100.0	89.4	-10.6	
	3.44	81.3	71.7	-11.7	
	4.19	22.5	35.5	57.8	
Non-uniform	1.23	105.0	99.1	-5.6	314
	1.83	106.3	98.3	-7.5	
	2.91	100.0	91.7	-8.3	
	3.44	81.3	78.0	-4.0	
	4.19	22.5	41.7	85.4	
Run 2					
Uniform	1.23	95.0	86.0	-9.5	298
	3.44	118.8	108.7	-8.5	
	4.19	62.5	77.6	24.1	
Non-uniform	1.23	95.0	86.3	-9.1	341
	3.44	118.8	108.8	-8.4	
	4.19	62.5	79.9	27.9	

* Relative error % = (Prediction - Measurement) / Measurement * 100

** The CPU times reported correspond to 1.60 GHz Intel Pentium M computer

7.2.4. Significance of Coupling of Radiation Model with System Model

For the investigation of significance of coupling of the radiation model with the system model, temperature predictions of the coupled code are compared with those obtained

by the original system model where radiation was taken into account by incorporation of particle to gas heat exchange through Stefan-Boltzmann law in freeboard energy conservation equation. Figures 7.9 and 7.10 show the comparison between predicted and measured temperature profiles for runs without and with recycle, respectively. As can be seen from the figures, the effect of incorporating a radiation model into the system model on the predictions of temperatures is not significant, because the high temperatures of refractory-lined freeboard walls and high surface to volume ratio *(Surface area/Volume=9.4)* of the test rig under consideration cause the incident radiative heat fluxes to be dominated by wall rather than particle laden gas emissions.

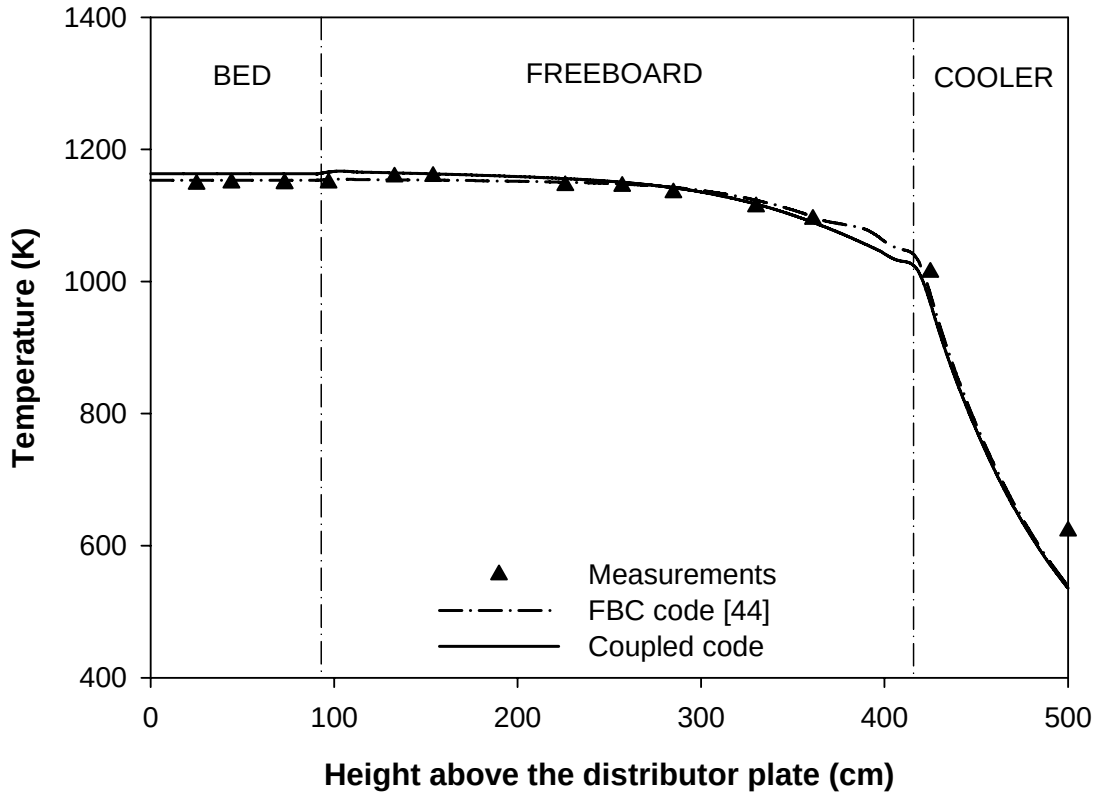

Figure 7.9: Comparison between the measurements and predictions of temperature profiles obtained from FBC code and coupled code for Run 1.

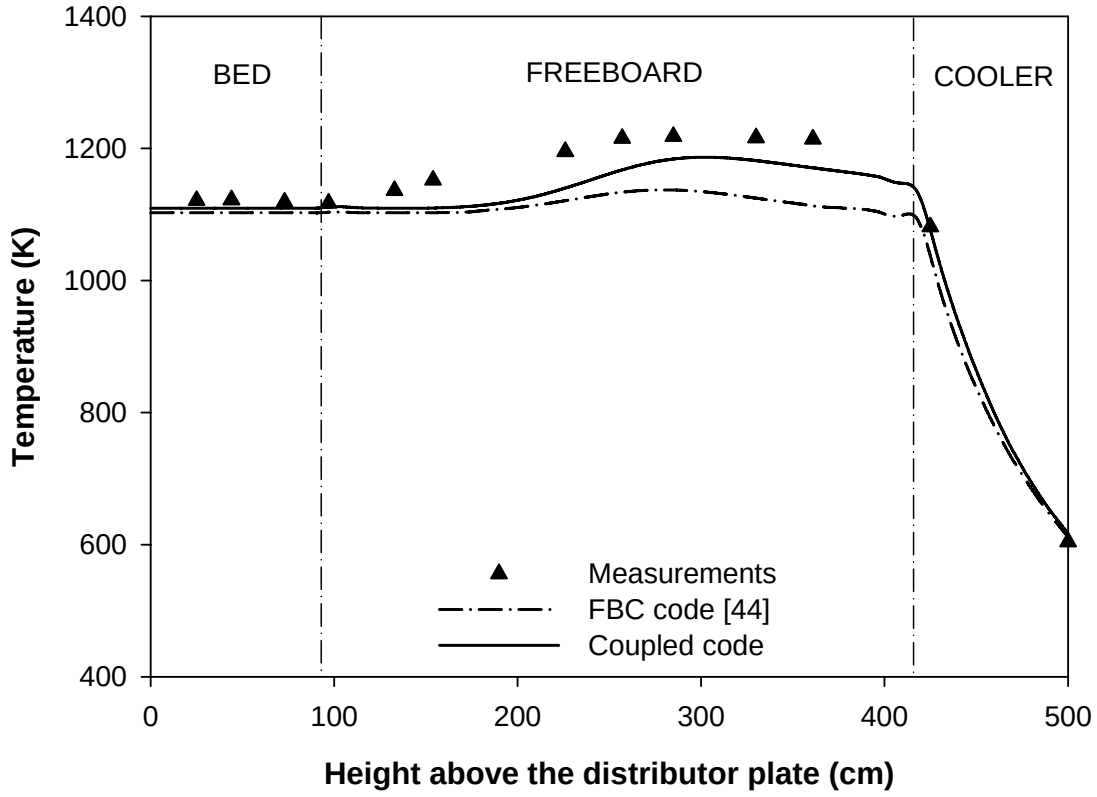

Figure 7.10: Comparison between the measurements and predictions of temperature profiles obtained from FBC code and coupled code for Run 2.

However, in industrial boilers, freeboard is surrounded by water-cooled membrane walls which are considerably cooler than the combustion gases. Boilers also have much lower surface to volume ratio. In order to examine the effects of both on radiation in industrial boilers, an investigation was carried out on 16 MW_t Stationary Fluidized Bed Boiler.

7.3. Performance of the Radiation Model on the Freeboard of 16 MW_t SFBB

The predictive accuracy of the radiation model based on MOL solution of DOM is assessed by applying it to the freeboard of the 16 MW_t Stationary Fluidized Bed Boiler

and comparing its predictions with measurements and with predictions obtained by Andersson et al. [97] by using single zone method. As can be seen in Figure 7.11, reasonably good agreement is achieved between the predictions of MOL solution of DOM and measurements, and MOL solution of DOM produces more accurate results compared to single zone method especially at the axial locations where particle load is higher. Discrepancy between predictions and measurements is considered to be due to low surface to volume ratio *(Surface area/Volume=1.7)* of SFBB which leads to incident heat fluxes to be dominated by particle laden gas emissions. Therefore, accurate treatment of the medium necessitates use of non-uniform radiative properties. However, it was not possible to calculate local absorption coefficients as the local gas concentrations and particle concentration, composition, and size distribution were not available.

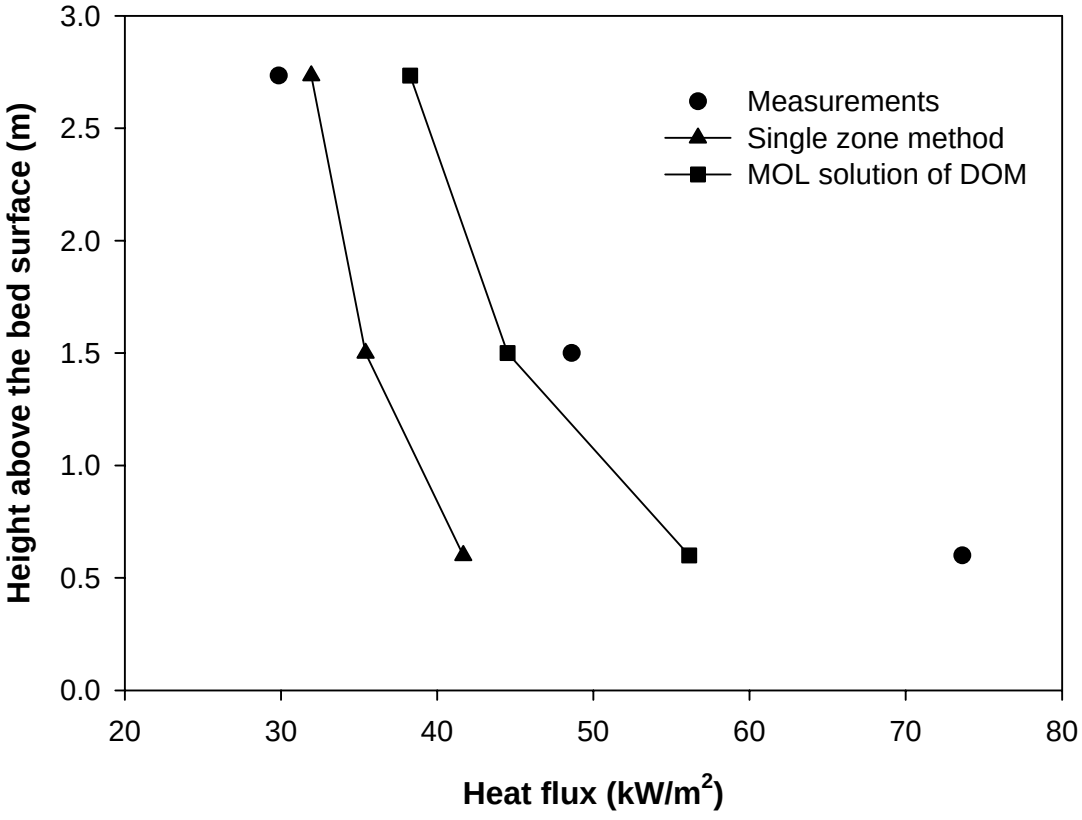

Figure 7.11: Comparison between the measurements and predictions of total heat fluxes with single zone method and MOL solution of DOM.

Many researchers showed that the particle load decreases exponentially as one proceeds higher along the freeboard [61, 99, 100]. Since particle absorption coefficient is directly proportional with the particle loading, it can be also represented by an exponential decay function. In this study, in an attempt to see the effect of using exponential decay function for estimation of particle absorption coefficient, constants of the function were adjusted to reproduce the measured heat fluxes. Heat fluxes predicted by MOL solution of DOM by using the decay function were compared with the measurements and comparison is shown in Figure 7.12. Favorable agreement demonstrates the significance of accurate particle loading and hence particle property estimation in prediction of performance of fluidized bed boilers.

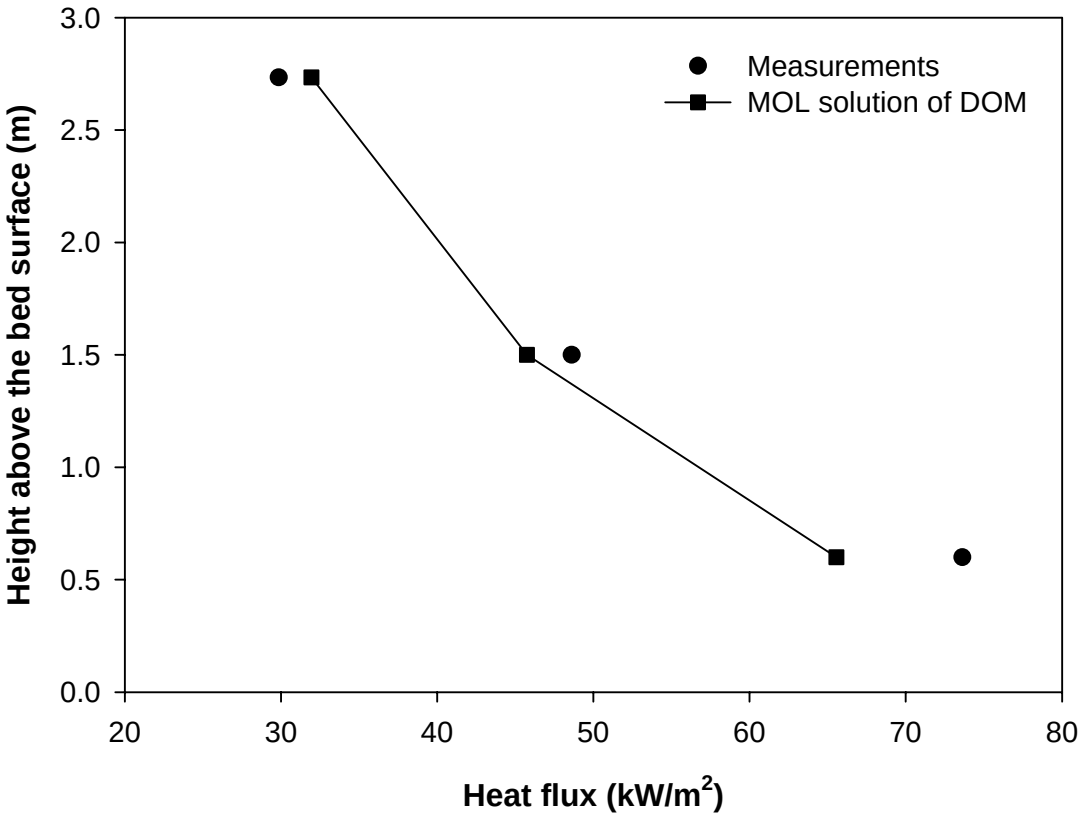

Figure 7.12: Comparison between the measurements and predictions of heat fluxes using non-uniform particle absorption coefficient.

CHAPTER 8

CONCLUSIONS

Simultaneous solution of the conservation equations for mass, momentum, energy and species in conjunction with radiative transfer equation was carried out by coupling two independent, previously developed and tested codes: (i) a FBC system model which accounts for bed and freeboard hydrodynamics, volatiles releases and combustion, char particles combustion and size distribution, attrition, sulfur retention and heat transfer, (ii) a radiation model for freeboard region, which is based on MOL solution of DOM for a 3-D rectangular enclosure containing gray, absorbing, emitting and isotropically scattering medium bounded by gray and diffuse walls.

The predictive performance of the coupled code was tested by comparing its predictions with measurements obtained from two combustion tests carried out by burning a typical Turkish lignite, Beypazarı, in a 0.3 MW_t Atmospheric Bubbling Fluidized Bed Combustor in its own ash with and without recycling of fly ash particles. On the basis of comparisons, the following conclusions have been reached:

- Temperature predictions of the model are found to be in good agreement with measurements. Recycling of fine particles leads to decrease in bed temperatures and increase in freeboard temperatures.

- O_2, CO and CO_2 concentration profiles predictions of the model are generally in good agreement with the experimental data. O_2 decreases and CO and CO_2 increase with recycle.
- Recycling of fine particles increases radiative properties of solid particles due to higher concentration of particles inside the freeboard.
- Predicted radiative heat fluxes incident on refractory-lined freeboard walls are in good agreement with measurement. Recycling fine particles increases radiative heat fluxes due to higher particle load and higher freeboard temperatures.
- Using non-uniform gas absorption coefficient was found to improve the accuracy only slightly.
- The effect of incorporating a radiation model into the system model on predictions is not significant, as high temperatures of refractory-lined freeboard walls and high surface to volume ratio *(Surface area/Volume=9.4)* of the test rig cause the incident radiative heat fluxes to be dominated by wall rather than particle laden gas emissions.

In order to investigate performance of the radiation model in an industrial boiler, the radiation model was also applied to North American bituminous coal fired 16 MW_t Stationary Fluidized Bed Boiler at Chalmers University of Technology. The predictive accuracy of the radiation model based on MOL solution of DOM is assessed by comparing its predictions with measurements and the predictions obtained by single zone method. Based on the results obtained following conclusions have been reached:

- Reasonably good agreement is achieved by MOL solution of DOM with measurements.
- MOL solution of DOM produces more accurate results compared to single zone method especially at the axial locations where particle load is higher.
- Discrepancy between predictions and measurements is considered to be due to low surface to volume ratio *(Surface area/Volume=1.7)* of SFBB which

leads to incident heat fluxes to be dominated by particle laden gas emissions.

- Using non-uniform absorption coefficient of solid particles was found to improve the accuracy significantly.

In consequence, the predictive ability, flexibility in the incorporation of various sub-models and the computational efficiency of this coupled code presented in this study makes it a promising tool for the evaluation performance of bubbling fluidized bed boilers.

8.1. Suggestions for Future Work

Based on the experience gained in the present study, the following recommendations for future extension of the work are suggested.

- Performance of coupled code is sensitive to the empirical correlations utilized for distribution of particle load along the freeboard region. Experimental investigation for particle load profile in freeboard is necessary.
- The wall energy balance is required to be coupled to freeboard heat transfer model to decrease the dependence on the measurements.
- Since the radiative properties of a medium depend on wavelength, a non-gray radiation model of the freeboard region is required to be incorporated into coupled code.

REFERENCES

1. Lindsay, J.J., Morton, W. and Newey, D.C., "Radiative Heat Transfer in the Freeboard of a Fluidised Bed", *Proceedings of the Fifth Engineering Foundation Conference on Fluidization*, Engineering Foundation, New York, N.Y., pp. 385-392, 1986.

2. Andersson, B.-Å., Johnsson, F. and Leckner, B., "Heat Flow Measurements in Fluidized Bed Boilers", *The 9th Int. Conf. on Fluidized Bed Combustion*, ASME Book No 10232, 1, New York, pp. 592-598, 1987.

3. Filla, M., Scalabrin, A., "Influence of Scattering of Thermal Radiation by Suspended Particles on the Rate of Heat Transfer in the Freeboard of a 1 MW_t Fluidized Bed Combustor", *Proceedings of the Eurotherm Seminar: Heat Transfer Radiating and Combusting System-2*, pp. 37-49, 1994.

4. Selçuk, N., Batu, A. and Ayranci, I., "Performance of Method of Lines Solution of Discrete Ordinates Method in the Freeboard of a Bubbling Fluidized Bed Combustor", *Journal of Quantitative Spectroscopy & Radiative Transfer*, vol. 73, no. 2-5, pp. 503-516, 2002.

5. Selçuk, N., Sivrioğlu, Ü., "Mathematical Modeling of Coal-Fired Fluidized Beds", *Journal of Thermal Sciences and Technology (in Turkish)*, vol. 3, no. 1, pp. 31-38, 1980.

6. Selçuk, N., Degirmenci, E. and Gogebakan, Y., "Modeling of a Bubbling AFBC with Volatiles Release", *Journal of Energy Resources Technology - Transactions of the ASME*, vol. 125, no. 1, pp. 72-81, 2003.

7. Altindag, H., Gogebakan, Y. and Selçuk, N., "Sulfur Capture for Fluidized-Bed Combustion of High-Sulfur Content Lignites", *Applied Energy*, vol. 79, no. 4, pp. 403-424, 2004.

8. Becker, H.A., Beér, J.M. and Gibbs, B.M., "A Model for Fluidized-Bed Combustion of Coal", *Institute of Fuel Symposium Series No. 1: Fluidised Combustion*, pp. A1-1-A1-10, 1975.

9. Gordon, A.L., Amundson, N.R., "Modeling of Fluidized Bed Reactors-IV: Combustion of Carbon Particles", *Chemical Engineering Science*, vol. 31, no. 12, pp. 1163-1178, 1976.

10. Chen, T.P., Saxena, S., "Mathematical Modeling of Coal Combustion in Fluidized Beds with Sulfur Emission Control by Limestone or Dolomite", *Fuel*, vol. 56, no. 4, pp. 401-413, 1977.

11. Horio, M., Wen, C.Y., "Simulation of Fluidized Bed Combustors: Part 1. Combustion Efficiency and Temperature Profile", *AIChE Symposium Series: Fluidization: Application to Coal Conversion Processes*, vol. 74, no. 176, pp. 101-110, 1978.

12. Sarofim, A.F., Beér, J.M., "Modelling of Fluidized Bed Combustion", *Proceedings of the 17th Symposium (International) on Combustion*, 1978.

13. Saxena, S.C., Grewal, N.S. and Venkataramana, M., *Modeling of a Fluidized Bed Combustor with Immersed Tubes*, University of Illinois, Chicago, Report FE-1787-10, 1978.

14. Gordon, A.L., Carami, H.S. and Amundson, N.R., "Modeling of Fluidized Bed Rectors-V: Combustion of Carbon Particles - An Extension", *Chemical Engineering Science*, vol. 33, no. 6, pp. 713-722, 1978.

15. Beér, J.M., Baron, R.E., Borghi, G., Hodges, J.L. and Sarofim, A.F., "A Model of Coal Combustion in Fluidized Bed Combustors", *Proceedings of the International Conference on Fluidized Bed Combustion*, ASME, pp. 437-456, 1978.

16. Fan, L.T., Tojo, K. and Chang, C.C., "Modeling of Shallow Fluidized Bed Combustion of Coal Particles", *Industrial Engineering Chemical Process Des. Dev.*, vol. 18, no. 2, pp. 333-337, 1979.

17. Rajan, R.R., Wen, C.Y., "A Comprehensive Model for Fluidized Bed Coal Combustors", *AIChE Journal*, vol. 26, no. 4, pp. 642-655, 1980.

18. Congalidis, J.P., Georgakis, C., "Multiplicity Patterns in Atmospheric Fluidized Bed Coal Combustors", *Chemical Engineering Science*, vol. 36, no. 9, pp. 1529-1546, 1981.

19. Chakraborty, R.K., Howard, J.R., "Combustion of Char in Shallow Fluidized Bed Combustors: Influence of Some Design and Operating Parameters", *Journal of the Institute of Energy*, vol. 48, no. 418, pp. 48-54, 1981.

20. Park, D., Levenspiel, O. and Fitzgerald, T.J., "Plume Model for Large Particle Fluidized-Bed Combustors", *Fuel*, vol. 60, no. 4, pp. 295-306, 1981.

21. Bukur, D., Amundson, N.R., "Fluidized Bed Char Combustion Kinetic Models", *Chemical Engineering Science*, vol. 37, no. 1, pp. 17-25, 1982.

22. Chang, C.C., Rong, S.X. and Fan, L.T., "Modelling of Shallow Fluidized Bed Reactors: Ii. Analytical and Numerical Solutions", *The Canadian Journal of Chemical Engineering*, vol. 60, pp. 781-795, 1982.

23. Chen, L.H., Wen, C.Y., "Model of Solid Gas Reaction Phenomena in the Fluidized Bed Freeboard", *AIChE Journal*, vol. 28, no. 6, pp. 1019-1027, 1982.

24. Overturf, B.W., Reklaitis, G.V, "Fluidized-Bed Reactor Model with Generalized Particle Balances", *AIChE Journal*, vol. 29, no. 5, pp. 813-828, 1983.

25. Walsh, P.M., Dutta, A. and Beér, J.M., "Char Combustion in the Freeboard above a Fluidized Bed Burning a High Volatile Bituminous Coal", *Proceedings of the 20th Symposium (International) On Combustion*, 1984.

26. Brem, G., *Overall Modeling of Atmospheric Fluidized Bed Combustion and Experimental Verification*, in *Atmospheric Fluidized Bed Coal Combustion Research Development and Application*, M. Valk, Editor, Elsevier: Amsterdam. pp. 185-225, 1995.

27. Dixit, V.B., Holmes, M.L. and Carson, W.R., "A Predictive Model for the Freeboard Performance in a Fluidized Bed Combustor Operating in the Bubbling Mode", *Proceedings of the 7th International Conference on Fluidization*, Engineering Foundation, New York, N.Y., pp. 604-612, 1986.

28. Lemcoff, N.O., "Fluidized Bed Combustion of High Ash Chars", *Combust. Sci. and Tech.*, vol. 62, pp. 131-147, 1988.

29. Brem, G., "A Mathematical Model as a Tool for Simulation and Optimization of Coal Combustion in an Atmospheric FBC", *Proceedings of the 4th International Fluidized Bed Conference: Fluidized Combustion in Practice: Clean, Versatile, Economic?* pp. II/11/1-14, 1988.

30. Ho, T.C., Kirkpatrick, M. and Hopper, J.R., "Mixing and Combustion in a Shallow Coal-Limestone Fluidized Bed Combustor", *The Canadian Journal of Chemical Engineering*, vol. 67, pp. 207-217, 1989.

31. de Souza-Santos, M.L., "Comprehensive Modeling and Simulation of Fluidized-Bed Boilers and Gasifiers", *Fuel*, vol. 68, no. 12, pp. 1507-1521, 1989.

32. Trevino, C., Herrera, C. and Ybarra, P.G., "Stability Analysis of a Simplified Model of a Fluidized Bed Combustor", *Combustion and Flame*, vol. 80, no. 3-4, pp. 399-411, 1990.

33. Adanez, J. and J.C. Abadanes, Labiano, F. G. and De Diego, L. F., "Carbon Efficiency in Atmospheric Fluidized Bed Combustion of Lignites", *Fuel*, vol. 71, pp. 417-424, 1992.

34. Lin, W., Bu, J., Korbee, R., Svoboda, K. and van der Bleek, C.M., "Modelling SO_2 and NO_x Emissions in Fluidized Bed Combustion of Coal", *Fuel*, vol. 72, no. 3, pp. 299-304, 1993.

35. Goel, S.K., Beér, J.M. and Sarofim, A.F., "Significance of Destruction Reactions in Determining Net Emission of Nitrogen Oxides", *13th International Conference on Fluidized Bed Combustion*, ASME, pp. 887-898, 1995.

36. Sriramulu, S., Sane, S., Agarwal, P. and Mathews, T., "Mathematical Modeling of Fluidized Bed Combustion: 1. Combustion of Carbon in Bubbling Beds", *Fuel*, vol. 75, no. 12, pp. 1351-1362, 1996.

37. Reddy, G.V., Sinha, A., "A Mathematical Model for Coal Combustion in a 10 MW FBC Power Plant", *Energy*, vol. 22, no. 4, pp. 381-387, 1997.

38. Huilin, L., Guangbu, Z., Ruoshan, B., Lidan, Y. and Yukun, Q., "Modelling of Coal Combustion in a 25-MW FBC Power Plant", *Energy*, vol. 24, no. 3, pp. 199-208, 1999.

39. Kulasekaran, S., Linjewile, T.M. and Agarwal, P.K., "Mathematical Modeling of Fluidized Bed Combustion 3. Simultaneous Combustion of Char and Combustible Gases", *Fuel*, vol. 78, no. 4, pp. 403-417, 1999.

40. Ilic, M.S., Oka, S.N. and Vesna, B.B., "Combustion of a Porous Char Particle in Fluidized Bed - Mathematical Model and Experimental Results", *Proceedings of the Mediterranean Combustion Symposium MSC-99*, pp. 866-877, 1999.

41. Mançuhan, E., "Modelling of Combustion of Low Grade Lignites in Fluidized Beds with Heat Extraction ", *Proceedings of the 15th International Conference on Fluidized Bed Combustion*, ASME, Paper No. FBC99-0015, 1999.

42. Değirmenci, E., *Dynamic Simulation of Fluidized Bed Combustors*, Ph.D. Thesis, METU, Ankara, Turkey, 2000.

43. Chen, Z., Lin, M., Ignowski, J., Kelly, B., Linjewile, T.M. and Agarwal, P.K., "Mathematical Modeling of Fluidized Bed Combustion. 4: N_2O and NO_x Emissions from the Combustion of Char", *Fuel*, vol. 80, no. 9, pp. 1259-1272, 2001.

44. Altındağ, H., *Mathematical Modeling of Sulfur Retention in Fluidized Bed Combustors*, M.Sc. Thesis, METU, Ankara, Turkey, 2003.

45. Afacan, O., *Mathematical Modeling of NO_x Emissions in Bubbling Fluidized Bed Combustors*, M.Sc. Thesis, METU, Ankara, Turkey, 2005.

46. Lindsay, J.J., *Radiative Heat Transfer in Fluidized Beds*, Ph.D. Thesis, Trinity College, University of Cambridge, Great Britain, 1983.

47. Andersson, B.-Å., *Heat Transfer in Stationary Fluidized Bed Boilers*, Ph.D. Thesis, Chalmers University of Technology, Göteborg, 1988.

48. Filla, M., Scalabrin, A. and Tonfoni, C., "Scattering of Thermal Radiation in the Freeboard of a 1 MW_t Fluidized Bed Combustor with Coal and Limestone Feeding", *Twenty-Sixth Symposium (Int.) on Combustion*, The Combustion Institute, pp. 3295-3300, 1996.

49. Kozan, M., Selçuk, N., "Investigation of Radiative Heat Transfer in Freeboard of a 0.3 MW_t AFBC Test Rig", *Combust. Sci. and Tech.*, vol. 153, pp. 113-126, 2000.

50. Batu, A., Selçuk, N., "Modeling of Radiative Heat Transfer in the Freeboard of a Fluidized Bed Combustor Using the Zone Method of Analysis", *Turkish J.Eng. Env. Sci.*, vol. 26, no. 1, pp. 49-58, 2002.

51. Selçuk, N., Ayranci, I. and Gogebakan, Y., "Effect of Recycle on Radiative Heat Transfer in the Freeboard of a Fluidized Bed Combustor", *18th International Conference on Fluidized Bed Combustion*, ASME, Paper No. FBC2005-060, 2005.

52. Leckner, B., "Spectral and Total Emissivity of Water Vapor and Carbon Dioxide", *Combust. Flame*, vol. 19, pp. 33-48, 1972.

53. Deirmendjian, D., *Electromagnetic Scattering of Spherical Polydispersions*, Elsevier, USA, 1969.

54. Hottel, H.C., Cohen, E.S., "Radiant Heat Exchange in Gas-Filled Enclosure: Allowance for Nonuniformity of Gas Temperature", *AIChE Journal*, vol. 4, pp. 3-14, 1958.

55. Rhine, J.M., Tucker, R.J., *Modeling of Gas-Fired Furnaces and Boilers*, British Gas plc, McGraw-Hill, Great Britain, Ed., 1991.

56. Yücel, A., "Solution of the Discrete Ordinates Equations for a Radiatively Participating Medium by the Method of Lines", *Advances in Computer Methods for Partial differential Equations VII*, pp. 838-844, 1992.

57. Selçuk, N., Kırbaş, G. and Tarhan, T., "Evaluation of Method of Lines Solution of Discrete Ordinates Method and Finite Volume Method in a Planar Medium", *Proceedings of the International Conference on Computational Heat and Mass Transfer (CHMT-99)*, pp. 358-364, 1999.

58. Selçuk, N., Kırbaş, G., "The Method of Lines Solution of Discrete Ordinates Method for Radiative Heat Transfer in Enclosures", *Numer. Heat Transfer, Part B*, vol. 37, pp. 379-392, 2000.

59. Incropera, F.P., De Witt, D. P., *Fundementals of Heat and Mass Transfer*, John Wiley and Sons, 3rd Ed., 1990.

60. Choi, J.H., I.Y. Chang, D.W. Shun, C.K. Yi, J.E. Son and S.D. Kim, "Correlation on the Particle Entrainment Rate in Gas Fluidized Beds", *Industrial & Engineering Chemistry Research*, vol. 38, no. 6, pp. 2491-2496, 1999.

61. Kunii, D., Levenspiel, O., *Fluidization Engineering*, Butterworth Heinemann, 2nd Ed., 1991.

62. Davidson, J.F., Clift, R. and Harrison, D., *Fluidization*, Academic Press, 2nd Ed., 1985.

63. Ergun, S., "Fluid Flow through Packed Columns", *Chemical Engineering Progress*, vol. 48, no. 2, pp. 89-94, 1952.

64. Mori, S., Wen, C. Y., "Estimation of Bubble Diameter in Gaseous Fluidized-Beds", *AIChE Journal*, vol. 21, no. 1, pp. 109-115, 1975.

65. Gogolek, P.E.G., Becker, H. A., "Calculation of the Expansion of a Bubbling Fluidized-Bed of Coarse Particles", *Powder Technology*, vol. 71, no. 1, pp. 107-110, 1992.

66. Denloye, A.O.O., Botterill, J. S. M., "Bed to Surface Heat-Transfer in a Fluidized-Bed of Large Particles", *Powder Technology*, vol. 19, no. 2, pp. 197-203, 1978.

67. Sleicher, C.A., Rouse, M. W., "A Convenient Correlation for Heat Transfer to Constant and Variable Property Fluids in Turbulent Pipe Flow", *International Journal of Heat and Mass Transfer*, vol. 18, pp. 677-683, 1975.

68. Field, M.A., Gill, D. W., Morgan, B. B. and Hawksley, P. G. W., *Combustion of Pulverized Coal*, British Coal Utilization Research Association, Ed., 1967.

69. Hottel, H.C., Williams, G. C., Nerheim, N. M. and Schneider, G. R., "Kinetic Studies on Stirred Reactors, Combustion of Carbon Monoxide and Propane", *Proceedings of the 10th Int. Symp. on Combustion*, The Combustion Institute, 975-986, 1965.

70. Grace, J.R., Clift, R., "2-Phase Theory of Fluidization", *Chemical Engineering Science*, vol. 29, no. 2, pp. 327-334, 1974.

71. Grace, J.R., Harrison, D., "Behavior of Freely Bubbling Fluidised Beds", *Chemical Engineering Science*, vol. 24, no. 3, pp. 497-508, 1969.

72. Davidson, J.F., Harrison, D., *Fluidised Particles*, Cambridge University Press, Ed., 1963.

73. Stubington, J.F., Chan, S. W. and Clough, S. J., "A Model for Volatiles Release into a Bubbling Fluidized-Bed Combustor", *AIChE Journal*, vol. 36, no. 1, pp. 75-85, 1990.

74. Anthony, D.B., Howard, J. B., "Coal Devolatilization and Hydrogasification", *AIChE Journal*, vol. 22, no. 4, pp. 625-656, 1976.

75. Gögebakan, Y., *Char Attrition in Fluidized Bed Combustors*, M.Sc. Thesis, METU, Ankara, Turkey, 2000.

76. Hazlett, J.D., Bergougnou, M. A., "Influence of Bubble-Size Distribution at the Bed Surface on Entrainment Profile", *Powder Technology*, vol. 70, no. 2, pp. 99-107, 1992.

77. Kunii, D. and O. Levenspiel, "Fluidized Reactor Models.1. For Bubbling Beds of Fine, Intermediate, and Large Particles. 2. For the Lean Phase - Freeboard and Fast Fluidization", *Industrial & Engineering Chemistry Research*, vol. 29, no. 7, pp. 1226-1234, 1990.

78. Botterill, J.S.M., *Fluid-Bed Heat Transfer*, Academic Press, Ed., 1975

79. Siegel, R., Howell, J.R., *Thermal Radiation Heat Transfer*, New York: McGraw-Hill, Inc., 1972.

80. Modest, M.F., *Radiative Heat Transfer*, New York: McGraw-Hill, Inc., 1993.

81. Ayrancı, I., *The Method of Lines Solution of Discrete Ordinates Method for Radiative Heat Transfer in 3-D Rectangular Enclosures Containing Scattering Media*, M.Sc. Thesis, METU, Middle East Technical University, Ankara, 2001.

82. Fiveland, W.A., "Discrete-Ordinates Solutions of the Radiative Transport Equation for Rectangular Enclosures", *J. Heat Transfer*, vol. 106, pp. 699-706, 1984.

83. Carlson, B.G., Lathrop, K.D., *Transport Theory- the Method of Discrete Ordinates in Computing Methods in Reactor Physics*, ed. H. Greenspan, C.N. Kelber and D. Okrent, New York: Gordon and Breach, Ed., 1968.

84. Selçuk, N., Kayakol, N., "Evaluation of Angular Quadrature and Spatial Differencing Schemes for Discrete Ordinates Method in Rectangular Furnaces", *Proceedings of 31st National Heat Transfer Conference*, ASME HTD, pp. 151-158, 1996.

85. Schiesser, W.E., *The Numerical Method of Lines in Integration of Partial Differential Equations*, Academic Press Inc., 1991.

86. Kozan, M., *Investigation of Radiative Heat Transfer in Freeboard of a 0.3 MW_t Afbc Test Rig*, M.Sc. Thesis, METU, Ankara, Turkey, 1999.

87. Viskanta, R., Ungan, A. and Mengüç, P., "Predictions of Radiative Properties of Pulverized Coal and Fly-Ash Polydispersion", *ASME Paper*, vol. 81-HT-24, 1981.

88. Tien, C.L., Drolen, B.L., "Thermal Radiation in Particulate Media with Dependent and Independent Scattering ", *Annual Review of Numerical Fluid Mechanics and Heat Transfer*, vol. 1, no. 1, pp. 1-32, 1987.

89. Neubronner, M., Vortmeyer, D., "Thermal Radiation of Fly Ashes - Dependence on Size Distribution and Chemical Composition", *Proceedings of The Tenth (Int.) Heat Transfer Conference*, Institution of Chemical Engineers, pp. 117-122, 1994.

90. Değirmenci, E., "Calculation of Scattering Coefficients", *Ch.E. 473 Term Project*, Chemical Engineering Department, METU, Turkey, 1996.

91. Hannes, J., *Mathematical Modeling of Circulating Fluidized Bed Combustion*, Ph.D. Thesis, RWTH, Aachen, Germany, 1996.

92. Radhakrishnan, K., Hindmarsh, A. C., *Description and Use of Lsode, the Livermore Solver for Ordinary Differential Equations*, Lawrance Livermore National Laboratory Report No: UCRL-ID-113855, 1993.

93. Harmandar, H., *Effect of Recycling on the Performance of Bubbling Fluidized Bed Combustors*, M.Sc. Thesis, METU, Ankara, Turkey, 2003.

94. Corporation, M., "Operating Manual of 64 Series Heat Flux Transducers", 1995.

95. Dereniak, E.L., Crowe, D.G., "Optical Radiation Detectors", John Wiley & Sons, Inc., 1984.

96. Degirmenci, E., Y. Gogebakan and N. Selcuk, "Assessment of Catalyst Deactivation Model for Sulfur Retention in Fluidized Bed Combustors", *Combustion Science and Technology*, vol. 153, pp. 95-111, 2000.

97. Andersson, B.-Å., Leckner, B. and Amand, L-E., "Fluidized Bed Combustion of Coals and Alternative Fuels", *The 8th International Conference on Fluidized Bed Combustion*, DOE/METC-85/6021, 2, pp. 1019-1029, 1985.

98. Svensson, G., Leckner, B., "The Fluidised Bed Boiler at Chalmers University of Technology", *The 7th Int. Conf. on Fluidized Bed Combustion,* 1982.

99. Lewis, W.K., Gilliland, E. R. and Lang, P. M., "Entrainment from Fluidized Beds", *Chemical Engineering Progress Symposium Series: Fluidization*, pp. 65-78, 1961.

100. Kunii, D., Levenspiel, O., "Entrainment and Elutriation from Fluidized Beds", *Journal Of Chemical Engineering Of Japan*, vol. 2, no. 1, pp. 84-88, 1969.

APPENDIX A

ORDINATES AND WEIGHTS FOR S_N APPROXIMATIONS

In this study, S_N angular quadrature was used for implementation of MOL solution of DOM. The ordinates and weights for various orders of approximation are presented in Table A.1.

Table A.1 Discrete ordinates for the S_N approximation.

Order of Approximation	Ordinates μ_m	η_m	ξ_m	Weights w_m
S_2	0.5000000	0.5000000	0.7071068	1.5707963
S_4	0.9082483	0.2958759	0.2958759	0.5235987
	0.2958759	0.9082483	0.2958759	0.5235987
	0.2958759	0.2958759	0.9082483	0.5235987
S_6	0.9656013	0.1838670	0.1838670	0.1609517
	0.6950514	0.6950514	0.1838670	0.3626469
	0.1838670	0.9656013	0.1838670	0.1609517
	0.6950514	0.1838670	0.6950514	0.3626469
	0.1838670	0.6950514	0.6950514	0.3626469
	0.1838670	0.1838670	0.9656013	0.1609517
S_8	0.9795543	0.1422555	0.1422555	0.1712359
	0.8040087	0.5773503	0.1422555	0.0992284
	0.5773503	0.8040087	0.1422555	0.0992284
	0.1422555	0.9795543	0.1422555	0.1712359
	0.8040087	0.1422555	0.5773503	0.0992284
	0.5773503	0.5773503	0.5773503	0.4617179
	0.1422555	0.8040087	0.5773503	0.0992284
	0.5773503	0.1422555	0.8040087	0.0992284
	0.1422555	0.5773503	0.8040087	0.0992284
	0.1422555	0.1422555	0.9795543	0.1712359
S_{10}	0.9809754	0.1372719	0.1372719	0.0944411
	0.8523177	0.1372719	0.5046889	0.148395
	0.8523177	0.5046889	0.1372719	0.148395
	0.7004129	0.1372719	0.7004129	0.0173701
	0.7004129	0.5046889	0.5046889	0.1149972
	0.7004129	0.7004129	0.1372719	0.0173701
	0.5046889	0.1372719	0.8523177	0.148395
	0.5046889	0.5046889	0.7004129	0.1149972
	0.5046889	0.7004129	0.5046889	0.1149972
	0.5046889	0.8523177	0.1372719	0.148395
	0.1372719	0.1372719	0.9809754	0.0944411
	0.1372719	0.5046889	0.8523177	0.148395
	0.1372719	0.7004129	0.7004129	0.0173701
	0.1372719	0.8523177	0.5046889	0.148395
	0.1372719	0.9809754	0.1372719	0.0944411